Microgrid Formation-based Service Restoration Using Deep Reinforcement Learning and Optimal Switch Placement in Distribution Networks

A Thesis Submitted to the College of
Graduate and Postdoctoral Studies
In Partial Fulfillment of the Requirements
For the Degree of Master of Science
In the Department of Electrical and Computer Engineering
University of Saskatchewan
Saskatoon, SK, Canada

By

Mosayeb Afshari Igder

Permission to Use

In presenting this thesis in partial fulfillment of the requirements for a Postgraduate degree from the University of Saskatchewan, I agree that the Libraries of this University may make it freely available for inspection. I further agree that permission for copying of this thesis in any manner, in whole or in part, for scholarly purposes may be granted by the professor or professors who supervised my thesis work or, in their absence, by the Head of the Department or the Dean of the College in which my thesis work was done. It is understood that any copying or publication or use of this thesis or parts thereof for financial gain shall not be allowed without my written permission. It is also understood that due recognition shall be given to me and to the University of Saskatchewan for any scholarly use which may be made of any material in my thesis.

Requests of permission to copy or to make other uses of materials in this thesis in whole or part should be addressed to:

Head of the Department of Electrical and Computer Engineering
57 Campus Drive
University of Saskatchewan
Saskatoon, Saskatchewan, S7N 5A9
Canada

OR

Dean
College of Graduate and Postdoctoral Studies
University of Saskatchewan
116 Thorvaldson Building, 110 Science Place
Saskatoon, Saskatchewan S7N 5C9
Canada

Abstract

A power distribution network that demonstrates resilience has the ability to minimize the duration and severity of power outages, ensure uninterrupted service delivery, and enhance overall reliability. Resilience in this context refers to the network's capacity to withstand and quickly recover from disruptive events, such as equipment failures, natural disasters, or cyber attacks. By effectively mitigating the effects of such incidents, a resilient power distribution network can contribute to enhanced operational performance, customer satisfaction, and economic productivity. The implementation of microgrids as a response to power outages constitutes a viable approach for enhancing the resilience of the system.

In this work, a novel method for service restoration based on dynamic microgrid formation and deep reinforcement learning is proposed. To this end, microgrid formation-based service restoration is formulated as a Markov decision process. Then, by utilizing the node cell and route model concept, every distributed generation unit equipped with the black-start capability traverses the power system, thereby restoring power to the lines and nodes it visits. The deep Q-network is employed as a means to achieve optimal policy control, which guides agents in the selection of node cells that result in maximum load pick-up while adhering to operational constraints.

In the next step, a solution has been proposed for the switch placement problem in distribution networks, which results in a substantial improvement in service restoration. Accordingly, an effective algorithm, utilizing binary particle swarm optimization, is employed to optimize the placement of switches in distribution networks. The input data necessary for the proposed algorithm comprises information related to the power system topology and load point data. The fitness of the solution is assessed by minimizing the unsupplied loads and the number of switches placed in distribution networks.

The proposed methods are validated using a large-scale unbalanced distribution system consisting of 404 nodes, which is operated by Saskatoon Light and Power, a local utility in Saskatoon, Canada. Additionally, a balanced IEEE 33-node test system is also utilized for validation purposes.

Acknowledgments

I express my sincere appreciation to my esteemed supervisor, Dr. Xiaodong Liang, for her invaluable guidance, patience, and unwavering support throughout my master's study at the University of Saskatchewan. Her profound expertise and extensive experience have played an indispensable role in the successful completion of this thesis.

I extend my profound gratitude to my esteemed parents and sisters for their unwavering support and unconditional love, without which the accomplishment of this achievement would not have been possible.

Lastly, I would like to express my heartfelt gratitude to my incredible friends - Ershad Ostadzadeh, Mehdi Abbasipour, Amir Hossein Dehghani, Sadegh Zandi, and Shiva Naserabadi - for their unwavering support and camaraderie, which have played a vital role in my achievements. Thank you for always being there for me!

Table of Contents

Permission to Use i

Abstract ii

Acknowledgments iii

Table of Contents iv

List of Figures vii

List of Tables x

List of Abbreviations xii

1 Introduction 1

1.1 Service Restoration in Distribution networks 1

1.2 Motivation and Problem Statement 2

1.3 Objectives of the research work 5

1.3.1 Service Restoration 5

1.3.2 Optimal Switch Placement 5

1.4 Thesis Outline 6

1.5 Reference 7

2 Microgrid Formation Techniques in Active Distribution Networks: A Review 10

2.1 Abstract 10

2.2 Introduction 11

2.3 Microgrid Construction Models 15

2.3.1 Graph Theory-based Technique 16

2.3.2 Heuristic Rule-based Algorithm 22

2.3.3 Clustering Algorithm 25

2.3.4 Mixed Integer Linear Programming 28

2.4 Microgrid Control 30

2.4.1 Traditional Hierarchical Control for Microgrid 30

2.4.2 Multiagent System-based Distributed Control 32

2.5 Microgrid Economic 34
2.6 Advantages and Disadvantages of Microgrid Formation Algorithms, and Future Research Direction 36
2.6.1 Advantages and Disadvantages of Microgrid Formation Algorithms 36
2.6.2 Future Research Direction 37
2.7 Conclusion 38
2.8 Reference 39
3 Service Restoration Using Deep Reinforcement Learning and Dynamic Microgrid Formation in Distribution Networks 50
3.1 Abstract 50
3.2 Introduction 50
3.3 The Proposed Service Restoration Method Using Deep Reinforcement Learning 53
3.4 Problem Formulation 55
3.4.1 Microgrid Formation-based Service Restoration 55
3.4.2 Modeling Microgrid Formation-based Service Restoration as a Markov Decision Process 57
3.5 Deep Reinforcement Learning Algorithm for Service Restoration 61
3.5.1 Deep Q-Learning 62
3.5.2 Enhance learning process of deep reinforcement learning 63
3.5.3 Offline Training and Online Applications of the Proposed Method 65
3.6 Validation Using IEEE 33-Node Test System 66
3.6.1 The Modified IEEE 33-Node Test System 66
3.6.2 Training 68
3.6.3 Testing and Implementation 69
3.6.4 Performance Comparison with Existing Methods 78
3.7 Validation Using a Real Large Distribution Network 80
3.7.1 Scenario 1 81
3.7.2 Scenario 2 84
3.7.3 Scenario 3 87
3.8 Conclusion 90
3.9 Appendix 91

3.10 Reference 93

4 Optimal Switch Placement to Enhance Microgrid Formation-based Service Restoration Using Reinforcement Learning in Distribution Networks 96

4.1 Abstract 96

4.2 Introduction 96

4.3 Problem Formulation 98

4.3.1 Particle Swarm Optimization Algorithm 98

4.3.2 Objective Function 100

4.4 The Switch Placement Algorithm 102

4.5 Validation of the Proposed Switch Placement Method Using the IEEE 33-node Test System 104

4.5.1 The Switch Placement Optimization 105

4.5.2 Service Restoration through Microgrid Formation using Deep Reinforcement Learning 106

4.6 Validation Through a Real Large 404-node Distribution System 107

4.6.1 Switch Placement Optimization 107

4.6.2 Service Restoration through Microgrid Formation using Deep Reinforcement Learning 108

4.7 Conclusion 112

4.8 Reference 113

5 Conclusions and Future Work 115

5.1 Summary and Conclusions 115

5.2 Future Work 115

Appendix 117

Publications (Jan. 2021 – Apr. 2023): 117

List of Figures

Figure 2.1. A resilience performance curve [4]. 11

Figure 2.2. (a) Resiliency improvement strategies in power distribution networks, (b) Islanding in power system. 13

Figure 2.3. The summary of microgrid formation techniques. 16

Figure 2.4. The coarsening first iteration in the graph partitioning technique [52]. 17

Figure 2.5. The coarsening second iteration in the graph partitioning technique [52]. 18

Figure 2.6. The partitioning stage in the graph partitioning technique [52]. 19

Figure 2.7. Uncoarsening stage in the graph partitioning technique [52]. 20

Figure 2.8. The distribution network graph in a normal mode [53]. 22

Figure 2.9. The distribution network graph in a self-healing mode [53]. 22

Figure 2.10. The flowchart of microgrid construction using the heuristic method [46]. 24

Figure 2.11. Microgrid formation of the 119-bust test system [57]. 25

Figure 2.12. Hierarchical algorithm, the dendrogram of IEEE 39-bus test system [49]. 27

Figure 2.13. The K-means algorithm [64]. 28

Figure 2.14. Traditional hierarchical control for microgrids [71]. 32

Figure 2.15. The structure of multiagent-based microgrid [71]. 33

Figure 2.16. Peak shaving and load leveling [95]. 35

Figure 3.1. The flow chart of the proposed service restoration method through dynamic MG formation and DRL in distribution networks. 54

Figure 3.2. The framework of DRL for MG-formation-based service restoration. 66

Figure 3.3.The modified IEEE 33-node test system. 67

Figure 3.4.The simplified IEEE 33-node test system with 14 node cells. 67

Figure 3.5. The average loss in the training process. 69

Figure 3.6.Three microgrids formed in the modified IEEE 33-node test system using DQN (Case 1). 70

Figure 3.7. The restoration sequences of modified IEEE 33-node system using the DQN in case1. 71

Figure 3.8. Voltage profile of the modified IEEE 33-node test system after forming three MGs (Case 1). 71

Figure 3.9. Power losses of the modified IEEE 33-node test system in each MG (Case 1). 72

Figure 3.10. Microgrid formation of the modified IEEE 33-node test system using DQN (Case 2). 73

Figure 3.11. Voltage profile of the modified IEEE 33-node test system after forming three MGs (Case 2). 74

Figure 3.12. Power losses of the modified IEEE 33-node test system in each MG (Case 2). 74

Figure 3.13. Microgrid formation of modified IEEE 33-node system using DQN for Case3. 75

Figure 3.14.Voltage profile of the modified IEEE 33-node test system after forming two MGs (Case 3). 76

Figure 3.15. Power losses of the modified IEEE 33-node test system in each MG (Case 3). 76

Figure 3.16. Microgrid formation of the modified IEEE 33-node test system using DQN (Case 4). 77

Figure 3.17. Voltage profile of the modified IEEE 33-node test system after forming three MGs (Case 4). 78

Figure 3.18. Power losses of the modified IEEE 33-node test system in each MG (Case 4). 78

Figure 3.19. The simplified system with 32 node cells through the node cell concept. 81

Figure 3.20. Microgrid formation of the 404-node system using DQN (Scenario 1). 83

Figure 3.21. Voltage profile of the 404-node system after restoration (Scenario 1). 84

Figure 3.22. Power losses in each MG for the 404-node system (Scenario 1). 84

Figure 3.23. Microgrid formation of the 404-node system using DQN (Scenario 2). 86

Figure 3.24.Voltage profile of the 404-node system after restoration (Scenario 2). 87

Figure 3.25. Power losses in each MG for the 404-node system (Scenario 2). 87

Figure 3.26. Microgrid formation of the 404-node system using DQN (Scenario 3). 89

Figure 3.27. Voltage profile of the 404-node system after restoration (Scenario 3). 90

Figure 3.28. Power losses in each MG for the 404-node system (Scenario 3). 90

Figure 4.1. Flowchart of the proposed switch placement algorithm. 104

Figure 4.2. The IEEE 33-node test system [16]. 105

Figure 4.3. Microgrid formation-based service restoration in IEEE 33-node test system. 107

Figure 4.4. Node cells formation of Saskatoon Light and Power system. 110

Figure 4.5. Microgrid formation-based service restoration in the Saskatoon Light and Power distribution network. 111

List of Tables

Table 2.1. Major blackouts across the globe..... 11

Table 2.2. Summary of literature review on microgrid formation for service restoration in distribution networks. 29

Table 2.3. Cost details of various power generation technologies [100]. 36

Table 3.1. DG parameters for the modified IEEE 33-node test system..... 67

Table 3.2.Hyper-parameter Settings of the DQN for the Modified IEEE 33-Node Test System. 68

Table 3.3. Restored nodes and power of the modified IEEE 33-node test system using DQN (Case 1) 70

Table 3.4. DG Output Power of the Modified IEEE 33-node Test System (Case 1) 70

Table 3.5. Restored Nodes and Power of the Modified IEEE 33-node Test System using DQN (Case 2) 73

Table 3.6. DG output power of the modified IEEE 33-node test system (Case 2)..... 73

Table 3.7. Restored nodes and power of the modified IEEE 33-node test system using DQN (Case 3) 75

Table 3.8. DG output power of the modified IEEE 33-node test system (Case 3)..... 75

Table 3.9. Restored nodes and power of the modified IEEE 33-node test system using DQN (Case 4) 77

Table 3.10. DG output power of the modified IEEE 33-node test system (Case 4)..... 77

Table 3.11.Comparison among the proposed method and three existing methods in [10], [11], and [15] for service restoration using the modified IEEE 33-node test system 79

Table 3.12. The number of variables and constraints for three existing methods [15]..... 79

Table 3.13.DG parameters in the modified 404-node system model 80

Table 3.14. Restored node cells and power of the modified 404-node system using DQN (Scenario 1) 82

Table 3.15. DG output power for the modified 404-node system (Scenario 1)..... 82

Table 3.16. The restored node cells and power of the 404-node system using DQN (Scenario 2) 85

Table 3.17 .DG output power for the 404-node system (Scenario 2)..... 85

Table 3.18. The restored node cells and power of the 404-node system using DQN (Scenario 3) 88

Table 3.19. DG output power for the 404-node system (Scenario 3)..... 88

Table 3.20. Node cell mapping for the modified IEEE 33-node test system..... 91

Table 3.21. node cell mapping for the 404-node system 92

Table 4.1. Comparative analysis of switching solutions with different objective weights in IEEE 33-node system 106

Table 4.2. Comparison of MG-based service restoration using DRL: optimal vs random switch placement 107

Table 4.3.Comparative Analysis of Switching Solutions with Different Objective Weights in the real world system 109

Table 4.4. Comparison of MG-based service restoration using DRL: optimal vs random switch placement 110

List of Abbreviations

ACO	Ant Colony Algorithm
ADS	Active Distribution Systems
BPSO	Binary Particle Swarm Optimization
DER	Distributed Energy Resource
DG	Distributed Generation
DGs	Distributed Generators
DQN	Deep Q-Network
DRL	Deep Reinforcement Learning
DSR	Distribution Service Restoration
GA	Genetic Algorithm
gbest	Global Best Value
GGGP	Greedy Graph Growing Partitioning
IA	Immune Algorithm
KL	Kernighan-Lin
MAS	Decentralized Multiagent System
MDP	Markov Decision Process
MG	Microgrid
MGs	Microgrids
MILP	Mixed-Integer Linear Program
MINLP	Mixed-Integer Non-Linear Programming
OF	Objective Function

pbest	Particle Best Value
PSO	Particle Swarm Optimization
PID	Proportional Integral Derivative
ReLU	Rectified Linear Units
SCADA	Supervisory Control and Data Acquisition
SEM	Shortest Edge Machine
STD	Standard Deviation

1 Introduction

1.1 Service Restoration in Distribution networks

Over the past few decades, large-scale blackouts and extreme weather events have been increasing, power system infrastructures must be designed and maintained to be able to withstand and recover from such outages/events [1], [2]. Improving resiliency of power systems is urgently needed considering significant impact of power outages on critical services, economics, and public safety [3], [4], [5]. For instance, devastating impacts of hurricanes, Harvey, Irma, and Maria, in 2017 resulted in significant damages to utility infrastructure and widespread power disruptions [6]. Effective service restoration to rapidly restore power to customers following an outage is essential.

In the United States, distribution networks account for more than 90% of power outages [7]. Unplanned incidents, such as fallen trees, lightning strikes, storms, and equipment malfunctions, and planned activities, such as regular maintenance and equipment installation, can all lead to power outages in distribution systems. Once power outages are identified and isolated, the distribution service restoration (DSR) procedure is initiated to expedite recovery of disrupted loads [8].

Previously, distribution utilities created pre-determined solutions for a wide range of fault scenarios [9], and most companies developed their own restoration plans. However, a fully pre-planned restoration approach for distribution networks has two drawbacks, which make them unsuitable for our modern power grids: 1) it is impractical to account for all potential fault scenarios in advance via the offline analysis; and 2) pre-planned scenarios are based on fixed assumptions of input data related to network infrastructure/topology and load consumption, which may be unreliable and subject to change.

Traditional passive distribution networks, which do not include active components, such as generators or voltage regulators, solely rely on topological reconfigurations for the restoration process, which involves transferring the load from the off/outage feeder to neighbouring feeders via tie-lines equipped with tie-switches [10]. Currently, distribution systems are transitioning to active distribution systems (ADS) due to a growing number of controllable devices, including distributed generation (DG) units, microgrids (MGs), and remotely-controllable switches, which

can actively regulate the voltage and frequency [11]. For active distribution systems, an advanced distribution service restoration (DSR) framework is critical to achieve optimal restoration solutions.

1.2 Motivation and Problem Statement

Recently, conventional distribution grids have experienced substantial changes [12], and electric utilities aim to reduce losses and improve system reliability, and integrate more renewable energy sources and energy storage units at the distribution level. To promote renewable energy sources integration, microgrid (MGs) serves as an effective solution. Microgrids are essentially small-scale power systems that can operate in grid-connected or island modes, providing greater flexibility and resilience during power outages. Microgrids have the ability to operate independently, so they can provide power to critical loads during disturbances and facilitate faster service restoration [13]. IEEE Std1547.4-2011 defines microgrids as intentionally designed systems that can enhance reliability by supplying power to the islanded portion of the distribution network during outages/disturbances, alleviate overloading issues, and enable disconnection and reconnection to the main distribution network [14].

Self-healing is a key attribute of smart grids, defined as the ability to autonomously restore services following a fault [15]. By incorporating solar PV panels, wind turbines, backup generators, and remotely controlled switches, distribution systems can be partitioned into multiple self-sufficient microgrids, enabling a self-healing distribution network. One major challenge is to determine effective boundaries of microgrids during contingencies. The current research on microgrid formation for service restoration can be classified into two types [16]: 1) predetermined microgrids with specified switching status and network configuration, which do not consider system operating conditions and customer priorities, and they mainly focus on optimal operation of distributed energy resources [12]; and 2) dynamic microgrids, which aim to find optimal boundary during a fault to minimize the outage duration and disrupted load [15].

Mathematical programming [17], [18] and heuristic search methodologies [12], [19] are commonly employed to identify optimal boundaries of microgrids. A new operational approach for distribution systems is proposed in [18], where multiple dynamic microgrids are formed and energized by DGs from a radial distribution system in real-time operations. The objective is to restore critical loads during a power outage. The approach involves formulating a mixed-integer

linear program (MILP) to optimize the critical load pickup while ensuring self-adequacy and operational constraints by controlling remotely controlled switches and DGs. In [17], the microgrid formation for service restoration is proposed as a mixed-integer non-linear programming (MINLP) model, and a commercial solver, DCOPT, is employed solve the optimization problem. In [12], an optimization algorithm based on tabu search and a graph theory-based method are proposed to partition a distribution network into multiple virtual microgrids. In [19], a heuristic methodology is proposed to efficiently solve the post-disturbance microgrid formation to maximize load pickup.

For mathematical programming methods, it is crucial to create a precise mathematical model, but it is a time-consuming process and may not always be practical for certain applications. The model-based approaches may also encounter difficulties in modelling complex objects, integrating new features, and maintaining computational efficiency when applied to large systems. Heuristic-based methods utilize heuristic algorithms to obtain solutions for complex optimization problems, but they cannot identify the optimal solution. Restoring electrical service during a natural disaster is a critical task that demands quick and accurate actions. Both mathematical and heuristic-based methods have been developed to solve complex optimization problems for service restoration, but they may not be suitable for real-time applications that require fast and precise results. This is particularly true in the context of natural disasters, where conditions are often uncertain and prone to change. The time-consuming nature of mathematical-based methods and the approximate nature of heuristic-based methods may limit their effectiveness in providing the rapid and accurate response needed for successful service restoration during a disaster. Therefore, alternative approaches that can balance speed, accuracy, and adaptability are needed to ensure that service restoration is effective and timely.

Since dynamic microgrid formation-based service restoration involves a sequence of decisions, it can be conceptualized as a Markov decision process [20]. Deep reinforcement learning (DRL)-based algorithms can be employed to address this problem through an iterative solution procedure. DRL involves continuous interactions with the environment and gathering of feedback, which facilitates increased adaptability of the MG formation scheme to variable conditions. DRL algorithm's adaptive nature allows it to learn from feedback and modify its behaviour, accordingly, makes it well-suited for real-time applications that may experience rapid changes in conditions, such as those that occur during natural disasters. Therefore, a well-trained DRL model can quickly

provide an online scheme for dynamic microgrid formation as a service restoration strategy, ensuring uninterrupted power supply to critical loads.

DRL has become increasingly popular to address complex problems in power systems, including voltage control [21], electrical vehicle charging navigation [22], demand response [23], microgrid power management [24], and enhancing resilience of distribution networks [25]. However, there is very limited research done on DRL-based microgrid (MG) formation for service restoration in the literature due to challenges associated with implementing a feasible radial topology and a high number of reconfigurations required in a large system.

Optimal switch placement is another crucial factor that influences performance and reliability of distribution systems, especially during service restoration [26]. In active distribution networks, sectionalizing and automatic switches play a key role in isolating faulted areas to prevent cascading failures and reduce customer outages. Sectionalizing switches in distribution systems are expensive, so potential investment costs must be balanced with the system reliability improvement. The optimal switch placement in distribution systems with distributed generation sources is addressed in [27] through a combined approach of mixed fuzzy logic and ant colony algorithm, impacts on costs and reliability are analysed using a weighted sum of objective functions. In [28], a three-state variation of the particle swarm optimization method is proposed to identify ideal number and location of sectionalizer switches in distribution networks by optimizing cost of the outage function. A MILP approach is introduced in [29] as an effective method for optimizing the system average interruption duration index.

These approaches are effective for optimal switch placement, but they rely on the failure rates of the network equipment, and these parameters are often not readily available and costly to obtain. The mathematical-based optimization is not practical because it can only solve the problem effectively for small networks.

To overcome these technical challenges, this thesis focuses on:

- Developing a dynamic microgrid formation-based service restoration approach using deep reinforcement learning for distribution networks.
- Developing optimal switch placement method to improve service restoration.

1.3 Objectives of the research work

Drawing on the motivations and challenges outlined earlier, the present study sets forth the following research objectives:

1.3.1 Service Restoration

To develop a service restoration method in distribution networks, a mathematical optimization model for microgrid formation is developed first; a Markov decision process (MDP) is then defined to formulate service restoration as a sequence of decisions, which involves identifying key elements of the process, such as state, action, and reward; and the optimization problem is solved through deep reinforcement learning. The objectives of this part of the research are provided below:

- Formulate a mathematical model for microgrid formation-based service restoration that accounts for operation and topology constraints.
- Define a novel Markov decision process for the service restoration problem.
- Develop a deep reinforcement learning framework and utilize deep Q-network to efficiently form microgrids and maximize load pick up.
- Validate the proposed method using the IEEE 33-node test system and the real 404-node unbalanced distribution system operated by Saskatoon Light and Power, a local electric utility in Saskatoon, SK, Canada.

1.3.2 Optimal Switch Placement

For optimal switch placement in distribution networks, a multi-objective optimization problem is formulated using binary particle swarm optimization to minimize unsupplied loads and the number of switches. The following objectives are specified for this section:

- Develop an optimization problem for optimal switch placement in distribution networks using binary particle swarm optimization algorithm to minimize unsupplied loads and the number of switches.
- Validate the proposed method using the IEEE 33-node test system and the real 404-node unbalanced distribution system operated by Saskatoon Light and Power.
- Evaluate service restoration using optimally placed switches.

1.4 Thesis Outline

This thesis is in manuscript format, and includes six chapters as explained below:

Chapter 1 presents an introduction of the thesis.

Chapter 2 is a literature review for microgrid formation techniques in active distribution networks, it has been published in *IEEE Access* in April 2022.

Chapter 3 presents a new approach for dynamic microgrid formation-based service restoration using deep reinforcement learning in distribution networks. The method considers operational and structural constraints of microgrids and is formulated as a Markov decision process (MDP). Optimal control strategies for microgrid formation are obtained through the utilization of a deep Q-network. By utilizing the deep Q-learning method, a new algorithm is proposed for the agent to select actions in the process of microgrid formation, which guarantees the feasibility of a radial structure.

Chapter 4 proposes an optimal switch placement method using a multi-objective optimization through binary particle swarm algorithm.

Chapter 6 provides a summary of the thesis, highlighting key findings and future research directions.

1.5 Reference

[1] B. Chen, Z. Ye, C. Chen, and J. Wang, "Toward a MILP modeling framework for distribution system restoration," IEEE Trans. Power Syst., vol. 34, no. 3, pp. 1749–1760, 2019.

[2] Y. Zhang, F. Qiu, T. Hong, Z. Wang, and F. Li, "Hybrid imitation learning for real-time service restoration in resilient distribution systems," IEEE Trans. Ind. Inform., vol. 18, no. 3, pp. 2089–2099, 2022.

[3] Y. Du and D. Wu, "Deep reinforcement learning from demonstrations to assist service restoration in islanded microgrids," IEEE Trans. Sustain. Energy, vol. 13, no. 2, pp. 1062–1072, 2022.

[4] B. Chen, C. Chen, J. Wang, and K. L. Butler-Purry, "Sequential service restoration for unbalanced distribution systems and microgrids," IEEE Trans. Power Syst., vol. 33, no. 2, pp. 1507–1520, 2018.

[5] Y. Wang, C. Chen, J. Wang, and R. Baldick, "Research on resilience of power systems under natural disasters—A review," IEEE Trans. Power Syst., vol. 31, no. 2, pp. 1604–1613, 2016.

[6] "Hurricanes Nate, Maria, Irma, and Harvey Situation Reports," Energy.gov. https://www.energy.gov/ceser/articles/hurricanes-nate-maria-irma-and-harvey-situation-reports (accessed Mar. 31, 2023).

[7] R. J. Campbell and S. Lowry, "Weather-related power outages and electric system resiliency," Congressional Research Service, Library of Congress Washington, DC, 2012.

[8] F. Shen, Q. Wu, and Y. Xue, "Review of service restoration for distribution networks," J. Mod. Power Syst. Clean Energy, vol. 8, no. 1, pp. 1–14, 2020.

[9] J. J. Ancona, "A framework for power system restoration following a major power failure," IEEE Trans. Power Syst., vol. 10, no. 3, pp. 1480–1485, 1995.

[10] H. Sekhavatmanesh and R. Cherkaoui, "A multi-step reconfiguration model for active distribution network restoration integrating DG start-up sequences," IEEE Trans. Sustain. Energy, vol. 11, no. 4, pp. 2879–2888, 2020.

[11] H. Sekhavatmanesh and R. Cherkaoui, "Analytical approach for active distribution network restoration including optimal voltage regulation," IEEE Trans. Power Syst., vol. 34, no. 3, pp. 1716–1728, 2018.

[12] S. A. Arefifar, Y. A.-R. I. Mohamed, and T. H. El-Fouly, “Supply-adequacy-based optimal construction of microgrids in smart distribution systems,” IEEE Trans. Smart Grid, vol. 3, no. 3, pp. 1491–1502, 2012.

[13] A. Arif and Z. Wang, “Networked microgrids for service restoration in resilient distribution systems,” IET Gener. Transm. Distrib., vol. 11, no. 14, pp. 3612–3619, 2017.

[14] D. G. Photovoltaics and E. Storage, “IEEE Guide for Design, Operation, and Integration of Distributed Resource Island Systems with Electric Power Systems,” 2011.

[15] A. Mohsenzadeh, C. Pang, and M.-R. Haghifam, “Determining optimal forming of flexible microgrids in the presence of demand response in smart distribution systems,” IEEE Syst. J., vol. 12, no. 4, pp. 3315–3323, 2017.

[16] M. Zadsar, M. R. Haghifam, and S. M. Miri Larimi, “Approach for self-healing resilient operation of active distribution network with microgrid,” IET Gener. Transm. Distrib., vol. 11, no. 18, pp. 4633–4643, 2017.

[17] Z. Wang and J. Wang, “Self-healing resilient distribution systems based on sectionalization into microgrids,” IEEE Trans. Power Syst., vol. 30, no. 6, pp. 3139–3149, 2015.

[18] C. Chen, J. Wang, F. Qiu, and D. Zhao, “Resilient distribution system by microgrids formation after natural disasters,” IEEE Trans. Smart Grid, vol. 7, no. 2, pp. 958–966, 2015.

[19] K. S. A. Sedzro, X. Shi, A. J. Lamadrid, and L. F. Zuluaga, “A heuristic approach to the post-disturbance and stochastic pre-disturbance microgrid formation problem,” IEEE Trans. Smart Grid, vol. 10, no. 5, pp. 5574–5586, 2018.

[20] J. Zhao, F. Li, S. Mukherjee, and C. Sticht, “Deep reinforcement learning-based model-free on-line dynamic multi-microgrid formation to enhance resilience,” IEEE Trans. Smart Grid, vol. 13, no. 4, pp. 2557–2567, 2022.

[21] Q. Huang, R. Huang, W. Hao, J. Tan, R. Fan, and Z. Huang, “Adaptive power system emergency control using deep reinforcement learning,” IEEE Trans. Smart Grid, vol. 11, no. 2, pp. 1171–1182, 2020.

[22] T. Qian, C. Shao, X. Wang, and M. Shahidehpour, “Deep reinforcement learning for EV charging navigation by coordinating smart grid and intelligent transportation system,” IEEE Trans. Smart Grid, vol. 11, no. 2, pp. 1714–1723, 2020.

[23] B. Wang, Y. Li, W. Ming, and S. Wang, “Deep reinforcement learning method for demand response management of interruptible load,” IEEE Trans. Smart Grid, vol. 11, no. 4, pp. 3146–3155, 2020.

[24] Q. Zhang, K. Dehghanpour, Z. Wang, and Q. Huang, “A learning-based power management method for networked microgrids under incomplete information,” IEEE Trans. Smart Grid, vol. 11, no. 2, pp. 1193–1204, 2020.

[25] M. M. Hosseini and M. Parvania, “Resilient operation of distribution grids using deep reinforcement learning,” IEEE Trans. Ind. Inform., vol. 18, no. 3, pp. 2100–2109, 2022.

[26] Z. Li, W. Wu, X. Tai, and B. Zhang, “Optimization model-based reliability assessment for distribution networks considering detailed placement of circuit breakers and switches,” IEEE Trans. Power Syst., vol. 35, no. 5, pp. 3991–4004, 2020.

[27] H. Falaghi, M.-R. Haghifam, and C. Singh, “Ant colony optimization-based method for placement of sectionalizing switches in distribution networks using a fuzzy multiobjective approach,” IEEE Trans. Power Deliv., vol. 24, no. 1, pp. 268–276, 2008.

[28] A. Moradi and M. Fotuhi-Firuzabad, “Optimal switch placement in distribution systems using trinary particle swarm optimization algorithm,” IEEE Trans. Power Deliv., vol. 23, no. 1, pp. 271–279, 2007.

[29] A. Shahbazian, A. Fereidunian, and S. D. Manshadi, “Optimal switch placement in distribution systems: A high-accuracy MILP formulation,” IEEE Trans. Smart Grid, vol. 11, no. 6, pp. 5009–5018, 2020.

2 Microgrid Formation Techniques in Active Distribution Networks: A Review

2.1 Abstract

[1] Microgrid formation is a promising solution to enhance resiliency of distribution networks. The self-adequacy feature of a microgrid enables continuity of power supply through distributed generation (DG) units during severe faults and natural disasters. In this paper, different methods commonly used to partition a distribution network into multiple microgrids are presented, including the graph theory, heuristic rule-based algorithm, cluster-based technique, and mixed integer programming. Advantages and disadvantages of these techniques and future research directions are presented. This review provides an excellent summary on service restoration through microgrid formation, and offers a valuable reference for researchers working on grid modernization of distribution networks.

Keywords. Distribution networks, microgrid formation, resiliency, reliability, service restoration.

[1]Mosayeb Afshari Igder1, Xiaodong Liang 1, and Massimo Mitolo, "Microgrid Formation Techniques in Active Distribution Networks: A Review" (River Publishers) on Oct. 19, 2022, pp. 253-285. IEEE Access, vol. 10, pp. 46618 – 46632, 2022.

2.2 Introduction

The resiliency improvement of power systems against extreme events is an essential aspect of the system design and operation [1], [2]. Extreme events can be either natural disasters or cyber-attacks, which not only affect the continuity of electrical service for a considerable number of consumers, but may also cause significant financial losses. For example, more than 50,000 electricity customers were knocked out of service due to weather disasters in the United States [1], and over $1 billion financial losses were caused by eight weather disasters (i.e., flooding, storms, and hurricanes) during the first half of 2016. In August 2017, the hurricane Harvey caused a total of $180 billion losses, and many towns were left without power for several weeks [3]. Other extreme weather events are shown in Table 2.1, which have caused catastrophic damages to power systems, resulting in massive power outages [1], [4]–[6]. These blackouts within bulk power networks across the globe indicate vulnerability of power systems, and their resiliency improvement is a fundamental task for power system operators.

Table 2.1. Major blackouts across the globe.

Country	Date	Reference
Australia	2016	[40]
Ukraine	2015	[41]
India	2012	[42]
US	2012	[1]
China	2008	[43]

Resiliency is defined as the power grid's capability to with- stand and recover quickly from severe incidents, react properly to changing conditions, and prevent future events [2]. Figure 2.1 illustrates the performance of a resilient system and a conventional system under extreme events [4].

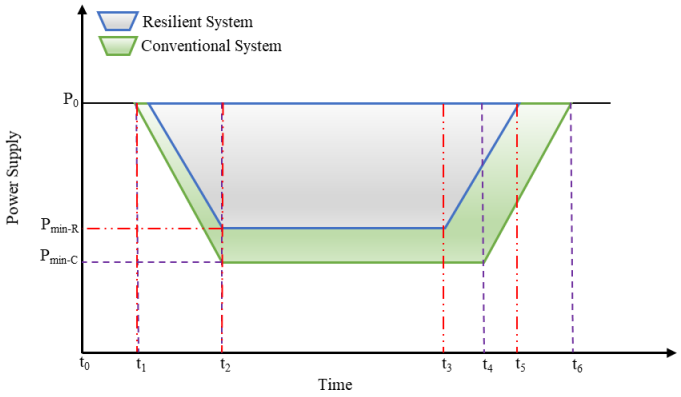

Figure 2.1. A resilience performance curve [4].

The power supply of the system is P_0 at time t_1 when a severe incidence happens. At time t_2, the power supply of the system quickly decreases to its minimum amount (P_{min-R} for a resilient system and P_{min-C} for a conventional system). The restoration is started for resilient and conventional systems at time t_3 and t_4, respectively. The normal power supply P_0 is resumed for resilient and conventional systems at time t_5 and t_6, respectively. Therefore, a resilient system equipped with resiliency-boosted strategies shows better performance in terms of load restoration.

The system's resiliency and resilience-based models have been recently investigated in [5]–[7]. In [8], a theoretical tutorial system is proposed to train distribution system opera- tors to effectively respond to emergencies. The study in [9] proposes a cooperative agents-based system for service restoration through artificial intelligence methods. In [10], a framework using a fuzzy logic is developed to manage out- ages. In [11], weather data are used to examine the probability of blackouts. The duration and frequency of occurrences have also been projected by selecting appropriate disaster response approaches.

Based on our literature review, techniques and strategies to improve the resiliency of distribution networks from both planning and operation point of view are provided in Figure 2.2 (a). An effective planning must be conducted prior to undesirable incidents to prepare for and lessen the impact of upcoming disasters. The disaster-specific planning may include hardening schemes [12], resource allocation [13], [14], prediction [15], repair crews [16], and switch design [17], [18]. Hardening of distribution networks refers to making the infrastructure sturdier and consequently more durable to failure, so that serious damages due to natural disasters can be minimized, and the restoration time can be reduced accordingly [12]. The system recovery capability can be improved by availability of spare and reliable resources, and their pre- event allocation [14]. Prediction models are used to forecast power outages, possible damages and restoration time; utilities can use these models to plan corrective actions prior to incidences [15]. Repair crews play a prominent role in recovering power systems after extreme events, proper management and optimal number of repair crews can improve the system resiliency [16].

After a power outage occurs, the imperative mission for system operators is to restore distribution networks as fast as possible to support critical loads and minimize financial losses to customers. Load restoration can be generally divided into conventional techniques [19], [20], automation [21], [22], and microgrid formation [23]–[25].

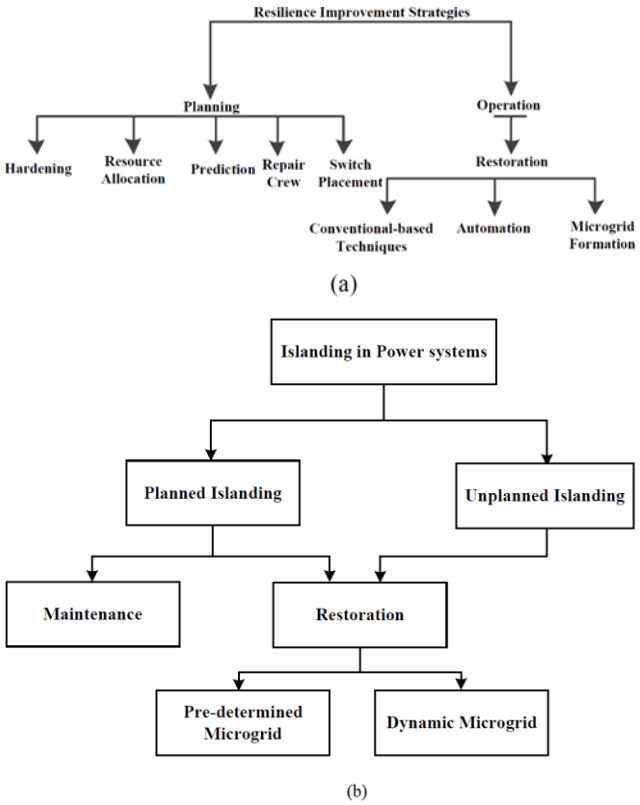

Figure 2.2. (a) Resiliency improvement strategies in power distribution networks, (b) Islanding in power system.

In conventional technique, the load from the off-outage area is transferred to the adjacent feeder through tie-lines and tie-switches [19]. Automation in distribution networks realized through sensors, communication networks, and remotely controlled switches can help distribution network operators to detect and separate faulty areas and recover unsupplied load by opening or closing remotely controlled switches after severe events [21].

Optimal implementation of switches in distribution networks aim to enhance service restoration process by designing an efficient sequence of switching operations [17]. The study of optimal placement of sectionalizer in radial distribution networks is conducted in [18], and an algorithm based on tree structure and dynamic programming is proposed to find sectionalizing switch locations while minimizing the cost of outages and improving reliability of the system. Ref [17] studies upgrading manual switches to remotely controlled switches to improve service restoration in distribution networks, where a greedy rule-based algorithm is used to maximize load restoration and minimize the investment cost.

However, during natural disasters, the distribution network may lose its connection with the main grid, and is not able to supply loads. In this case, traditional restoration techniques may not work properly. To address this issue, microgrid formation/islanding can be a promising solution because loads can be fed through local distributed generators within microgrids [23].

Figure 2.2 shows different types of islanding in power systems, which can be categorized into two groups [26]: planned islanding and unplanned islanding. Planned islanding, also known as intentional islanding, is initiated by power system operators or supervisory control and data acquisition (SCADA) systems; while unplanned islanding usually occurs due to faults in the system [27]. Sudden unplanned islanding should be detected quickly, it may trigger all control operations to maintain power generation and delivery despite islanding separation [26].

Both planned and unplanned islanding operations could be used in service restoration for distribution networks during severe events to supply load in their original or extended boundary. Based on their boundary [28]: microgrids can be divided into pre-determined microgrids and dynamic microgrids. A pre-determined microgrid has a fixed boundary, which is determined based on the supply adequacy, maximum distribution coverage, and reliability indices [29]–[32]. In [29], a systematic approach is proposed to sectionalize a distribution network into several virtual microgrids with optimized self-adequacy. An optimum design of microgrids in distribution networks based on reliability index, and active power and reactive power balance for the supply-security purpose is proposed in [30], [31]. In [32], the maximum coverage criterion, and optimized communication and control infrastructure are used to partition a distribution network into several microgrids.

A dynamic microgrid has boundaries that can be expanded or shrunk, while still maintains a balance between power generation and load demand. To avoid imbalance between local distributed generation (DG) units and loads, or to maximize the load pick-up during extreme events are main reasons that microgrids have dynamic boundaries. In [33], microgrid formation with flexible boundaries is proposed to improve reliability and resiliency of distribution networks.

To solve optimization problems associated with microgrid formation, the genetic algorithm and mixed integer linear programming can be used. In [34], smart switches are used as automatic sectionalizers to determine flexible boundaries of microgrids during natural disasters. In [35], adaptive self-adequate microgrids using dynamic boundaries is proposed, where clusters of nodes based on self-adequacy measures are built first, each cluster is then assigned with an agent with

the capability of supervisory control of all power generation sources within the cluster, communication with customers' smart meters within the cluster, and communication with neighbors' agents. Afterward, desirable adaptive microgrids can be formed by merging a group of clusters. Ref [2] proposes the formation of adaptive microgrids using graph theory and load switching sequence. Microgrid formation based on time and location of faults using mixed integer programming is presented in [36].

Planned microgrid formation/islanding can be used to supply load for expected conditions, such as maintenance in upstream grids [27]. Microgrids in island mode can provide electricity to remote communities, where the expansion of power systems is not economical [37]. Islanded microgrids can also improve energy security for critical load demands of industrials and militaries [38], reduce power losses, and improve voltage profile, power quality, and reliability [39].

In this paper, a comprehensive literature review is conducted on service restoration through microgrid formation techniques in distribution networks. The main contribution of the paper includes:

1. Various microgrid formation methods and their advantages and disadvantages are discussed.
2. Control and economic prospects of microgrids are summarized.
3. Future research directions are recommended.

The paper is arranged as follows: microgrid construction models and microgrid control are provided in Sections 2.3 and 2.4. Section 2.5 introduces microgrid economic prospect. Section 2.6 discusses advantages and disadvantages of microgrid formation algorithms and future research directions. The conclusion is drawn in Section 2.7.

2.3 Microgrid Construction Models

The most challenging aspect of the distribution network's partitioning is to form an optimal microgrid while maintain operational constraints, such as power balance and voltage limits at each node [44], [45]. Existing microgrid formation strategies can be broadly categorized into four techniques as shown in Figure 2.3 [12]: heuristic rule-based strategy [46], mixed integer linear programming (MILP) [14], [47], graph theory [48], and cluster-based models [49]. The cluster-based models can be categorized into 1) spectral clustering, 2) hierarchical algorithms, and 3) K-Means approach.

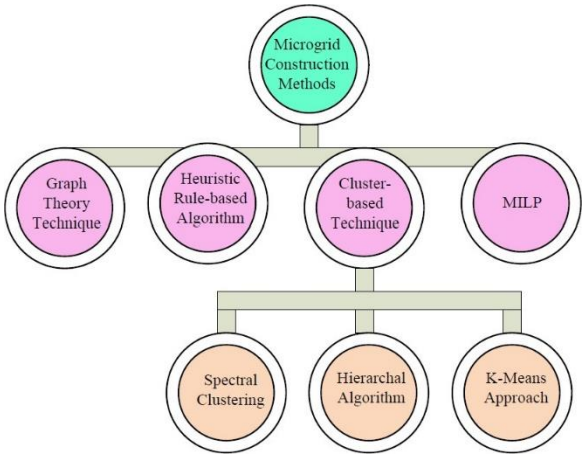

Figure 2.3. The summary of microgrid formation techniques.

2.3.1 Graph Theory-based Technique

Graph theory employs mathematical formulations to specify pairwise relations between objects. Each graph is composed of vertices and edges, which are also known as nodes and links, respectively. In power distribution networks, the graph-based concepts, such as graph partitioning, spanning tree, and spanning forest, are used to form microgrids in two different topologies: 1) loop-based microgrid topology, and 2) radial-based microgrid topology. In [2], both radial and loop-based microgrid topologies are considered as part of the load restoration strategy. The linearized DisFlow model is employed to consider power flow and voltage characteristics in each constructed microgrid. In [50], spanning tree and spanning forest concepts are applied to form post-disturbance radial-based microgrids energized by DGs. The LinDistFlow model is also used to satisfy operational constraints. In [51], the graph partitioning technique and linear integer programming are proposed to form an optimal loop-based microgrid to improve system reliability. In the following subsections, radial- and loop-based models are discussed.

2.3.1.1 Loop-based Model

The graph partitioning concept, which is employed to determine potential loops based on existing DG units, sectionalizes a graph G with the vertex set V and the edge set E into the Q subset ($V_{1,.,.,.}V_{i,...}, V_Q$), so that $Vi \subset V$, $Vi \cap Vj = \varnothing$ for $i \neq j$. In distribution systems, energized buses and distribution lines are defined as the vertex set and the edge set of the graph, respectively. Objective functions may include the maximization of load pick-up,

minimization of switching operations, generation-load balancing, minimization of neighboring loops interactions, and combinations of the above. The graph partitioning is composed of three stages, 1) coarsening, 2) partitioning, and 3) uncoarsening [52].

A. Stage1: Coarsening

The coarsening stage iteratively simplifies the distribution network graph until it can no longer be partitioned. The Shortest Edge Machine (SEM) is widely employed in this process. An initial node is firstly selected randomly and matched with the nearest adjacent node. Afterward, the nodes are combined into a single node and the process is repeated until all possible matches in the graph have been achieved. This process will end when the number of nodes reaches an established percentage of the original number. The graphs shown in Figure 2.4 and Figure 2.5 demonstrate the coarsening process using the IEEE 37-bus distribution network. Figure 2.4 (a) indicates the coarsening first iteration, where each red line indicates that the two nodes should be merged according to the SEM strategy. The outcome of the first iteration is shown in Figure 2.4 (b), in which the number of nodes is decreased from 37 to 23. The second iteration of coarsening is illustrated in Figure 2.5 (a), and its outcome is shown in Figure 2.5 (b). The coarsening process will end in the second iteration because the number of nodes is decreased to 16, which meets the termination criterion (obtaining less than 50% of the original number of nodes of the graph) [52].

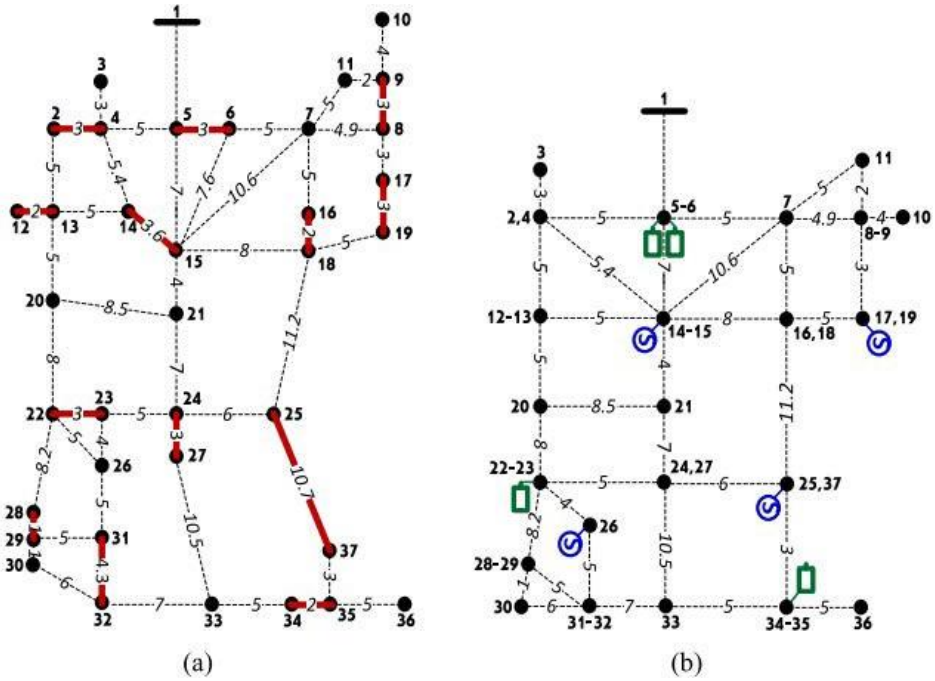

Figure 2.4. The coarsening first iteration in the graph partitioning technique [52].

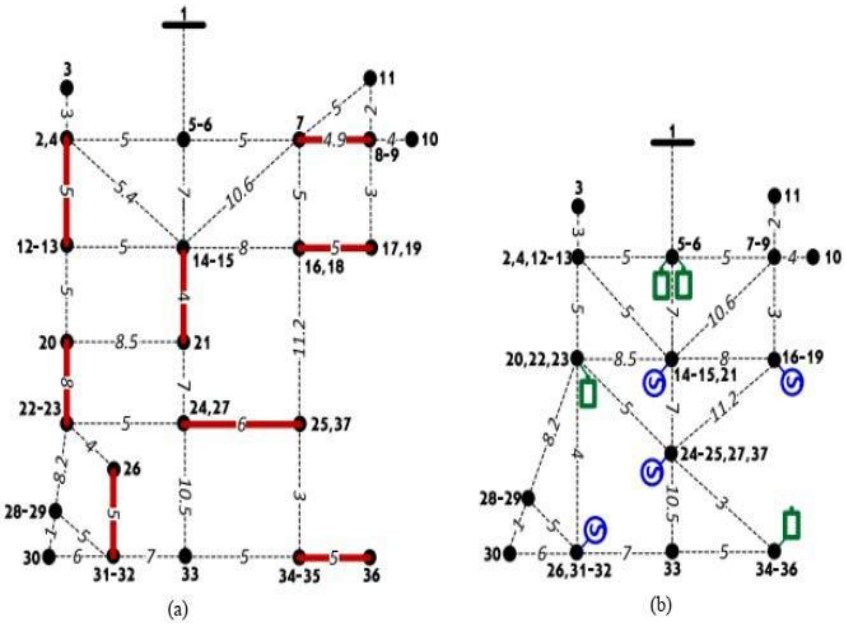

Figure 2.5. The coarsening second iteration in the graph partitioning technique [52].

B. Stage2: Partitioning

In partitioning stage, the graph obtained in the last iteration of coarsening process is partitioned into Q parts. The heuristic approaches, such as Kernighan-Lin (KL) and Greedy Graph Growing Partitioning (GGGP) algorithms, are used in [52]. With the GGGP algorithms, the solution is found by selecting the initial vertex and expanding it to comprise a large part of the graph. Since the main goal of service restoration is to form microgrids with self-healing capabilities, the potential cluster is expanded around controllable DGs. Power mismatches and the distance between nodes are employed to ensure that growing loops satisfy power balancing and the nearest nodes are used [52]. The partitioning stops when all nodes are covered by the loops. This process is shown in Figure 2.6, which includes three iterations, and the ultimate outcome is shown in Figure 2.6 (c). Since four controllable DG sources are present, four potential microgrids are formed, and four points evolve autonomously from those sources in Figure 2.6 (a). The process terminates once all nodes are covered by one of the loops in Figure 2.6 (c).

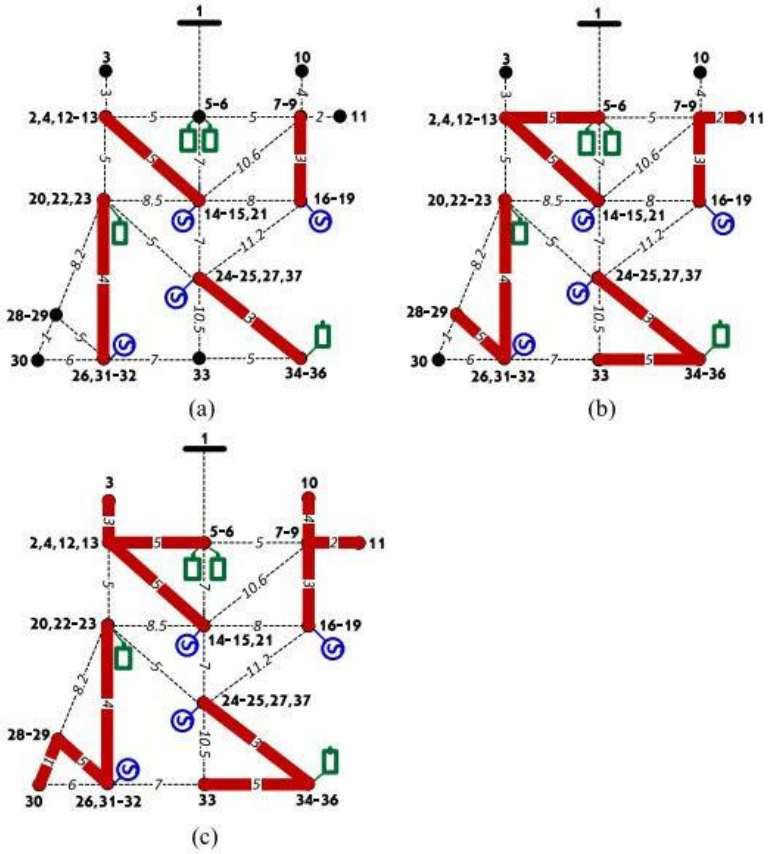

Figure 2.6. The partitioning stage in the graph partitioning technique [52].

C. Stage 3: Uncoarsening

In uncoarsening stage, the partitions obtained in previous stage should be reversed into the original graph based on the sequence of coarsening process. Refinement strategies, such as KL algorithm, should be employed. In this algorithm, the edge weight serves as a criterion to transfer a vertex between neighboring loops. However, it is more logical to consider power balancing criterion in microgrid formation to transfer nodes between adjacent loops. This modification should be implemented for refinement when used in microgrid formation [52].

Figure 2.7 illustrates the uncoarsening process, which also contains two iterations because the graph coarsening is also performed in two iterations. The first and second iterations of uncoarsening are demonstrated in Figure 2.7 (a) and Figure 2.7 (c), respectively; the refinement is shown in Figure 2.7 (b) and Figure 2.7 (d) based on the power mismatch amount in per unit. In the first iteration of the refinement, Node 20 is transferred from the lower left loop to the upper left loop to balance the power.

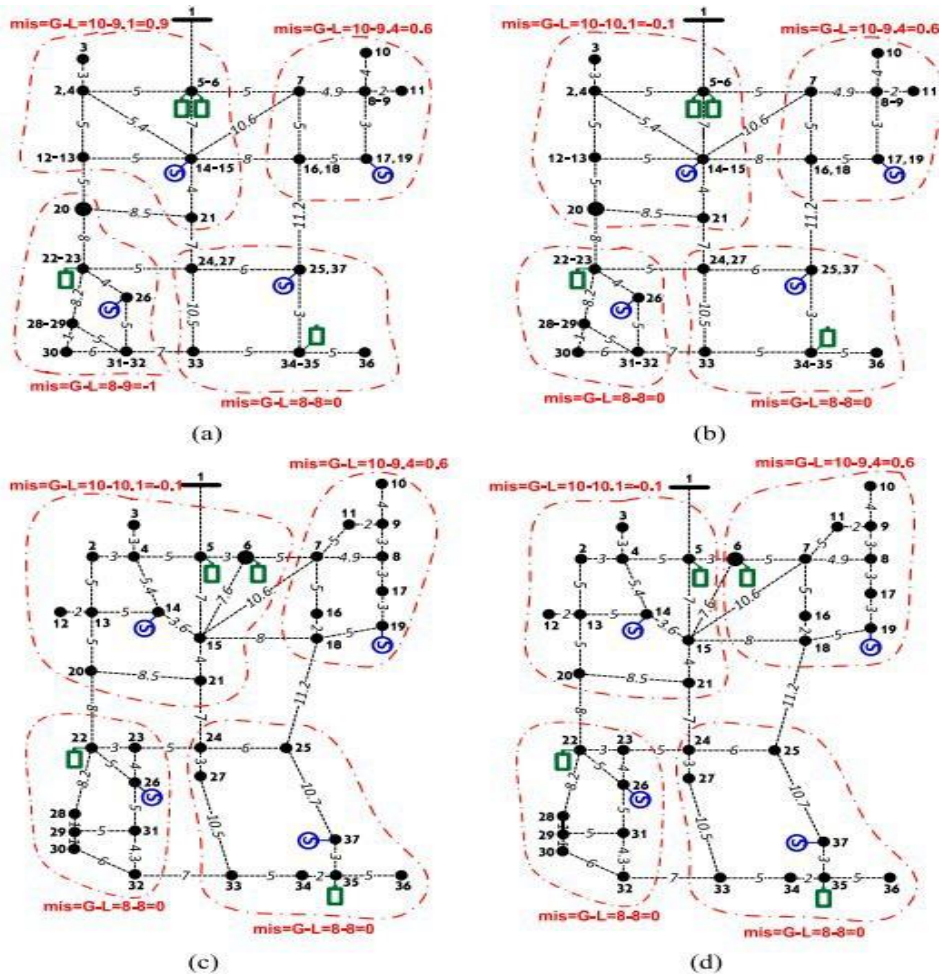

Figure 2.7. Uncoarsening stage in the graph partitioning technique [52].

2.3.1.2 Radial-based Model

The radial topology in distribution networks can be defined as a graph, where all nodes are put together into one energy source node without any loops. Two graph-based concepts, spanning tree and spanning forest, are used to model the radiality constraint in the microgrid formation problem. A spanning tree is a graph connecting all nodes with links without forming any loops. A spanning forest is a graph, whose connected constituents are spanning trees.

Distribution networks may be modelled with graphs consisting of vertexes and edges as shown in Figure 2.8 [53]. There are controllable switches at the edges of this graph, and the source nodes have feeders connected to the main grid, or to DG units. The fundamental loops of a graph defined by vectors, whose values are edges of the constructed loops, should be specified.

In Figure 2.9, there are four loops, C1 to C4, defined by the following vectors:

$V1 = \{10, 11, 12\}$
$V2 = \{1, 2, 3, 4, 5, 6, 8, 9, 10, 11\}$
$V3 = \{1, 2, 3, 13, 14, 16, 17, 18\}$
$V4 = \{15, 16, 17, 18\}$.

These fundamental loops can be categorized as real loops (C2 and C3) and virtual loops (C1 and C4). The virtual loops are those with DG units and the frequency control capability. The frequency control is one fundamental requirement for power systems operation. In island mode, microgrids must be able to realize voltage and frequency control through their controllers. DGs are usually connected to power systems with interfacing power electronics converters, which enables advanced controllers to be designed to realize frequency control [54]. Frequency control has been widely studied for DGs in microgrids [55], [56]. In [55], a dual-stage fractional order proportional integral derivative (PID) controller is used to improve the frequency control of microgrids when operating in island mode, and the imperialist competitive algorithm is implemented to optimize the PID gains. The Fuzzy tilt integral derivative using a filter and the double integral control are employed for frequency control of DGs in [56], and coefficients of the controller are optimized through the Whale optimization algorithm.

Following the designation of fundamental loops, spanning tree and spanning forest algorithms are employed to determine microgrid formation, taking into account the radiality constraint and the load supply. The spanning tree in a graph is not used with all nodes connected, thus some edges should be eliminated. A spanning forest, which is a graph with several trees, is used to model a distribution network [50]. To create a spanning forest and ensure the radiality of the network, it is sufficient to open only one switch in each loop that is not shared with any adjacent loop. In addition, if the switch is selected from virtual loops, a microgrid energized by DGs is formed. For instance, if switches 10 and 17 are opened, two microgrids (MG1 and MG2) are formed (Figure 2.9). Accordingly, by considering the switch status as a decision variable in the optimization problem, optimal microgrids are formed in load restoration process.

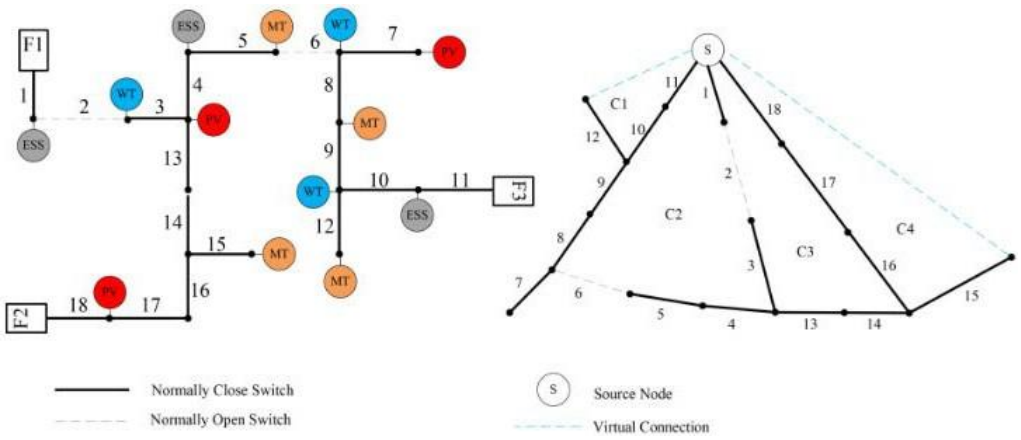

Figure 2.8. The distribution network graph in a normal mode [53].

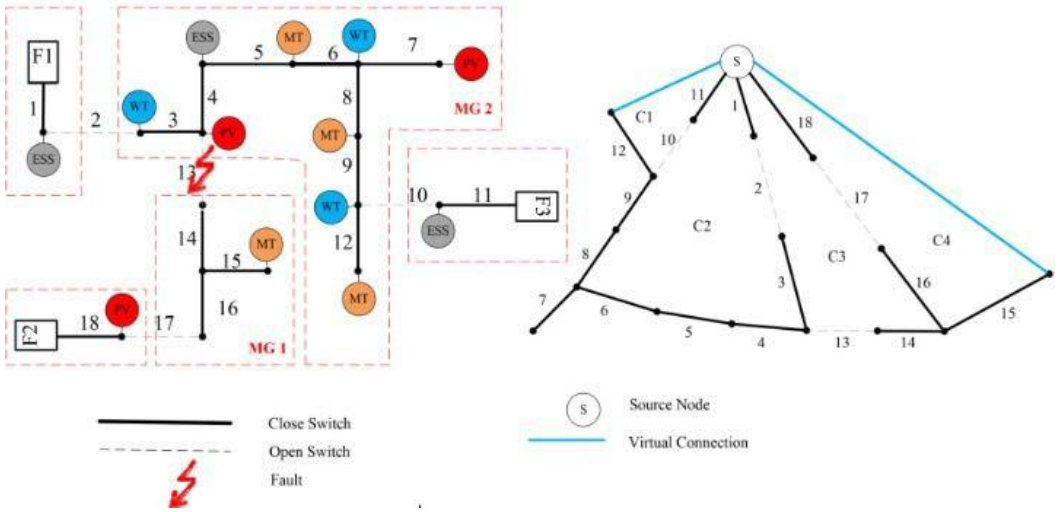

Figure 2.9. The distribution network graph in a self-healing mode [53].

2.3.2 Heuristic Rule-based Algorithm

Heuristic rule-based algorithms employ heuristics or rules to find solutions. The goal of this method is to solve the problem within an acceptable time frame. The solution may not be the best, but it is near the optimal one. As this algorithm is computationally efficient, it can be used in the optimization problem with many decision variables. The microgrid formation problem based on the heuristic rule-based algorithm utilizes rules to achieve solutions.

In [46], a post-disturbance microgrid construction solution is proposed for medium to large distribution networks using the heuristic algorithm in three steps. In the first step, DG units are placed optimally without considering microgrid formation constraints. Load dispatch, nodal

balance, line flow, generation placement, and voltage constraints are considered in the optimization problem with the objective of maximizing the load pick-up. Locations of DGs are provided in the first step. In the second step, the non-isolated nodes are clustered into microgrids using k-means method and DG nodes are considered as centroids. The network configuration for the constructed microgrids must meet the total load demand. In the third step, the dispatch assessment is implemented, where the capacity of the constructed microgrids is evaluated based on power system operation constraints. Figure 2.10 illustrates the heuristic method process in microgrid formation.

In [57], [58], a decentralized multiagent system (MAS) strategy and the heuristic rule-based algorithm are employed to form microgrids using load priority and switching operations as objective functions. The following ten steps are proposed, and the controlled DG unit is used as the power source for critical load restoration [58]:

- Step 1: *entire nodes* = a set of all nodes, which is demanded by the DG agent for restoration.
- Step 2: *node to restore* = a set of the nodes to be restored is selected by calculating the objective function (i.e., load priority order) and following the branch
  current limits, voltage limits, and consumed power constraints.
- Step 3: *min priority load* = the least priority node in the node to restore set.
- Step 4: *lower priority nodes* = a set of nodes in the entire nodes with a priority less than *min priority node*.
- Step 5: new loads to restore are initialized as a set of the nodes from nodes to restore by removing the min priority node.
- Step 6: the new load to restore is chosen from *lower priority nodes*, based on the load priority objective and operational constraints.
- Step 7: *max priority node* = the highest priority node chosen from the new nodes to restore set.
- Step 8: *priority factor* = the priority order of *min priority node* divided by the priority order of *max priority node*.
- Step 9: Compute the number of switching operations for *nodes to restore* and *new nodes to restore* as X and Y , respectively.

Step 10: If *Y* smaller than *X* multiplied by *priority factor*, then *nodes to restore* is *new nodes to restore* and go to Step 4. Else, *lower priority nodes = lower priority nodes – max priority nodes*. If *lower priority nodes* is an empty set, the algorithm ends, else go to Step 6.

Figure 2.11 shows the islanding of the 119-bus test system using the above-mentioned heuristic rule-based algorithm. In out of service areas, each dispatchable DG unit with the assistance of other types of renewable-based DGs build an individual microgrid to restore critical loads with an optimum number of switching operations.

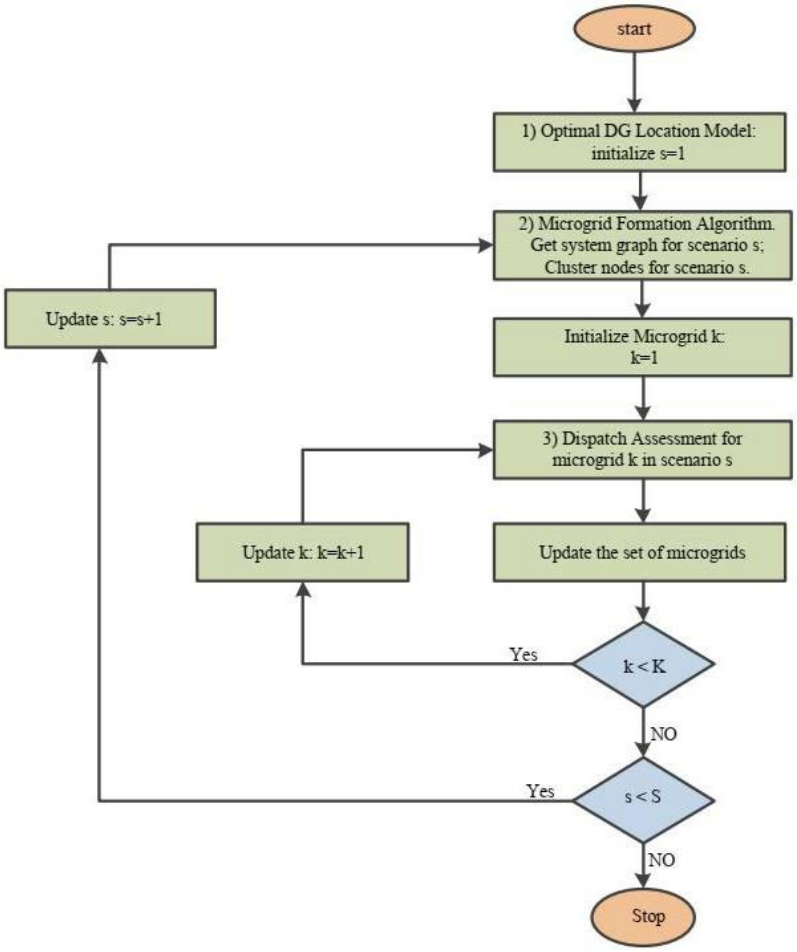

Figure 2.10. The flowchart of microgrid construction using the heuristic method [46].

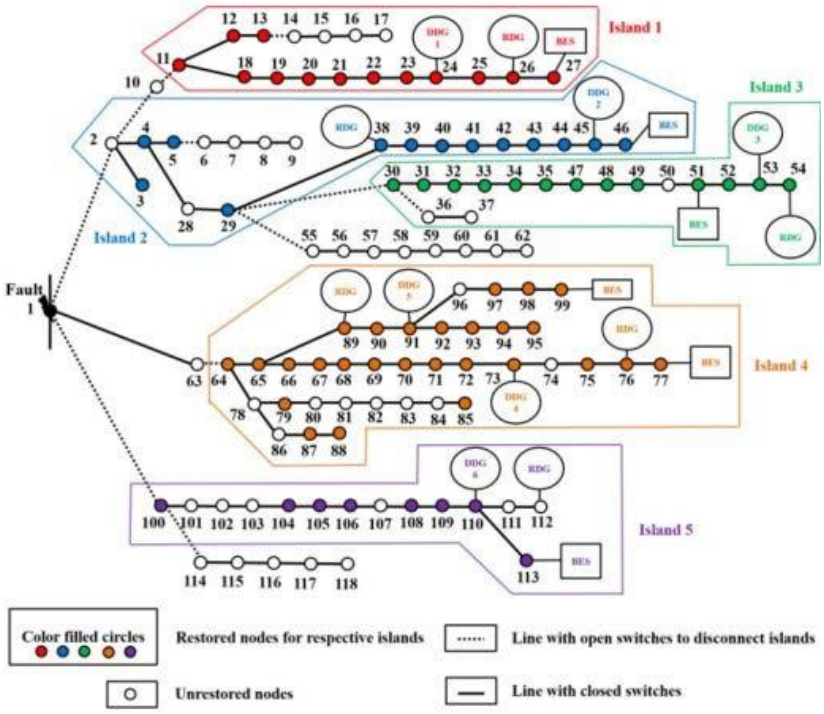

Figure 2.11. Microgrid formation of the 119-bust test system [57].

2.3.3 Clustering Algorithm

The clustering analysis splits a set of objects into uniform groups based on similarity measures, so the similarity of objects in one constructed group is greater than that in another group. Three clustering algorithms including spectral clustering [59], hierarchical algorithm [60], and k-means method [61] are widely used in distribution network partitioning.

2.3.3.1 Spectral Clustering

Spectral clustering is a type of graph partitioning that uses the affinity between two components within the dataset, which is the computational coupling between two nodes in power systems [59]. Since this method clusters buses by using the affinity matrix, buses with a greater affinity become a cluster. It is required that the affinity matrix must be obtained with high accuracy. The affinity between any two nodes is determined by the Hessian matrix related to AC optimal power flow. The Hessian matrix is the second derivative of the Lagrange function, and a larger amount of entry in this matrix indicates a stronger coupling.

To calculate the Hessian matrix, AC optimal power flow must be performed. After computing the Hessian matrix, the spectral clustering method is used to group buses with greater affinity together. The process of partitioning a distribution network with B buses into N clusters using spectral clustering is given by [59] as follows:

- Determine the components of the affinity matrix based on $A_{i,j} = (1 - w)\sum_{k=1}^{m}\sum_{l=1}^{n}|H_{k.l}| + w * Y_{i,j}$if $i \neq j$ and set $A_{ii}=0$.
- Form the diagonal matrix D based on $D_{i,i} = \sum_{n=1}^{B} A_{i,n}$ and build the matrix $P = D^{-1/2}AD^{-1/2}$.
- Specify the *N* largest eigenvalues associated with the matrix *P* and construct the matrix *V* by stacking the eigenvectors in columns. To have unit length, normalize the *V*'s rows.
- Consider each row of *V* as a data point and group these data points into *N* partitions using an algorithm, such as k-means or hierarchical.
- Give bus *i* to cluster *A* if row *i* of *V* was given to cluster *A*.

$Y_{i,j}$ is the component of the admittance matrix, and *w* is the affinity weight.

In [62], an adaptive spectral splitting technique is proposed. The primary splitting of the distribution network is achieved through the spectral clustering strategy first. When the primary partitioning is obtained, the boundary nodes/buses transfer from the present location to the neighboring partition in every iteration to acquire the corresponding power balance ratio of each partition, which is defined as a ratio of the total power demand to the total generation capacity, while maintaining power balance constraints.

2.3.3.2 Hierarchical Algorithm

In hierarchical clustering, nodes are grouped into hierarchical structures based on power system specifications of the line including average power flow or line impedance (admittance), and the obtained results are known as tree or dendrogram. A dendrogram's root point corresponds to the entire set of nodes, whereas each leaf represents a separate node. To what degree the nodes are similar to each other is shown by intermediate points. The distance between clusters or objects can be determined by the dendrogram height. Dendrograms can be cut at various levels to gain the final clustering results [63]. Figure 2.12 depicts the dendrogram related to IEEE 39-bus test system in which at the height level one, the blue, green, yellow and red clusters are formed; cutting

dendrogram at the height level three will result in combining the green and red clusters and forming three islands.

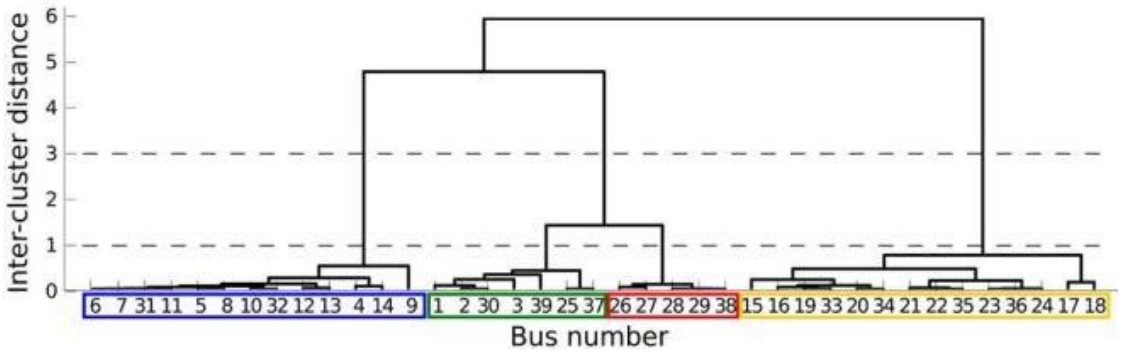

Figure 2.12. Hierarchical algorithm, the dendrogram of IEEE 39-bus test system [49].

2.3.3.3 K-means Method

The K-means algorithm falls into centroid or distance-based algorithms, and the distances are computed to assign an object to a cluster with its own centroid point [61]. The purpose of K-means method is to partition the network with n nodes into k clusters and to ensure that the distances are minimal within each cluster. This strategy begins by selecting k nodes randomly as initial centroid points within the networks. The remaining nodes are assigned to the closest among them. After that, the centroids are repositioned from each cluster to ensure that there is a minimum distance between the centroid and any other node within the cluster. Afterward, the distance between each node and k points is calculated, and the node is assigned to a cluster with the nearest centroid.

In this method, k centroid points are moved in succession until they reach a minimal threshold, and a stable cluster is obtained. In the distribution network's partitioning, nodes with controllable DGs are regarded as centroid points, and the electrical distance is utilized for distance metric. The process of the K-means algorithm is illustrated in Figure 2.13.

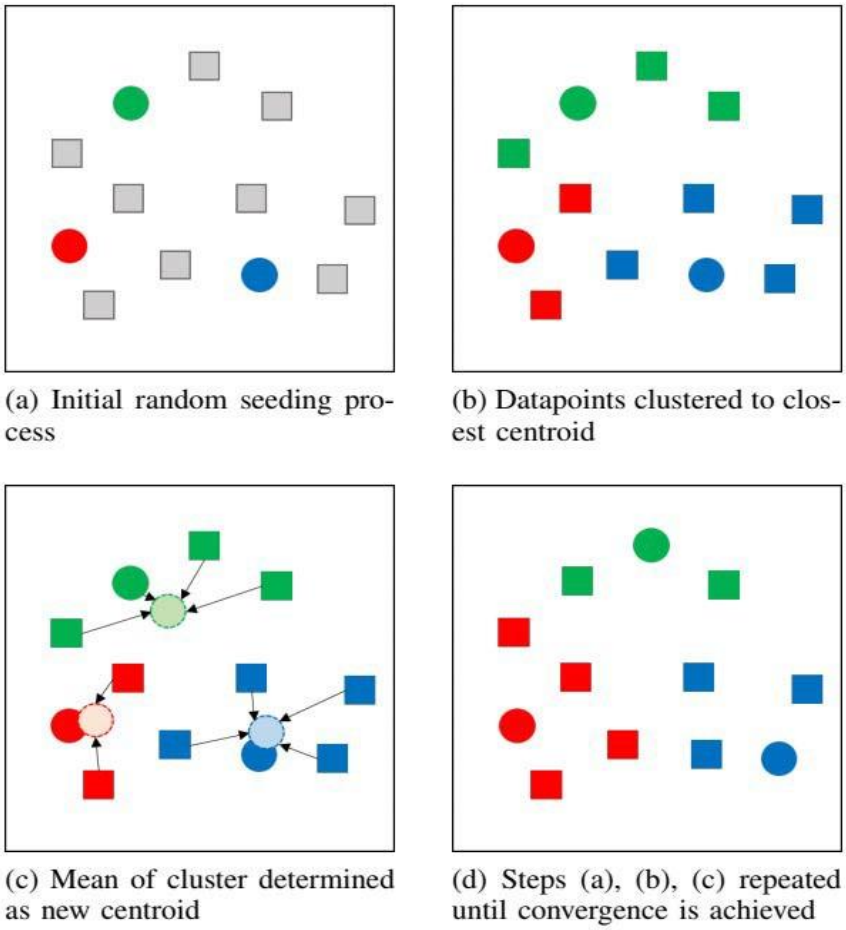

Figure 2.13. The K-means algorithm [64].

2.3.4 Mixed Integer Linear Programming

Mixed integer linear programming (MILP) is a mathematical optimization problem with integer decision variables, linear objective functions and constraints. This approach is broadly used in load restoration and microgrid formation [23], [33], [65]. Ref. [21] develops a MILP to form a microgrid energized by DGs through controlling the status of remotely controlled switches after natural disasters, where critical load pick-up is maximized with self-adequacy and operational constraints satisfied.

In [65], a MILP-based method is proposed to form multiple microgrids to restore prioritized load in distribution networks after extreme events. Flexible microgrid formation is investigated in [33], where MILP is used to solve the optimization problem based on utility profits and customer satisfactions. Implementation of MILP-based microgrids requires a large number of

control variables. To address this problem, a MILP with radiality constraints is proposed in [66]. In the MILP- based method, the following constraints must be satisfied when forming a microgrid:

- Splitting constraints.
- Power system physical constraints.
- Subgraph connectivity constraints.

Mathematically, MILP optimization can be handled by branch-and-bound, branch-and-cut, or cutting plane approaches. Currently, several commercial optimizers, such as CPLEX, GUROBI, and MOSEK, are available to provide flexible, parallel-processing and high-performance solvers for MILP.

According to our literature review, a summary on micro- grid formation for service restoration in distribution networks can be found in Table 2.2. Different studies are compared from application, information discovery, construction approach, objective function, and optimization problem aspects.

Table 2.2. Summary of literature review on microgrid formation for service restoration in distribution networks.

Reference Number		[2]	[16]	[23]	[58]	[25]	[51]	[68]	[29]	[30]	[33]	[47]	[50]	[52]	[60]	[61]	[69]	[70]
Application	Pre-determined Microgrid					*			*	*	*		*	*	*	*		*
	Dynamic Microgrid	*	*	*	*		*	*				*					*	
Information Discovery	Distributed MAS Scheme			*	*													
	Centralized Scheme	*																
Construction Approach	Graph Theory (Loop-Based)	*												*				
	Graph Theory (Radial-Based)	*	*				*		*		*						*	
	Heuristic Rule-Based				*						*	*					*	
	Spectral Clustering												*		*	*		
	Hierarchical Algorithm												*			*		
	K-Means Method											*						
	MILP		*	*		*		*		*							*	*
Objective Function	Supply-adequacy								*	*	*			*				
	Load Pickup	*	*	*	*		*	*				*						
	Switching Operation				*		*											
	Running Cost					*									*		*	*
	Power Exchange Between Microgrids								*	*				*				
	Islanding Success Probability										*							
	Subgraph Expansion												*					
Optimization Problem	Stochastic Problem	*			*							*				*		*
	Deterministic Problem		*	*		*	*	*	*	*	*		*	*	*		*	

2.4 Microgrid Control

Renewable energy-based DG units in microgrids use interfacing power electronics converters to connect to the system, and controllers are designed and implemented on these power electronics converters to achieve power, voltage and frequency control of DGs and the microgrid. In grid-connected mode, the voltage and frequency of microgrids are governed by the utility grid, controllers are used for real and reactive power or power factor control. In island mode, the microgrid must be able to control its voltage and frequency through advanced DG controllers. Hierarchical control techniques are extensively utilized for microgrid control and power management [70], [71].

2.4.1 Traditional Hierarchical Control for Microgrid

The traditional hierarchical control framework is illustrated in Figure 2.14, including primary, secondary, and tertiary control. The widely used primary control is droop control to adjust the local voltage and power, prevent system instability, and handle proper power sharing among DGs [70], [71]. The following well-recognized droop control technique is used to reach primary control objectives [71]:

$$\omega_{MG} = \omega^* - m.(P - P^*) \quad (2.1)$$

$$E_{MG} = E^* - n.(Q - Q^*) \quad (2.2)$$

where, frequency and output voltage amplitude are detonated by ω_{MG} and E_{MG}, respectively. ω^* and E^* represents reference frequency and voltage amplitude, respectively. Droop coefficients are represented by *m* and *n*.

The deviation of output voltage and frequency caused by primary control can be eliminated by secondary control [72]. The frequency and voltage restoration controllers are demonstrated in Fig. 14 [71].

$$\delta_\omega = k_{pw}(\omega^*_{MG} - \omega_{MG}) + k_{iw}\int(\omega^*_{MG} - \omega_{MG})dt + \Delta\omega_s \quad (2.3)$$

$$\delta E = k_{pE}(E_{MG}^{*} - E_{MG}) + k_{iE}\int (E_{MG}^{*} - E_{MG})dt \quad (2.4)$$

The frequency and amplitude values, ω_{MG} and E_{MG} inside microgrid are identified and evaluated by references ω_{MG}^{*} and E_{MG}^{*}, the obtained errors through compensators, δ_{ω} and δE, are send to each unit to recover output-voltage frequency and amplitude. The secondary control parameters are represented by k_{pw}, k_{iw}, k_{pE}, and k_{iE}. $\Delta\omega_s$ indicates the synchronization term.

Centralized control [73], [74] and decentralized control [65], [76] are two major techniques used in secondary control. For centralized control, the main drawback is its high reliance on the microgrid control center and the bidirectional communication structure. When the microgrid control center is faulted or the communication system fails, the centralized control no longer works well. Accordingly, the stability of the microgrid is decreased and its cost is increased [77].

Decentralized control, on the other hand, can overcome above issues, errors caused by one DG will not cause a whole system's failure, and it does not rely on communication networks, and can be simply expanded to several DGs, which improves the system's scalability [78].

Tertiary control is employed to identify power flow to achieve optimal operation for economic and service restoration purposes [79]. In Figure 2.14, by calculating *P/Q* via the static bypass switch, P_G and Q_G can be evaluated by the preferred references, P^* and Q^*.

$$\omega_{MG}^{*} = k_{pP}(P_G^{*} - P_G) + K_{iP}\int (P_G^{*} - P_G)dt \quad (2.5)$$

$$E_{MG}^{*} = k_{pQ}(Q_G^{*} - Q_G) + K_{iQ}\int (Q_G^{*} - Q_G)dt \quad (2.6)$$

The tertiary control parameters are represented by k_{pP}, K_{iP}, k_{pQ}, andK_{iQ}.

Power quality adjustment and economic operation can be achieved by the hierarchical control strategy, which enhances the flexibility of microgrids. The microgrid control center is utilized in this strategy to manage DGs and loads, which contributes to reliable operation of multiple microgrids [80].

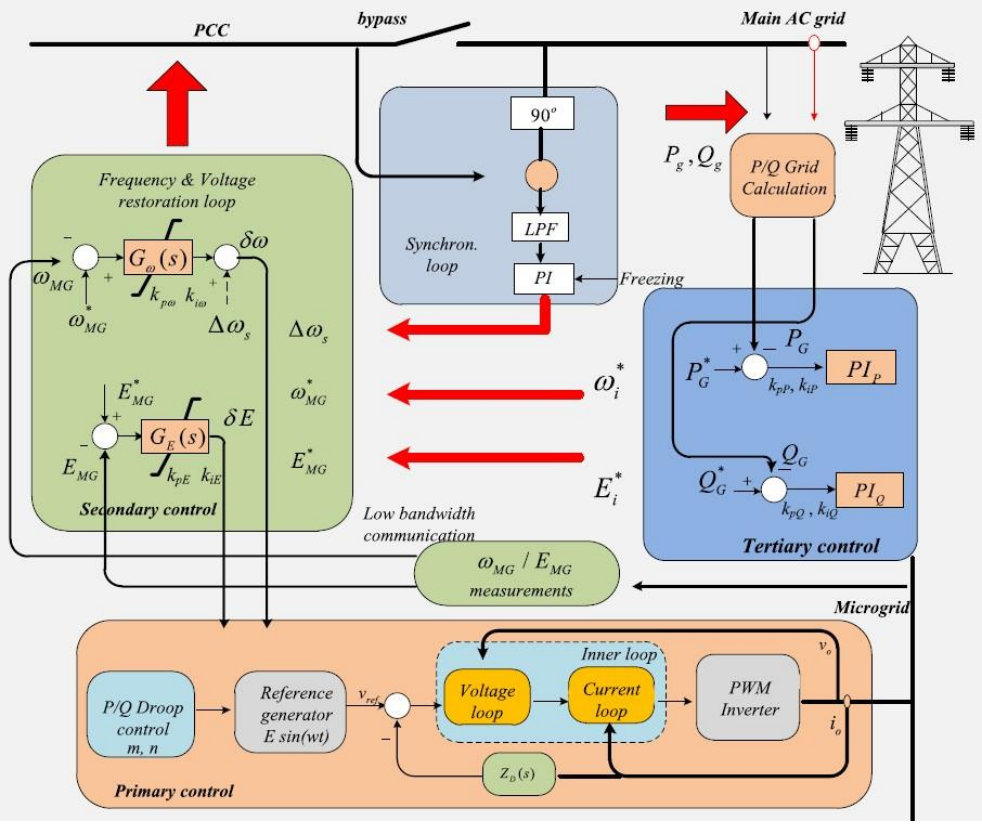

Figure 2.14. Traditional hierarchical control for microgrids [71].

2.4.2 Multiagent System-based Distributed Control

Multiagent control strategy splits a large system into a number of autonomous subsystems, which can communicate with each other [71]. Each agent has intelligent features [81], [82]. Using these intelligent agents, the multiagent system-based distributed control can achieve coordinated operation of the entire system. Figure 2.15 demonstrates the structure of a multi- agent control-based microgrid [71]. Various electrical components, such as wind turbine generation units, loads, gas turbines, and energy storage systems, are assigned to each agent. These agents observe control operations and the status of each electrical component, and the microgrid control center coordinates activities among all agents. Once there is a command from an agent, the microgrid control center notifies and coordinates all agents [83]. Communication and coordination are crucial during the entire decision-making process. Ref [84] uses the contact net protocol in such process.

Each agent generally contains two-level control blocks: the upper-level control block identifies the power supply reference and demand, and measures optimal increment cost; the

lower-level control block applies the power reference tracking of related electrical components [85]. Accordingly, each agent controls local load and power generation, and exchanges information with other agents.

There are many reported multiagent system-based distributed control schemes in the literature [86]–[91]. A multiagent distributed control with a frequency control framework is proposed in [86] by employing consensus method. Power sharing among distributed energy resources in microgrids through a multiagent-based technique is suggested in [87]. Ref [90] can overcome the weakness of droop control by using multiagent distributed control, and realize voltage and frequency control and proportional reactive power sharing among DGs. Ref [91] can regulate frequency, where each local controller shares information with neighboring controllers.

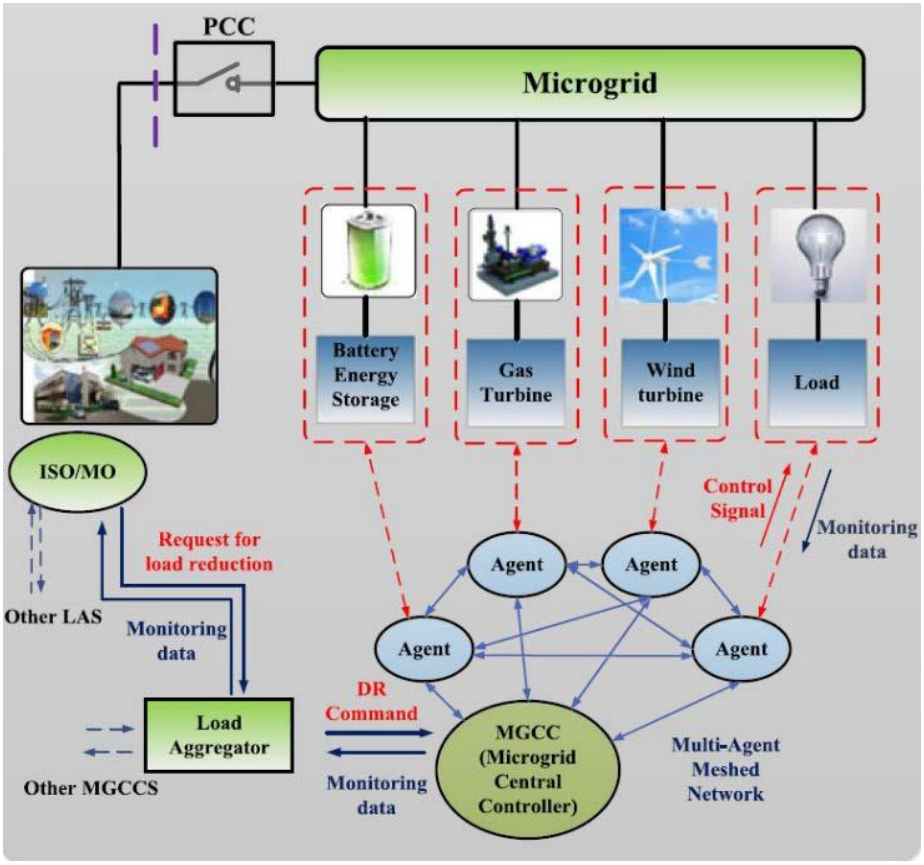

Figure 2.15. The structure of multiagent-based microgrid [71].

2.5 Microgrid Economic

Economic benefits from microgrid formation is an essential feature to address. Microgrids have several economic benefits, such as load leveling and peak shaving [92], power export and net metering [93], loss and emission reduction [94], power quality improvement [95], and resiliency enhancement [96].

DGs and energy storage along with advanced control technologies enables flexible power management within a micro- grid. It can be especially economically influential when the utility's Time-of-Use tariff comprises power and volumetric charges [95]. This type of tariff is usually a powerful motivation to facilitate peak shaving and load leveling as shown in Figure 2.16. In this example, an optimized load profile is achieved by implementing load shifting and peak shaving, which minimizes power demand and volumetric charges.

Exporting electricity to power systems is one main source of income brought by microgrid formation [93]. Net metering and feed-in tariffs are two general methods used to specify surplus power generated by microgrids [95]. Net metering utilizes a bidirectional meter to calculate a customer's net power consumption [95]. If the generation is more than the consumption, the meter turns backward. In the feed-in tariff method, all power producers receive a payment when they inject power into the system [97].

As microgrids are located locally, power generation can be consumed locally, which avoids long distance transmitting electricity, and thus, power losses along the feeders are reduced [98]. Power quality and the system's reliability can be also improved because the decentralized power supply can better match power supply and demand locally, and the influence due to transmission and generation outages can be reduced [99]. Due to increasing penetration of renewable energy-based DGs, microgrids can reduce green- house gas (GHG) emission compared to conventional power generation.

Table 2.3 provides a summary of cost details for various power generation technologies, including their technology cost, operation and maintenance (O & M) cost, capacity factor, fuel cost, efficiency, GHG emission, renewable potential, and the life time [100]. DGs in microgrids are mainly renewable energy sources, which makes microgrid formation economically viable.

In [101], the economic analysis is conducted for a microgrid with PV and battery storage in Northampton, Massachusetts, USA by considering the outage mitigation, emission reduction and resiliency improvement. The system is modeled using the battery storage evaluation tool for a

one-year period, and its efficiency is demonstrated through historical data and randomly generated large outages.

A lifecycle analysis is conducted for a microgrid with wind turbines, PV, diesel generators, and energy storage to evaluate its commercial aspect in [102], and it shows significant reduction in costs of GHG emission and loss, and improvement in reliability indices. An industrial microgrid with PV in China is analyzed from the economic aspect in [103] regarding emission reduction costs, levelized energy costs, and the payback period. This study demonstrates the economic benefit gained by a PV-based microgrid through real microgrid output data. In [104], economic benefits of microgrids are assessed according to reliability improvement, emission reduction, power quality of services, and the lessened peak loading.

Participation in electricity market is considered one benefit behind microgrid formation [105]. In the restructured electricity market, microgrids can participate in both energy and ancillary service markets as autonomous entities. Power generated by microgrids can be traded in electricity markets. The microgrid control center conducts the optimal power management of the electricity market, and aims to satisfy local demand during the system operation through optimal allocation of local energy sources [106]. Microgrids with renewable energy sources and energy storage can also participate in the emission trading market, where the energy price and emission data are sent to the microgrid control center, and the microgrid will be paid based on these data.

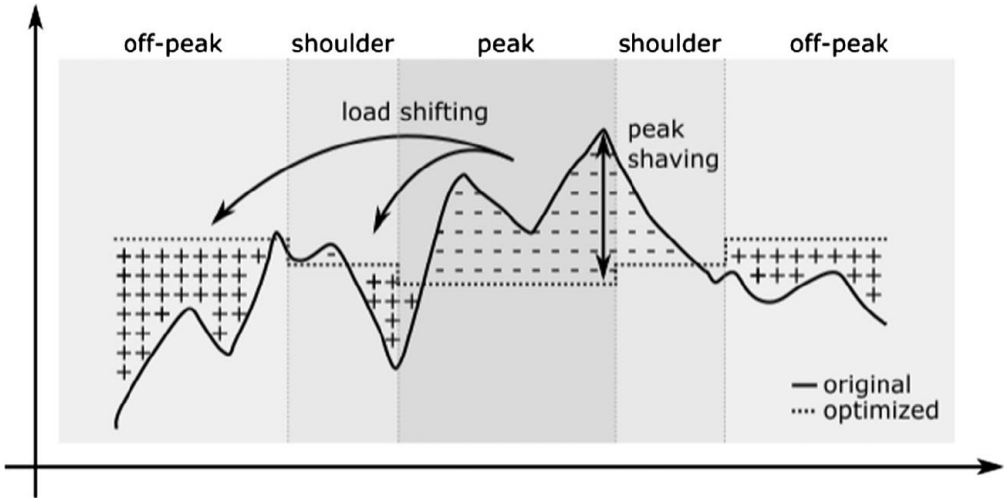

Figure 2.16. Peak shaving and load leveling [95].

Table 2.3. Cost details of various power generation technologies [100].

Generation Technology	Capital Cost ($/MW)	O & M Cost ($/M)	Fuel Cost ($/MWh)	Capacity Factor	Efficiency (%)	GHG Emission (tCO_2/MWh)	Renewable Potential (MW)	Lifetime (years)
Hydro	1260	28	-	0.46	85	-	1400	40
Wind	1620	43	-	0.37	30	-	2400	25
Solar	2160	27	-	0.25	30	-	6487	30
Geothermal	1200	30	-	0.7	20	-	3442	30
Coal Fired	1125	35	6.14	0.75	38	1.08	-	30
Coal IGCC	1315	28	6.14	0.8	43	1.08	-	30
Gas Fired	810	21	30.7	0.85	47	0.5	-	30
Gas IGCC	510	8	30.7	0.8	57	0.5	-	25
Biomass	1900	43	5.86	0.75	35	0	4807	25
Nuclear	2070	45	3.07	0.85	33	-	-	40

2.6 Advantages and Disadvantages of Microgrid Formation Algorithms, and Future Research Direction

2.6.1 Advantages and Disadvantages of Microgrid Formation Algorithms

A fast and effective service restoration strategy is vital to improve resiliency of distribution networks. Due to high penetration of DGs, microgrid formation can be an effective strategy to enhance the system's resiliency via critical load restoration during contingency. To form optimal microgrids, different algorithms have been reported in the literature. Each approach has its advantage and disadvantage, which will be discussed below:

- The mixed integer linear programming-based techniques can provide a complete picture of microgrid formation by modeling all components of a distribution network in details, but an optimal solution can be computationally expensive or practically infeasible when the size of the system is large.
- The heuristic rule-based algorithm can quickly find feasible microgrid formation after faults, but it needs problem-dependent information and may not guarantee an optimal solution.
- The graph theory can be successful to find optimal solution rapidly in a small system, however, its efficiency degrades for medium to large systems since the number of trees is increasing, and implementing the graph partitioning concept takes time to form a microgrid, which makes this method unattractive in the service restoration problem.

- In the spectral algorithm, to determine affinity between two components, the Hessian matrix needs to be calculated for AC power follow at a specific operating point. Although this algorithm provides a reliable solution for a particular operating point, it may not be a promising solution for service restoration problem because the system operating condition varies and the partitioning should be run for many operating points.
- The hierarchical clustering technique employs structural characteristics of distribution networks rather than the operating point, which makes partitioning more reasonable than the spectral algorithm. K-means method clusters objects by minimizing the distance within each cluster, but it may not be able to guarantee radiality constraints of distribution networks.

Based on advantages and disadvantages of various algorithms for microgrid formation, the combination of different strategies may contribute to a more reliable solution for service restoration problem. For example, the combination of k-means method with mixed integer programming technique can result in less decision variables, which improves convergence speed of the optimization problem and satisfies operational constraints.

2.6.2 Future Research Direction

In the area of service restoration using microgrid formation, the distributed optimization technique can be a suitable method to tackle microgrid formation problem, as it decomposes a large optimization problem into several subproblems and handles them in a parallel fashion, and thus, the convergence speed increases and the global optimal solution is obtained.

To develop efficient service restoration strategies through microgrid formation, more realistic models of distribution networks are needed. For example, most distribution networks have unbalanced configurations, which has not been sufficiently investigated in microgrid formation. In addition, supplying power to different types of loads (static and dynamic loads) needs to be further investigated following outages as each constructed microgrid must have the capability to manage motor starting transients as an efficient service restoration strategy.

Artificial intelligent and machine learning-based methods can be developed in service restoration to realize intelligent control actions. For example, deep reinforcement learning has a big potential to realize microgrid formation and intelligent service restoration in distribution networks.

2.7 Conclusion

In this paper, service restoration through microgrid formation techniques in the literature is extensively reviewed. Various approaches to construct microgrids are introduced, such as graph theory, heuristic rule-based algorithm, clustering algorithm, and mixed integer linear programming. Control and economic aspects of microgrids are summarized. The future research directions are recommended in the paper. The paper offers valuable information to engineers and researchers working on renewable energy sources and distribution system modernization.

2.8 Reference

[1] M. N. Ambia, K. Meng, W. Xiao, and Z. Y. Dong, ‘‘Nested formation approach for networked microgrid self-healing in islanded mode,’’ IEEE Trans. Power Del., vol. 36, no. 1, pp. 452–464, Feb. 2021.

[2] L. Che and M. Shahidehpour, ‘‘Adaptive formation of microgrids with mobile emergency resources for critical service restoration in extreme conditions,’’ IEEE Trans. Power Syst., vol. 34, no. 1, pp. 742–753, Jan. 2019.

[3] United States Environmental Protection Agency. (Mar. 15, 2009). U.S. Billion-Dollar Weather and Climate Disasters, 1980—Present (NCEI Accession 0209268). Accessed: Mar.16,2022.[Online].Available:https://hero.epa.gov/hero/index.cfm/reference/details/referenceid/7310466

[4] D. K. Mishra, M. J. Ghadi, A. Azizivahed, L. Li, and J. Zhang, ‘‘A review on resilience studies in active distribution systems,’’ Renew. Sustain. Energy Rev., vol. 135, Jan. 2021, Art. no. 110201.

[5] J. Lopez, J. E. Rubio, and C. Alcaraz, ‘‘A resilient architecture for the smart grid,’’ IEEE Trans. Ind. Informat., vol. 14, no. 8, pp. 3745–3753, Aug. 2018.

[6] A. Shaker, A. Safari, and M. Shahidehpour, ‘‘Reactive power management for networked microgrid resilience in extreme conditions,’’ IEEE Trans. Smart Grid, vol. 12, no. 5, pp. 3940–3953, Sep. 2021.

[7] Q. Zhou, M. Shahidehpour, A. Alabdulwahab, and A. Abusorrah, ‘‘Flexible division and unification control strategies for resilience enhancement in networked microgrids,’’ IEEE Trans. Power Syst., vol. 35, no. 1, pp. 474–486, Jan. 2020.

[8] L. Faria, A. Silva, Z. Vale, and A. Marques, ‘‘Training control centers’ operators in incident diagnosis and power restoration using intelligent tutoring systems,’’ IEEE Trans. Learn. Technol., vol. 2, no. 2, pp. 135–147, Apr. 2009.

[9] H. Liu, R. A. Davidson, and T. V. Apanasovich, ‘‘Statistical forecasting of electric power restoration times in hurricanes and ice storms,’’ IEEE Trans. Power Syst., vol. 22, no. 4, pp. 2270–2279, Nov. 2007.

[10] P.-C. Chen and M. Kezunovic, ‘‘Fuzzy logic approach to predictive risk analysis in distribution outage management,’’ IEEE Trans. Smart Grid, vol. 7, no. 6, pp. 2827–2836, Nov. 2016.

[11] R. B. Duffey and T. Ha, ‘‘The probability and timing of power system restoration,’’ IEEE Trans. Power Syst., vol. 28, no. 1, pp. 3–9, Feb. 2013.

[12] X. Liang, M. A. Saaklayen, M. A. Igder, S. M. R. H. Shawon, S. O. Faried, and M. Janbakhsh, ‘‘Planning and service restoration through microgrid formation and soft open points for distribution network modernization: A review,’’ IEEE Trans. Ind. Appl., vol. 58, no. 2, pp. 1843–1857, Mar. 2022.

[13] T. Ding, Z. Wang, W. Jia, B. Chen, C. Chen, and M. Shahidehpour, ‘‘Multiperiod distribution system restoration with routing repair crews, mobile electric vehicles, and soft-open-point networked microgrids,’’ IEEE Trans. Smart Grid, vol. 11, no. 6, pp. 4795–4808, Nov. 2020.

[14] K. S. A. Sedzro, A. J. Lamadrid, and L. F. Zuluaga, ‘‘Allocation of resources using a microgrid formation approach for resilient electric grids,’’ IEEE Trans. Power Syst., vol. 33, no. 3, pp. 2633–2643, May 2018.

[15] Y. Wang, C. Chen, J. Wang, and R. Baldick, ‘‘Research on resilience of power systems under natural disasters—A review,’’ IEEE Trans. Power Syst., vol. 31, no. 2, pp. 1604–1613, Mar. 2016.

[16] S. Lei, C. Chen, Y. Li, and Y. Hou, ‘‘Resilient disaster recovery logistics of distribution systems: Co-optimize service restoration with repair crew and mobile power source dispatch,’’ IEEE Trans. Smart Grid, vol. 10, no. 6, pp. 6187–6202, Nov. 2019.

[17] Y. Xu, C.-C. Liu, K. P. Schneider, and D. T. Ton, ‘‘Placement of remote- controlled switches to enhance distribution system restoration capability,’’ IEEE Trans. Power Syst., vol. 31, no. 2, pp. 1139–1150, Mar. 2016.

[18] Z. Galias, ‘‘Tree-structure based deterministic algorithms for optimal switch placement in radial distribution networks,’’ IEEE Trans. Power Syst., vol. 34, no. 6, pp. 4269–4278, Nov. 2019.

[19] S. P. Singh, G. S. Raju, G. K. Rao, and M. Afsari, ‘‘A heuristic method for feeder reconfiguration and service restoration in distribution networks,’’ Int. J. Electr. Power Energy Syst., vol. 31, nos. 7–8, pp. 309–314, 2009.

[20] M. B. Jorge, V. O. Héctor, L. G. Miguel, and P. D. Héctor, ‘‘Multi- fault service restoration in distribution networks considering the operating mode of distributed generation,’’ Electr. Power Syst. Res., vol. 116, pp. 67–76, Nov. 2014.

[21] F. Shen, Q. Wu, and Y. Xue, ‘‘Review of service restoration for distribution networks,’’ J. Mod. Power Syst. Clean Energy, vol. 8, no. 1, pp. 1–14, 2020.

[22] H. Sekhavatmanesh and R. Cherkaoui, ‘‘Distribution network restoration in a multiagent framework using a convex OPF model,’’ IEEE Trans. Smart Grid, vol. 10, no. 3, pp. 2618–2628, May 2019.

[23] C. Chen, J. Wang, F. Qiu, and D. Zhao, ‘‘Resilient distribution system by microgrids formation after natural disasters,’’ IEEE Trans. Smart Grid, vol. 7, no. 2, pp. 958–966, Mar. 2016.

[24] M. Khederzadeh and S. Zandi, ‘‘Enhancement of distribution system restoration capability in single/multiple faults by using microgrids as a resiliency resource,’’ IEEE Syst. J., vol. 13, no. 2, pp. 1796–1803, Jun. 2019.

[25] G. Patsakis, D. Rajan, I. Aravena, and S. Oren, ‘‘Strong mixed-integer formulations for power system islanding and restoration,’’ IEEE Trans. Power Syst., vol. 34, no. 6, pp. 4880–4888, Nov. 2019.

[26] A. Llaria, O. Curea, J. Jiménez, and H. Camblong, ‘‘Survey on micro- grids: Unplanned islanding and related inverter control techniques,’’ Renew. Energy, vol. 36, no. 8, pp. 2052–2061, Aug. 2011.

[27] P. Fuangfoo, T. Meenual, W.-J. Lee, and C. Chompooinwai, ‘‘PEA guidelines for impact study and operation of DG for islanding operation,’’ IEEE Trans. Ind. Appl., vol. 44, no. 5, pp. 1348–1353, Sep. 2008.

[28] L. Zhu, C. Zhang, H. Yin, D. Li, Y. Su, I. Ray, J. Dong, F. Wang, L. M. Tolbert, Y. Liu, Y. Ma, B. Rogers, J. Glass, L. Bruce, S. Delay, P. Gregory, M. Garcia-Sanz, and M. Marden, ‘‘A smart and flexible microgrid with a low-cost scalable open-source controller,’’ IEEE Access, vol. 9, pp. 162214–162230, 2021.

[29] S. A. Arefifar, Y. A.-R. I. Mohamed, and T. H. El-Fouly, ‘‘Supply- adequacy-based optimal construction of microgrids in smart distribution systems,’’ IEEE Trans. Smart Grid, vol. 3, no. 3, pp. 1491–1502, Sep. 2012.

[30] M. Barani, J. Aghaei, M. A. Akbari, T. Niknam, H. Farahmand, and M. Korpas, ‘‘Optimal partitioning of smart distribution systems into supply-sufficient microgrids,’’ IEEE Trans. Smart Grid, vol. 10, no. 3, pp. 2523–2533, May 2019.

[31] S. A. Arefifar, Y. A.-R. I. Mohamed, and T. H. M. El-Fouly, ‘‘Optimum microgrid design for enhancing reliability and supply-security,’’ IEEE Trans. Smart Grid, vol. 4, no. 3, pp. 1567–1575, Sep. 2013.

[32] S. A. Arefifar, Y. A.-R.-I. Mohamed, and T. El-Fouly, ‘‘Optimized multi- ple microgrid-based clustering of active distribution systems considering communication and control requirements,’’ IEEE Trans. Ind. Electron., vol. 62, no. 2, pp. 711–723, Feb. 2015.

[33] A. Mohsenzadeh, C. Pang, and M.-R. Haghifam, ‘‘Determining optimal forming of flexible microgrids in the presence of demand response in smart distribution systems,’’ IEEE Syst. J., vol. 12, no. 4, pp. 3315–3323, Dec. 2018.

[34] Y. Du, H. Tu, X. Lu, J. Wang, and S. Lukic, ‘‘Black-start and service restoration in resilient distribution systems with dynamic microgrids,’’ IEEE J. Emerg. Sel. Topics Power Electron., early access, Apr. 8, 2021, doi: 10.1109/JESTPE.2021.3071765.

[35] M. E. Nassar and M. M. A. Salama, ‘‘Adaptive self-adequate microgrids using dynamic boundaries,’’ IEEE Trans. Smart Grid, vol. 7, no. 1, pp. 105–113, Jan. 2016.

[36] R. Hemmati, H. Mehrjerdi, and S. M. Nosratabadi, ‘‘Resilience-oriented adaptable microgrid formation in integrated electricity-gas system with deployment of multiple energy hubs,’’ Sustain. Cities Soc., vol. 71, Aug. 2021, Art. no. 102946.

[37] M. E. Khodayar, ‘‘Rural electrification and expansion planning of off-grid microgrids,’’ Electr. J., vol. 30, no. 4, pp. 68–74, May 2017.

[38] P. Siritoglou, G. Oriti, and D. L. Van Bossuyt, ‘‘Distributed energy- resource design method to improve energy security in critical facilities,’’ Energies, vol. 14, no. 10, May 2021, Art. no. 10.

[39] A. Naderipour, Z. Abdul-Malek, M. Hajivand, Z. M. Seifabad, M. A. Farsi, S. A. Nowdeh, and I. F. Davoudkhani, ‘‘Spotted hyena optimizer algorithm for capacitor allocation in radial distribution system with distributed generation and microgrid operation considering different load types,’’ Sci. Rep., vol. 11, no. 1, Feb. 2021, Art. no. 1.

[40] R. Yan, N.-A. Masood, T. K. Saha, F. Bai, and H. Gu, ‘‘The anatomy of the 2016 South Australia blackout: A catastrophic event in a high renew- able network,’’ IEEE Trans. Power Syst., vol. 33, no. 5, pp. 5374–5388, Sep. 2018.

[41] G. Liang, S. R. Weller, J. Zhao, F. Luo, and Z. Y. Dong, ‘‘The 2015 Ukraine blackout: Implications for false data injection attacks,’’ IEEE Trans. Power Syst., vol. 32, no. 4, pp. 3317–3318, Jul. 2017.

[42] S. Sreekumar, D. S. Kumar, and J. S. Savier, ‘‘A case study on self-healing of smart grid with islanding and inverter volt–VAR function,’’ IEEE Trans. Ind. Appl., vol. 56, no. 5, pp. 5408–5416, Oct. 2020.

[43] H. Hou, X. Yin, Q. Chen, D. You, G. Tong, and D. Shao, ‘‘Review on the wide area blackout of 500 kV main power grid in some areas of south China in 2008 snow disaster,’’ Autom. Electr. Power Syst., vol. 32, no. 11, pp. 12–15, 2008.

[44] S. Cai, Y. Xie, Q. Wu, M. Zhang, X. Jin, and Z. Xiang, ‘‘Distributionally robust microgrid formation approach for service restoration under random contingency,’’ IEEE Trans. Smart Grid, vol. 12, no. 6, pp. 4926–4937, Nov. 2021.

[45] W. T. El-Sayed, H. E. Z. Farag, H. H. Zeineldin, and E. F. El-Saadany, ‘‘Formation of islanded droop-based microgrids with optimum load- ability,’’ IEEE Trans. Power Syst., vol. 37, no. 2, pp. 1564–1576, Mar. 2022.

[46] K. S. A. Sedzro, X. Shi, A. J. Lamadrid, and L. F. Zuluaga, ‘‘A heuristic approach to the post-disturbance and stochastic pre-disturbance micro- grid formation problem,’’ IEEE Trans. Smart Grid, vol. 10, no. 5, pp. 5574–5586, Sep. 2019.

[47] L. H. Macedo, G. Muñoz-Delgado, J. Contreras, and R. Romero, ‘‘Optimal service restoration in active distribution networks considering micro- grid formation and voltage control devices,’’ IEEE Trans. Ind. Appl., vol. 57, no. 6, pp. 5758–5771, Nov. 2021.

[48] J. Li, X.-Y. Ma, C.-C. Liu, and K. P. Schneider, ‘‘Distribution system restoration with microgrids using spanning tree search,’’ IEEE Trans. Power Syst., vol. 29, no. 6, pp. 3021–3029, Nov. 2014.

[49] R. J. Sánchez-García, M. Fennelly, S. Norris, N. Wright, G. Niblo, J. Brodzki, and J. W. Bialek, ‘‘Hierarchical spectral clustering of power grids,’’ IEEE Trans. Power Syst., vol. 29, no. 5, pp. 2229–2237, Sep. 2014.

[50] S. Lei, C. Chen, Y. Song, and Y. Hou, ‘‘Radiality constraints for resilient reconfiguration of distribution systems: Formulation and appli- cation to microgrid formation,’’ IEEE Trans. Smart Grid, vol. 11, no. 5, pp. 3944–3956, Sep. 2020.

[51] C. A. Cortes, S. F. Contreras, and M. Shahidehpour, ‘‘Microgrid topology planning for enhancing the reliability of active distribution networks,’’ IEEE Trans. Smart Grid, vol. 9, no. 6, pp. 6369–6377, Nov. 2018.

[52] L. Che, X. Zhang, M. Shahidehpour, A. Alabdulwahab, and Y. Al-Turki, ‘‘Optimal planning of loop-based microgrid topology,’’ IEEE Trans. Smart Grid, vol. 8, no. 4, pp. 1771–1781, Jul. 2017.

[53] M. Zadsar, M. R. Haghifam, and S. M. M. Larimi, ‘‘Approach for self- healing resilient operation of active distribution network with microgrid,’’ IET Gener., Transmiss. Distrib., vol. 11, no. 18, pp. 4633–4643, Dec. 2017.

[54] J. Morren, S. W. H. de Haan, and J. A. Ferreira, ‘‘Contribution of DG units to primary frequency control,’’ Eur. Trans. Electr. Power, vol. 16, no. 5, pp. 507–521, 2006.

[55] K. Singh, M. Amir, F. Ahmad, and S. S. Refaat, ‘‘Enhancement of frequency control for stand-alone multi-microgrids,’’ IEEE Access, vol. 9, pp. 79128–79142, 2021.

[56] Zaheeruddin, K. Singh, and M. Amir, ‘‘Intelligent fuzzy TIDF-II con- troller for load frequency control in hybrid energy system,’’ IETE Tech. Rev., pp. 1–17, Nov. 2021.

[57] A. Sharma, D. Srinivasan, and A. Trivedi, ‘‘A decentralized multi-agent approach for service restoration in uncertain environment,’’ IEEE Trans. Smart Grid, vol. 9, no. 4, pp. 3394–3405, Jul. 2018.

[58] A. Sharma, D. Srinivasan, and A. Trivedi, ‘‘A decentralized multiagent system approach for service restoration using DG islanding,’’ IEEE Trans. Smart Grid, vol. 6, no. 6, pp. 2784–2793, Nov. 2015.

[59] J. Guo, G. Hug, and O. K. Tonguz, ‘‘Intelligent partitioning in distributed optimization of electric power systems,’’ IEEE Trans. Smart Grid, vol. 7, no. 3, pp. 1249–1258, May 2016.

[60] X. Xu, F. Xue, S. Lu, H. Zhu, L. Jiang, and B. Han, ‘‘Structural and hierarchical partitioning of virtual microgrids in power distribution network,’’ IEEE Syst. J., vol. 13, no. 1, pp. 823–832, Mar. 2019.

[61] E. Cotilla-Sanchez, P. D. Hines, C. Barrows, S. Blumsack, and M. Patel, ‘‘Multi-attribute partitioning of power networks based on electrical distance,’’ IEEE Trans. Power Syst., vol. 28, no. 4, pp. 4979–4987, Nov. 2013.

[62] C. Shah and R. Wies, ‘‘Adaptive day-ahead prediction of resilient power distribution network partitions,’’ in Proc. IEEE Green Technol. Conf. (GreenTech), Apr. 2021, pp. 477–483.

[63] R. Xu and D. Wunsch, ‘‘Survey of clustering algorithms,’’ IEEE Trans. Neural Netw., vol. 16, no. 3, pp. 645–678, May 2005.

[64] D. M. L. K. Cheong, T. Fernando, H. C. Iu, M. Reynolds, and J. Fletcher, ‘‘Review of clustering algorithms for microgrid formation,’’ in Proc. IEEE Innov. Smart Grid Technol. Asia (ISGT-Asia), Dec. 2017, pp. 1–6.

[65] M. A. Gilani, A. Kazemi, and M. Ghasemi, ‘‘Distribution system resilience enhancement by microgrid formation considering distributed energy resources,’’ Energy, vol. 191, Jan. 2020, Art. no. 116442.

[66] T. Ding, Y. Lin, G. Li, and Z. Bie, ‘‘A new model for resilient distribution systems by microgrids formation,’’ IEEE Trans. Power Syst., vol. 32, no. 5, pp. 4145–4147, Sep. 2017.

[67] T. Zhao, B. Chen, S. Zhao, J. Wang, and X. Lu, ‘‘A flexible operation of distributed generation in distribution networks with dynamic boundaries,’’ IEEE Trans. Power Syst., vol. 35, no. 5, pp. 4127–4130, Sep. 2020.

[68] R. A. Osama, A. F. Zobaa, and A. Y. Abdelaziz, ‘‘A planning framework for optimal partitioning of distribution networks into microgrids,’’ IEEE Syst. J., vol. 14, no. 1, pp. 916–926, Mar. 2020.

[69] Z. N. Popovic, S. D. Knezevic, and B. S. Brbaklic, ‘‘A risk management procedure for island partitioning of automated radial distribution networks with distributed generators,’’ IEEE Trans. Power Syst., vol. 35, no. 5, pp. 3895–3905, Sep. 2020.

[70] L. Meng, E. R. Sanseverino, A. Luna, T. Dragicevic, J. C. Vasquez, and J. M. Guerrero, ‘‘Microgrid supervisory controllers and energy management systems: A literature review,’’ Renew. Sustain. Energy Rev., vol. 60, pp. 1263–1273, Jul. 2016.

[71] Y. Han, K. Zhang, H. Li, E. A. A. Coelho, and J. M. Guerrero, ‘‘MAS- based distributed coordinated control and optimization in microgrid and microgrid clusters: A comprehensive overview,’’ IEEE Trans. Power Electron., vol. 33, no. 8, pp. 6488–6508, Aug. 2018.

[72] J. M. Guerrero, J. C. Vasquez, J. Matas, L. G. de Vicuna, and M. Castilla, ‘‘Hierarchical control of droop-controlled AC and DC microgrids—A general approach toward standardization,’’ IEEE Trans. Ind. Electron., vol. 58, no. 1, pp. 158–172, Jan. 2011.

[73] M. M. A. Abdelaziz, M. F. Shaaban, H. E. Farag, and E. F. El-Saadany, ‘‘A multistage centralized control scheme for islanded microgrids with PEVs,’’ IEEE Trans. Sustain. Energy, vol. 5, no. 3, pp. 927–937, Jul. 2014.

[74] N. L. Díaz, A. C. Luna, J. C. Vasquez, and J. M. Guerrero, ‘‘Centralized control architecture for coordination of distributed renewable generation and energy storage in islanded AC microgrids,’’ IEEE Trans. Power Electron., vol. 32, no. 7, pp. 5202–5213, Jul. 2017.

[75] Q. Shafiee, V. Nasirian, J. C. Vasquez, J. M. Guerrero, and A. Davoudi, ‘‘A multi-functional fully distributed control framework for AC micro- grids,’’ IEEE Trans. Smart Grid, vol. 9, no. 4, pp. 3247–3258, Jul. 2018.

[76] X. Lu, X. Yu, J. Lai, Y. Wang, and J. M. Guerrero, ‘‘A novel distributed secondary coordination control approach for islanded microgrids,’’ IEEE Trans. Smart Grid, vol. 9, no. 4, pp. 2726–2740, Jul. 2018.

[77] A. Bidram, A. Davoudi, F. L. Lewis, and J. M. Guerrero, ‘‘Distributed cooperative secondary control of microgrids using feedback linearization,’’ IEEE Trans. Power Syst., vol. 28, no. 3, pp. 3462–3470, Aug. 2013.

[78] Y. Han, H. Li, P. Shen, E. A. A. Coelho, and J. M. Guerrero, ‘‘Review of active and reactive power sharing strategies in hierarchical controlled microgrids,’’ IEEE Trans. Power Electron., vol. 32, no. 3, pp. 2427–2451, Mar. 2017.

[79] S. M. Mohiuddin and J. Qi, ‘‘Optimal distributed control of AC microgrids with coordinated voltage regulation and reactive power sharing,’’ IEEE Trans. Smart Grid, vol. 13, no. 3, pp. 1789–1800, May 2022.

[80] X. Yu, A. M. Khambadkone, H. Wang, and S. T. S. Terence, ‘‘Control of parallel-connected power converters for low-voltage microgrid—Part I: A hybrid control architecture,’’ IEEE Trans. Power Electron., vol. 25, no. 12, pp. 2962–2970, Dec. 2010.

[81] A. Mehrizi-Sani, ‘‘Chapter 2 - Distributed Control Techniques in Micro- grids,’’ in The Book of Microgrid: Advanced Control Methods and Renew- able Energy System Integration, Amsterdam, The Netherlands: Elsevier, Imprint Butterworth-Heinemann, 2017, pp. 43–62.

[82] M. Yazdanian and A. Mehrizi-Sani, ‘‘Distributed control techniques in microgrids,’’ IEEE Trans. Smart Grid, vol. 5, no. 6, pp. 2901–2909, Nov. 2014.

[83] V. N. Coelho, M. W. Cohen, I. M. Coelho, N. Liu, and F. G. Guimarães, ‘‘Multi-agent systems applied for energy systems integration: State-of- the-art applications and trends in microgrids,’’ Appl. Energy, vol. 187, pp. 820–832, Feb. 2017.

[84] C.-H. Yoo, I.-Y. Chung, H.-J. Lee, and S.-S. Hong, ‘‘Intelligent control of battery energy storage for multi-agent based microgrid energy management,’’ Energies, vol. 6, no. 10, pp. 4956–4979, Sep. 2013.

[85] Y. Xu and Z. Li, ‘‘Distributed optimal resource management based on the consensus algorithm in a microgrid,’’ IEEE Trans. Ind. Electron., vol. 62, no. 4, pp. 2584–2592, Apr. 2015.

[86] W. Liu, W. Gu, W. Sheng, X. Meng, Z. Wu, and W. Chen, ‘‘Decentralized multi-agent system-based cooperative frequency control for autonomous microgrids with communication constraints,’’ IEEE Trans. Sustain. Energy, vol. 5, no. 2, pp. 446–456, Apr. 2014.

[87] T. Morstyn, B. Hredzak, and V. G. Agelidis, ‘‘Cooperative multi-agent control of heterogeneous storage devices distributed in a DC microgrid,’’ IEEE Trans. Power Syst., vol. 31, no. 4, pp. 2974–2986, Jul. 2016.

[88] C. Dou, M. Lv, T. Zhao, Y. Ji, and H. Li, ‘‘Decentralised coordinated control of microgrid based on multi-agent system,’’ IET Gener., Transmiss. Distrib., vol. 9, no. 16, pp. 2474–2484, Dec. 2015.

[89] C. M. Colson and M. H. Nehrir, ‘‘Comprehensive real-time microgrid power management and control with distributed agents,’’ IEEE Trans. Smart Grid, vol. 4, no. 1, pp. 617–627, Mar. 2013.

[90] Z. Li, C. Zang, P. Zeng, H. Yu, and H. Li, ‘‘MAS based distributed automatic generation control for cyber-physical microgrid system,’’ IEEE/CAA J. Autom. Sinica, vol. 3, no. 1, pp. 78–89, Jan. 2016.

[91] J. Yang, J. Dai, H. B. Gooi, H. Nguyen, and A. Paudel, ‘‘A proof- of-authority blockchain based distributed control system for islanded microgrids,’’ IEEE Trans. Ind. Informat., early access, Jan. 13, 2022.

[92] M. M. Rana, A. Rahman, M. Uddin, M. R. Sarkar, S. A. Shezan, M. F. Ishraque, S. M. S. H. Rafin, and M. Atef, ‘‘A comparative analysis of peak load shaving strategies for isolated microgrid using actual data,’’ Energies, vol. 15, no. 1, p. 330, Jan. 2022.

[93] A. Rauf, A. T. Awami, M. Kassas, and M. Khalid, ‘‘Optimizing a residential solar PV system based on net-metering approaches,’’ in Proc. CIRED 26th Int. Conf. Exhib. Electr. Distrib. IET, Sep. 2021, pp. 1–5.

[94] L. Zhang, Y. Yang, Q. Li, W. Gao, F. Qian, and L. Song, ‘‘Economic optimization of microgrids based on peak shaving and CO2 reduction effect: A case study in Japan,’’ J. Cleaner Prod., vol. 321, Oct. 2021, Art. no. 128973.

[95] M. Stadler, G. Cardoso, S. Mashayekh, T. Forget, N. DeForest, A. Agarwal, and A. Schönbein, ‘‘Value streams in microgrids: A literature review,’’ Appl. Energy, vol. 162, pp. 980–989, Jan. 2016.

[96] Y. Wang, A. O. Rousis, and G. Strbac, ‘‘On microgrids and resilience: A comprehensive review on modeling and operational strategies,’’ Renew. Sustain. Energy Rev., vol. 134, Dec. 2020, Art. no. 110313.

[97] R. Ma, H. Cai, Q. Ji, and P. Zhai, ‘‘The impact of feed-in tariff degression on R&D investment in renewable energy: The case of the solar PV industry,’’ Energy Policy, vol. 151, Apr. 2021, Art. no. 112209.

[98] Y. Parag and M. Ainspan, ‘‘Sustainable microgrids: Economic, environmental and social costs and benefits of microgrid deployment,’’ Energy Sustain. Develop., vol. 52, pp. 72–81, Oct. 2019.

[99] S. Chowdhury, S. P. Chowdhury, and P. Crossley, Microgrids and Active Distribution Networks (The Institution of Engineering and Technology (IET)), London, U.K.: 2009.

[100] S. R. Thangavelu, A. M. Khambadkone, and I. A. Karimi, ‘‘Long-term optimal energy mix planning towards high energy security and low GHG emission,’’ Appl. Energy, vol. 154, pp. 959–969, Sep. 2015.

[101] P. Balducci, K. Mongird, D. Wu, D. Wang, V. Fotedar, and R. Dahowski, ‘‘An evaluation of the economic and resilience benefits of a microgrid in Northampton, Massachusetts,’’ Energies, vol. 13, no. 18, p. 4802, Sep. 2020.

[102] T. Adefarati and R. C. Bansal, ‘‘Reliability, economic and environmental analysis of a microgrid system in the presence of renew- able energy resources,’’ Appl. Energy, vol. 236, pp. 1089–1114, Feb. 2019.

[103] M. Mao, P. Jin, Y. Zhao, F. Chen, and L. Chang, ‘‘Optimal allocation and economic evaluation for industrial PV microgrid,’’ in Proc. IEEE Energy Convers. Congr. Expo., Sep. 2013, pp. 4595–4602.

[104] G. Y. Morris, C. Abbey, S. Wong, and G. Joós, ‘‘Evaluation of the costs and benefits of microgrids with consideration of services beyond energy supply,’’ in Proc. IEEE Power Energy Soc. Gen. Meeting, Jul. 2012, pp. 1–9.

[105] M. J. Ghadi, A. Rajabi, S. Ghavidel, A. Azizivahed, L. Li, and J. Zhang, ‘‘From active distribution systems to decentralized microgrids: A review on regulations and planning approaches based on operational factors,’’ Appl. Energy, vol. 253, Nov. 2019, Art. no. 113543.

[106] M. H. Imani, P. Niknejad, and M. R. Barzegaran, ‘‘The impact of customers’ participation level and various incentive values on implementing emergency demand response program in microgrid operation,’’ Electr. Power Energy Syst., vol. 96, pp. 114–125, Mar. 2018.

3 Service Restoration Using Deep Reinforcement Learning and Dynamic Microgrid Formation in Distribution Networks

3.1 Abstract

A resilient power distribution network can reduce length and impact of power outages, maintain continuous services, and improve reliability. One effective way to enhance the system's resilience is to form microgrids during outages. In this paper, a novel dynamic microgrid formation-based service restoration method using deep reinforcement learning is proposed, and it is treated as a Markov decision process (MDP) while taking operational and structural limitations of microgrids into account. The deep Q-network is employed to obtain optimal control strategies for microgrid formation. We have introduced a new way for the agent to choose actions when building a microgrid using the deep Q-learning method, which ensures that the microgrid has a feasible radial structure. The proposed service restoration method enables real-time computing to facilitate online formation of dynamic microgrids and adapts to changing conditions. Its effectiveness is validated by case studies using the modified IEEE 33-node test system and a real 404-node distribution system operated by Saskatoon Light and Power in Saskatoon, Canada.

3.2 Introduction

Improving resiliency is crucial to ensure that power grids can withstand and recover from disruptions, such as natural disasters and cyber-attacks [1]. Service restoration capability to critical loads after disruptions on the main grid is a key indicator of a resilient distribution system. The traditional practice is to redirect affected loads from areas without power to areas with power through the network reconfiguration [2]. Today, forming microgrids (MGs) with dynamic boundaries is a promising service restoration solution to improve resiliency of distribution systems [3], [4]. By incorporating a variety of energy sources, such as solar panels, wind turbines and backup generators, along with remotely control switches, a distribution network can be partitioned into multiple self-adequate MGs, through which the restoration is improved and the power supply continuity to critical loads is maintained [5]-[9]. Optimal construction of multiple MGs to restore

critical loads during a fault in the primary grid is proposed in [10], [11]. In [12], distributed energy resources (DER) and isolate switches are allocated in a distribution network to form resilience-oriented MGs. In [13], a two-stage service restoration method is proposed for the mobile emergency resource allocation, MG formation, and sequential service restoration for contingencies. In [14], a self-healing control strategy is proposed to minimize unused capacities of distributed generation (DG) for service restoration in islanded mode during a contingency.

The main challenge of a multi-MGs formation problem is to find the most suitable topology that satisfies various operational constraints. Mathematical programming [15]–[17] and heuristic search [18], [19] approaches are commonly used to achieve the topology determination. In [15], a novel mixed-integer linear programming (MILP) method is used to create an optimization model to form MGs in distribution networks after a disturbance. In [16], a MILP-based service restoration method is developed to determine the optimal hardening plan, allocation of DGs, and topology reconfiguration, which ensures that a predetermined level of load is supplied after natural disasters. The MG formation problem is formulated as a mixed-integer non-linear programming (MINLP) model in [17], and a commercial solver, DCOPT, is used to address the optimization problem. A heuristic-based method is proposed to identify optimal reconfiguration of a large-scale distribution network in [18]. In [19], a tabu search optimization algorithm and a graph theory-based method are used to form several virtual MGs in a distribution network. These MG formation strategies are primarily focused on present conditions/environment. However, conditions during a natural disaster may be uncertain and prone to change [20], causing constructed MGs lose their effectiveness or get damaged.

To use mathematical programming methods, creating a precise mathematical model is essential, but this process can be time-consuming, and thus, may become not practical. Model-based schemes may also have difficulty to model complex objects, integrate new features, and maintain efficiency for large systems. To overcome these challenges, novel adaptive dynamic MG formation strategies are urgently needed for distribution networks.

Deep reinforcement learning (DRL) continuously interacts with the environment and gathers feedback, so it can form MGs that are adaptable to variable conditions [21]. DRL is effective in handling Markov decision process (MDP), and becomes popular to tackle many problems in power systems, such as voltage control [22], electrical vehicles charging navigation [23], demand response [24], MG power management [25], and resiliency improvement of

distribution networks [26]. However, to implement a feasible radial topology, a high number of reconfiguration actions are required for a large system. To date, service restoration methods using DRL-based MG formation are very limited in the literature.

In this paper, a novel dynamic microgrid formation-based service restoration method using deep reinforcement learning for distribution networks is proposed. We have adopted the node cell and route model concept in [1] to start the process. Each DG with the black-start capability is treated as an energization agent, and it travels through the system to energize lines and nodes it visits. Using the node cell concept, nodes connected by non-switchable lines are grouped into a single unit, known as a "node cell", and all nodes within a node cell are activated simultaneously when an energization agent visits, which greatly reduces the search space. Next, the deep Q-network algorithm guides the agent to select the node cell and pick up as many loads as possible while following operational constraints. To ensure radiality constraints for each constructed MG, we propose a novel algorithm to pick up node cells by an energization agent. A simulator-based environment is created using the software, OpenDSS, integrated for power flow studies. A simulator offers a variety of features and can perform a range of tasks, and thus, facilitates complex object-oriented learning, and new features can be integrated through agent-environment interactions in a simulator. This adaptable capability makes simulators suitable for real-world application.

The main contributions of this paper include:

- Proposed a novel dynamic MG formation-based service restoration method using DRL in distribution networks.
- Developed a new DRL framework through MDP to form dynamic MGs by incorporating the node cell and route model concept (The deep Q-network is trained offline, and then used for online decision-making to provide fast, near-optimal solutions).
- Validated the proposed method using the IEEE 33-node system and a real unbalanced three-phase 404-node distribution system operated by Saskatoon Light and Power, a Canadian electric utility in Saskatoon, Canada.

The paper is organized as follows: the proposed method is introduced in Section 3.3; its problem formulation is given in Section 3.4; the DRL algorithm is provided in Section 3.5; the

proposed approach is validated by case studies in Sections 3.6 and 3.7; and conclusions are drawn in Section 3.8.

3.3 The Proposed Service Restoration Method Using Deep Reinforcement Learning

Modern distribution systems with renewable DGs and controllable devices have significant potential to enhance service restoration. In this paper, the proposed service restoration method can maximize the restored load by forming multiple dynamic microgrids. DRL is trained offline and then applied online for fast and efficient decision-making. DRL is used to create control actions, while ensures that operational and topological constraints are met.

The proposed service restoration method can be implemented by the following eight steps (Figure 3.1).

Step 1: *Define the problem and set up the environment as an MDP*. The objective of the service restoration, state and action spaces, and rewards or penalties related to different actions are defined.

Step 2: *Data collection and preprocessing.* Gather data on the electrical distribution system, including details on generation and load. To establish an appropriate input format for the neural network, the data are preprocessed.

Step 3: *Node Cell Formation.* The node cell concept is used to convert a distribution network to a smaller simplified network with only switchable lines.

Step 4: *Fault isolation.* Open upstream switches of node cells containing faults.

Step 5: *Deep reinforcement learning model construction*. Construct a deep neural network-based reinforcement learning model that is capable of making decisions for service restoration. The model consists of an input layer that receives data on the state of the distribution network, and an output layer that generates a probability distribution for possible actions.

Step 6: *Model training using the deep Q-learning approach.* Train the deep reinforcement learning model using the preprocessed data and a Q-learning approach, which involves optimizing the model's decision-making process based on rewards and penalties associated with different actions.

Step 7: *Model testing and evaluation.* Test the trained deep reinforcement learning model using a new dataset to evaluate its performance in correctly restoring loads in the distribution network. This step ensures the effectiveness and accuracy of the trained model.

Step 8: *Real-world deployment of the trained model.* Deploy the trained deep reinforcement learning model in a real-world distribution network for service restoration once it has demonstrated satisfactory performance. This involves integrating the model into the operational environment of the distribution network and utilizing it to guide actual service restoration decisions based on its learned decision-making capabilities.

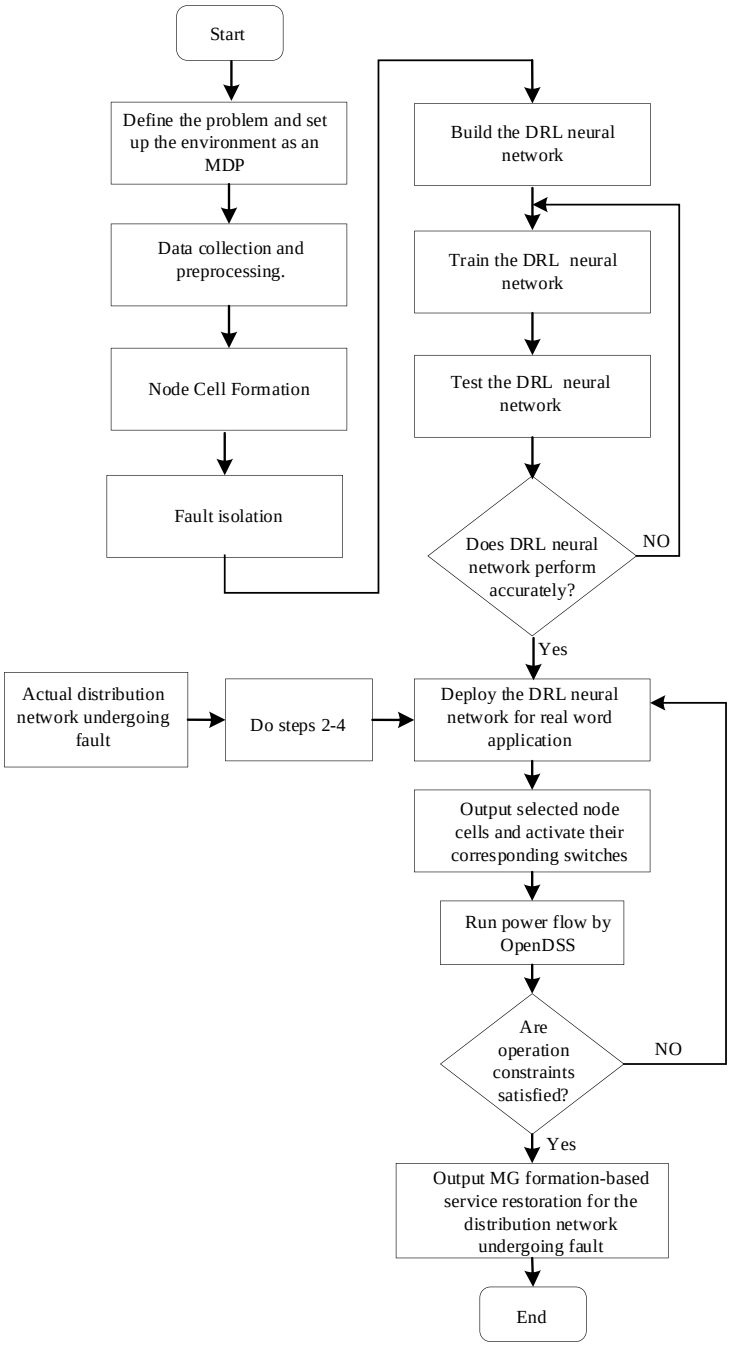

Figure 3.1. The flow chart of the proposed service restoration method through dynamic MG formation and DRL in distribution networks.

3.4 Problem Formulation

In this section, the MG formation-based service restoration problem is formulated and its MDP formulation is presented.

3.4.1 Microgrid Formation-based Service Restoration

A graph *G = (V, E)* is used to represent the distribution network, where *V* and E refer to the sets of nodes and edges, respectively, $|V| = N$, $|E| = L$ At each node *i* in *V*, there is a load that demands active and reactive power, $\mathcal{p}_i$ and $\mathcal{q}_i$, respectively. Before converting the MG formation-based service restoration problem into a MDP, the object, operation and topology constraints are discussed to lay the foundation for the MDP elements definition.

1) Objective function: The restoration aims to maximize the amount of restored priority-weighted loads based on the capacity of DGs. The objective function is expressed by

$$\mathrm{OF} = \max \sum_{i \in V} z_i \mathcal{w}_i \mathcal{P}_i \tag{3.1}$$

where $\mathcal{P}_i$ is the restored load. z_i is a binary variable determining if load *i* is picked up. $\mathcal{w}_i$ is the priority weight of load *i*.

2) Operational constraints*:* The linearized DistFlow model [10] is used to represent operational constraints in MG formation-based service restoration. (**3.2**) and (**3.3**) ensure active and reactive power balance, respectively.

$$\mathcal{P}_i^{\mathcal{g}} - z_i \mathcal{p}_i + \sum_{(j,i) \in E} \mathcal{P}_{ji}^{\mathcal{BR}} - \sum_{(i,j) \in E} \mathcal{P}_{ij}^{\mathcal{BR}} = 0, \qquad \forall i \in V \tag{3.2}$$

$$\mathcal{Q}_i^{\mathcal{g}} - z_i \mathcal{q}_i + \sum_{(j,i) \in E} \mathcal{Q}_{ji}^{\mathcal{BR}} - \sum_{(i,j) \in E} \mathcal{Q}_{ij}^{\mathcal{BR}} = 0, \qquad \forall i \in V \tag{3.3}$$

where $\mathcal{P}_i^{\mathcal{g}}$ and $\mathcal{Q}_i^{\mathcal{g}}$ are active and reactive power output of DGs at node *i*, respectively. $\mathcal{p}_i$ and $\mathcal{q}_i$ are real and reactive demand of the load at node *i*, respectively. Real and reactive power flow on branch *(i, j)* are $\mathcal{P}_{ij}^{\mathcal{BR}}$ and $\mathcal{Q}_{ij}^{\mathcal{BR}}$, respectively. Limits for DG output power are expressed by (3.4).

$$\underline{\mathcal{P}}_m^{min} \le \mathcal{P}_m^{\mathcal{G}} \le \overline{\mathcal{P}}_m^{max}, \underline{\mathcal{Q}}_m^{min} \le \mathcal{Q}_m^{\mathcal{G}} \le \overline{\mathcal{Q}}_m^{max}, \forall m \in V_{DG} \quad (3.4)$$

where $\overline{\mathcal{P}}_m^{max}$ and $\underline{\mathcal{P}}_m^{min}$ are upper and lower limits of active power output of DGs, respectively. $\overline{\mathcal{Q}}_m^{max}$ and $\underline{\mathcal{Q}}_m^{min}$ are upper and lower limits of reactive power output of DGs, respectively. V_{DG} is the set of nodes containing DGs. (**3.5**) enforces the relation between the voltage difference of two end nodes and the power flow of each closed line.

$$-M(1-\alpha_{ij}) + \frac{(r_{ij}.\mathcal{P}_{ij}^{\mathcal{BR}} + x_{ij}.\mathcal{Q}_{ij}^{\mathcal{BR}})}{v_0} \le v_j - v_i \le M(1-\alpha_{ij}) + \frac{(r_{ij}.\mathcal{P}_{ij}^{\mathcal{BR}} + x_{ij}.\mathcal{Q}_{ij}^{\mathcal{BR}})}{v_0}, \forall (i,j) \in E \quad (3.5)$$

where α_{ij} is a binary variable with a value of 1 if line *(i, j)* is closed, and 0 if otherwise. r_{ij} and x_{ij} are the resistance and reactance of line *(i, j)*, respectively. v_0 is the reference voltage. In order to ensure that the voltages at two unconnected buses remain separated, the Big M method is employed. The range of the voltage (v_i) is defined as

$$v^{min} \le v_i \le v^{max} \quad (3.6)$$

where v^{max} and v^{min} are the maximum and minimum voltage magnitude squared. Safe margins should be maintained for line loading conditions.

$$-\mathcal{P}_{ij}^{max} \le \alpha_{ij}.\mathcal{P}_{ij}^{\mathcal{BR}} \le \mathcal{P}_{ij}^{max} \quad (3.7)$$

$$-Q_{ij}^{max} \le \alpha_{ij}.Q_{ij}^{\mathcal{BR}} \le Q_{ij}^{max} \quad (3.8)$$

3) Topological constraints: The multicommodity flow-based model [15] is widely used to ensure a radial topology of MGs. The topological constrains are provided as follows:

$$\sum_{(j,\, i_s) \in E} \mathcal{F}_{ji_s}^k - \sum_{(i_s, j) \in E} \mathcal{F}_{i_s j}^k + 1 = 0, \ \forall\, k \in V \backslash i_s \quad (3.9)$$

$$\sum_{(j,\,k)\in E} \mathcal{F}_{jk}^{k} - \sum_{(k,j)\in E} \mathcal{F}_{kj}^{k} - 1 = 0\,, \qquad \forall\, k \in V\backslash i_s \tag{3.10}$$

$$\sum_{(j,\,i)\in E} \mathcal{F}_{ji}^{k} - \sum_{(i,j)\in E} \mathcal{F}_{ij}^{k} = 0,\ \forall\, k \in V\backslash i_s, \forall\, i \in V\{k, i_s\} \tag{3.11}$$

$$0 \le \mathcal{F}_{ij}^{k} \le \lambda_{ij},\ 0 \le \mathcal{F}_{ji}^{k} \le \lambda_{ji},\ \forall\, k \in V\backslash i_s,\ (\mathrm{i,j}) \in E \tag{3.12}$$

$$\sum_{(i,j)\in E} \lambda_{ij} + \lambda_{ji} - |V| + 1 = 0 \tag{3.13}$$

$$\lambda_{ij} + \lambda_{ji} = \sigma_{ij},\ \forall(\mathrm{i,j}) \in E \tag{3.14}$$

$$\alpha_{ij} - \sigma_{ij}\ \le 0 \tag{3.15}$$

where $\mathcal{F}_{ij}^{k}$ is the flow of electric power (commodity) k from nodes *i* to *j*. λ_{ij} is a binary variable with a value of 1 if arc *(i, j)* is part of the directed spanning tree, and 0 if otherwise. σ_{ij} represents a fictitious status of branch *(i, j)*, it is 1 when closed, and 0 when otherwise. i_s is the index for the substation or DG buses.

The constraints (3.9) - (3.14) are used to create this fictitious tree-like structure, which is called a "spanning tree". The spanning tree connects all the nodes in the network, but it may not be the same as the actual physical layout of the network. The constraint (3.15) is used to restrict the network to only use certain connections in the spanning tree that are specified by a variable called σ. Detailed explanation of these constraints can be found in [15].

3.4.2 Modeling Microgrid Formation-based Service Restoration as a Markov Decision Process

Markov Decision Process (MDP) is a mathematical framework that is used to model decision-making problems. In an MDP, the decision-maker makes a sequence of decisions over time, and the outcomes of those decisions depend on the current state of the system, and the actions taken by the decision-maker. MG-based service restoration in power systems is a decision-making

problem that can be formulated as an MDP. In service restoration, the goal is to restore power to customers after an outage by selectively closing and opening switches in the distribution network. By formulating MG-based service restoration as an MDP, the decision-making problem can be broken down into a sequence of simpler decision problems, where the decision-maker (agent) must choose which load should be picked up based on the current state of the network and the expected future outcomes of each decision. A MDP can be defined by following elements.

State $\boldsymbol{s_{m,t}} \in \boldsymbol{S}$: The state of the MG formation for service restoration consists of: 1) the current location of the agent, $LA_{m,t}$, 2) all visited node cells, VN_t, 3) the load condition, P_t, and 4) the remaining capacity of the DG, $C_{m,t}$.

$$s_{m,t} = \left[LA_{m,t}, VN_t, P_t, C_{m,t}\right] \quad (3.16)$$

Action $\boldsymbol{a_{m,t}} \in \boldsymbol{A}$: The action is to pick up a node cell and switch on a corresponding branch. Nodes connected by non-switchable lines are treated as a node cell, and all nodes within a node cell are activated and supplied power simultaneously if this node cell is visited by an energization agent. The simplified network topology only contains node cells and switchable lines, and the action space contains only candidate node cells. The agents travel through the network, chooses node cells by following topological constraints, and ensures that: 1) each MG is isolated from other MGs, and 2) all constructed MGs operate in a tree topology to ensure radiality constraints. This problem is built over a graph $\mathcal{G}(\mathcal{V}, \mathcal{E})$, where the node cell is represented by node $n \in \mathcal{V}$, and the energization path is indicated by edge $e \in E$, which connects two node cells. The adjacent $\mathcal{V} \times \mathcal{V}$ matrix A is used to represent this graph, its element a_{ij} is 1 when there is an edge from node cells i to j, and 0 when there is no such edge. For an agent to choose a node cell as an action, there should be a connection between its current position or all previously visited node cells and the candidate node cell to maintain connectivity within a MG.

To ensure the radiality operation of a MG, the following steps should be followed when an agent wants to take an action:

Step 1: The energization path must begin from either a DG or a substation.

Step 2: When an agent travels, its path shouldn't include any loop, i.e., a node cell cannot be visited more than once.

Step 3: The agent can pick up a node cell only if its upstream node cell has already been energized.

Power generation in the system is observed by agents. Agents select the next node cell to visit at each step based on their current power capacity. If an agent chooses the next location to visit, all loads within the selected node cell will be restored at the same time. When an agent restores a node cell, its capacity is updated as follows:

$$\mathcal{P}_{m,t}^{max} = \overline{\mathcal{P}}_{m}^{max} - \sum_{l \in N_{t-1}^{L}} \sum_{k=1}^{t-1} \mathcal{P}_{l,k}^{L} \quad (3.17)$$

$$\mathcal{Q}_{m,t}^{max} = \overline{\mathcal{Q}}_{m}^{max} - \sum_{l \in N_{t-1}^{L}} \sum_{k=1}^{t-1} \mathcal{Q}_{l,k}^{L} \quad (3.18)$$

where $\mathcal{P}_{m,t}^{max}$ and $\mathcal{Q}_{m,t}^{max}$ are the maximum active and reactive power of DG m at time *t*, respectively. $\overline{\mathcal{P}}_{m}^{max}$ and $\overline{\mathcal{Q}}_{m}^{max}$ are the maximum active and reactive power capacities of DG m, respectively. $\mathcal{P}_{l}^{L}$ and $\mathcal{Q}_{l}^{L}$ are active and reactive power demand of node cell *l*. The second term of (3.17) and (3.18) indicates the amount of active and reactive power being restored already.

The procedure of selecting an action by agents is demonstrated in algorithm 1 below.

Algorithm 1: Action Selection

```
for agent m = 1 to number of agents do
    Observe state s_{m,t} and adjacent matrix
     Condition1 = False, Condtion2 = False, Condtion3 = False
    Select action
        Via exploration or exploitation
    if selected action not in visited nodes
        Condition1 = True
     end if
    if selected action load ≤ agent DG capacity
        Condition2 = True
        end if
     Check the connection between selected action and agent current position or visited
     Nodes
    if there is any connection
        Condition3 = True
     end if
    if Condition1 and Condtion2 and Condition3
        Take action
         break
     else:
        select another action and check three conditions again
     end if
    if agent couldn't take any action
        agent's done = True
    end if
end for
```

Reward $r_{m,t}(s_t, a_t)$: The agents fulfill the power balance, branch limits, and voltage constraints while taking actions. There are two methods in the literature to address the MDP under constraints: 1) use a safety layer to tune control actions, and 2) add penalty functions to the reward signal. In this paper, the second method is adopted using penalty terms to solve a constrained MDP with the following reward signal:

$$r_{m,t} = w_l \mathcal{D}_l + C_p + C_q + C_b + C_v \quad (3.19)$$

$$\mathcal{D}_l = \sqrt{\mathcal{P}_l^{L^2} + \mathcal{Q}_l^{L^2}} \quad (3.20)$$

$$C_p = \begin{cases} -|\Delta\mathcal{P}| & |\Delta\mathcal{P}| \le \partial_p \\ -\eta * |\Delta\mathcal{P}| & |\Delta\mathcal{P}| > \partial_p \end{cases} \quad (3.21)$$

$$C_q = \begin{cases} -|\Delta\mathcal{Q}| & |\Delta\mathcal{Q}| \le \partial_q \\ -\eta * |\Delta\mathcal{Q}| & |\Delta\mathcal{Q}| > \partial_q \end{cases} \quad (3.22)$$

$$\Delta\mathcal{P} = \sum_{i=1}^{N} \left(\sum_{h:(h,i)\in B} \mathcal{P}_{hi}^{\mathcal{BR}} + \mathcal{P}_i^{\mathcal{G}} - \sum_{j:(i,j)\in B} \mathcal{P}_{ij}^{\mathcal{BR}} - \mathcal{P}_t^{L} \right) \quad (3.23)$$

$$\Delta\mathcal{Q} = \sum_{i=1}^{N} \left(\sum_{h:(h,i)\in B} \mathcal{Q}_{hi}^{\mathcal{BR}} + \mathcal{Q}_i^{\mathcal{G}} - \sum_{j:(i,j)\in B} \mathcal{Q}_{ij}^{\mathcal{BR}} - \mathcal{Q}_t^{L} \right) \quad (3.24)$$

$$C_b = -\sum_{(i,j)\in B} \left(max\left(0, \mathcal{P}_{ij}^{\mathcal{BR}} - \mathcal{P}_{ij}^{max}\right) + max\left(0, -\mathcal{P}_{ij}^{max} - \mathcal{P}_{ij}^{\mathcal{BR}}\right) \right) \quad (3.25)$$
$$- \sum_{(i,j)\in B} \left(max\left(0, \mathcal{Q}_{ij}^{\mathcal{BR}} - \mathcal{Q}_{ij}^{max}\right) + max\left(0, -\mathcal{Q}_{ij}^{max} - \mathcal{Q}_{ij}^{\mathcal{BR}}\right) \right)$$

$$C_v = -\sum_{i=1}^{N} \left(max(\mathcal{V}_i - \mathcal{V}^{max}, 0) + max\left(\mathcal{V}^{min} - \mathcal{V}_i, 0\right) \right) \quad (3.26)$$

where $\mathcal{D}_l$ is of node cell *l* obtained by (3.20). Active and reactive power imbalances are $\Delta\mathcal{P}$ and $\Delta\mathcal{Q}$, respectively. The first term of (3.19), $w_l\mathcal{D}_l$, represents the load pick-up with its priority weight. C_p and C_q are penalty terms for active and reactive power imbalance, obtained by (3.21) and (3.22), respectively. $\Delta\mathcal{P}$ and $\Delta\mathcal{Q}$ are computed by (3.23) and (3.24), respectively. C_b is the penalty term for the branch limit violation, calculated by (3.25). C_v is a penalty term for the voltage limit violation, calculated by(3.26). ∂_p and ∂_q are thresholds to maintain power imbalance within a permissible range. η is a penalty factor when power imbalance is greater than a threshold.

3.5 Deep Reinforcement Learning Algorithm for Service Restoration

Reinforcement learning (RL) concerns about decision making, and how intelligent agents take actions in an environment to maximize the cumulative reward [27]. The agent interacts with the environment in discrete time steps, and receives the state of an environment, based on which

the agent takes action to alter the state of the environment. Then the environment will send the agent a reward for the current time step, and the state for the next time step. The primary purpose of RL is to identify the best strategy that yields the highest long-term reward through the best combination of actions. A RL algorithm can tackle problems expressed as MDP. In Section III, the MG formation-based service restoration problem has been designed as an MDP. The optimal solution of this problem can then be identified using the Deep Q-learning algorithm.

3.5.1 Deep Q-Learning

The deep Q-learning algorithm is the core concept in RL, and it takes advantage of the strength of deep learning to improve the learning capability [29]. A deep Q-network (DQN) is utilized to approximate Q-values (the estimated optimal future values) that the agent will learn. The input of a DQN is the state of the environment, its outputs are Q-values for available actions, and these Q-values are updated iteratively. For a policy φ, which is a neural network, and maps its input to output, the Q-value function $\mathcal{Q}^{\varphi}(s_{m,t}, a_{m,t})$ is formulated as follows [30]:

$$\begin{aligned}\mathcal{Q}^{\varphi}(s_{m,t}, a_{m,t}) &= \mathbb{E}\left[\sum_{t'=t}^{T} \gamma^{t'-t}\left[r_{m,t'}(s_{m,t'}, a_{m,t'})\right]\right] \\ &= \mathbb{E}\left[r_{m,t} + \gamma \mathcal{Q}^{\varphi}(s_{m,t+1}, \varphi(s_{m,t+1})\right]\end{aligned} \tag{3.27}$$

where $\mathcal{Q}^{\varphi}(s_{m,t}, a_{m,t})$ is the expected Q-value for state-action pair $s_{m,t}$ and $a_{m,t}$ at time step t. γ is the discount factor. $r_{m,t}$ is the immediate reward at time step t. The Q-value is a measure of the expected cumulative reward that the agent can achieve by taking a specific action $a_{m,t}$ in a particular state $s_{m,t}$, considering the policy φ as the decision-making mechanism. The DRL aims to find an optimal policy φ^* to achieve the maximum expected cumulative reward. In a DQN, the neural network with parameters ϑ, $\mathcal{Q}(s_{m,t}, a_{m,t}|\vartheta)$, is trained to minimize the following loss function, $\mathcal{L}(\vartheta)$, known as a mean-squared Bellman error [30]:

$$\mathcal{L}(\vartheta) = \left[r_{m,t} + \gamma \max_{a_{m,t+1}} \mathcal{Q}(s_{m,t+1}, a_{m,t+1}|\vartheta) - \mathcal{Q}(s_{m,t}, a_{m,t}|\vartheta)\right]^2 \tag{3.28}$$

where 1st term represents the immediate reward obtained by the agent for taking action $a_{m,t}$ in

state $s_{m,t}$, the 2nd term reflects the estimated future rewards that the agent can obtain by selecting the best action in the next state, and the 3rd term represents the current estimated Q-value for the current state-action pair ($s_{m,t}$, $a_{m,t}$),obtained from the neural network with parameters ϑ.

By minimizing the loss function in (3.28(**3.27**), a DQN learns to produce Q-values, leading to proper selection of actions. To minimize this loss, the Adam optimization algorithm is used as follows:

$$\vartheta \leftarrow Adam(\vartheta, \nabla_{\vartheta}\mathcal{L}(\vartheta)) \quad (3.29)$$

where ∇_{ϑ} is the policy gradient.

3.5.2 Enhance learning process of deep reinforcement learning

One essential part of DRL is to ensure the Q-network learn appropriate reactions in the MDP. Three most successful approaches are the Epsilon-greedy-based exploration, the fixed Q-network, and the experience replay.

3.5.2.1 Epsilon-greedy-based exploration

Due to the random initialization of weights and biases in the Q-network prior to training, it is challenging to recognize actions that result in the greatest long-term reward. At the start of training, instead of relying solely on the Q-network to select actions, the agent can randomly select actions to explore all potential outcomes and receive a satisfactory reward. After being trained, the agent can then exploit the environment by selecting actions based on the DQN approximation. The epsilon-greedy strategy is an effective way to balance exploration and exploitation in deep reinforcement learning, allowing the agent to efficiently learn and adapt its actions to achieve optimal performance in the environment. The agent makes random action choices with a probability of epsilon (ε), allowing it to explore different actions and gather information about their associated rewards and consequences. The exploration rate (ε) can be adjusted using an exponential decay, and its value gradually decreases over the course of Q-network training. At each time step, the agent generates a random number between 0 and 1. If the generated number is below the exploration rate, the agent selects the action with the highest Q-value; otherwise, the agent randomly selects an action. The exploration rate ε is formulated by

$$\varepsilon = \varepsilon_F + (\varepsilon_{int} - \varepsilon_F) * e^{-\varepsilon_{decay} * episode} \quad (3.30)$$

where ε_F, ε_{int}, and ε_{decay} are the final, initial, and decay rate of exploration, respectively. $episode$ is the episode number.

3.5.2.2 Fixed Q-network

Determining the maximum Q-value of the next state and the Q-value of the current state using the same Q-network during an update process and loss calculation may cause overestimation in deep Q-learning. To address this concern, a separate Q-network, known as the target Q-network, is established to obtain the Q-value of the next state. The target Q-network has the same structure and parameters as the Q-network, and it is periodically updated with the Q-network parameters during training.

$$\mathcal{L}(\vartheta) = \begin{cases} \left[r_{m,t} - Q\left(s_{m,t,} a_{m,t} | \vartheta\right)\right]^2 & t = T \\ \left[r_{m,t} + \gamma \max_{a_{m,t+1}} Q^{Target}\left(s_{m,t+1}, a_{m,t+1} | \vartheta^{Target}\right) - Q\left(s_{m,t,} a_{m,t} | \vartheta\right)\right]^2 & t \neq T \end{cases} \quad (3.31)$$

where Q^{Target} is the expected Q-value for the target Q-network. ϑ^{Target} are the neural network parameters for the target Q-network.

3.5.2.3 Experience replay and multi-buffers

The DQN can be trained based on prior experiences. For this purpose, an experience replay mechanism with memory and replay components is employed. This mechanism stores the agent's experiences (the state, action, reward, and next state at time step t) in the memory. Once enough experiences have been stored, the replay process is initiated, and a random selection of experiences is drawn from the memory. This helps to remove any bias due to correlations between data samples. The learning of DQN also relies heavily on the stored experiences, so aligning experiences with high reward values can enhance its learning and lead to improved selection of actions. As a result, a multi-buffer approach with two memories is employed. The first memory

(*memo1*), denoted as the "original memory," is used to store all the experiences collected during the training process. The second memory (*memo2*), referred to as the "reward-based memory," is specifically designed to store experiences with high reward values extracted from the original memory. Subsequently, the Q-network is trained using mini-batch that is generated from two separate memories, *memo1* and *memo2*. During the training process, mini-batch ((3.34)) is randomly sampled from both memories. This allows for a diverse set of experiences to be used for training.

$$memo1 = \left[\dots, \left(s_{m,t}, a_{m,t}, r_{m,t}, s_{m,t+1}\right), \dots\right] \quad (3.32)$$

$$memo2 = \left[\dots, \left(s_{m,t}, a_{m,t}, {r_{m,t}}^{\dagger}, s_{m,t+1}\right), \dots\right] \quad (3.33)$$

$$minibatch = \begin{bmatrix} random.sample(memo1, BatchSize1) \\ random.sample(memo2, BatchSize2) \end{bmatrix} \quad (3.34)$$

The batch sizes, denoted as *BatchSize1* and *BatchSize2*, represent the number of samples used in each training step from the first and second memories, respectively.

3.5.3 Offline Training and Online Applications of the Proposed Method

The framework of the proposed method, including offline training and online applications, is shown in Figure 3.2. During the training phase, the agent interacts with a simulator-based environment that provides feedback (S_t, A_t, r_t, S_{t+1}) based on the agent's actions. The feedback, referred to as experience, is saved in the replay memory and later utilized to train the deep Q-network and adjust parameters of the neural network. The training ends when a set number of steps have been completed and the loss function reaches the threshold. Afterwards, the trained Q-network is saved as the policy Q-network, and used in online applications for service restoration during faults. The input layer of the policy Q-network receives the state of a distribution system, and optimal MGs are formed by selecting actions with the highest Q-values in the output layer of the policy Q-network.

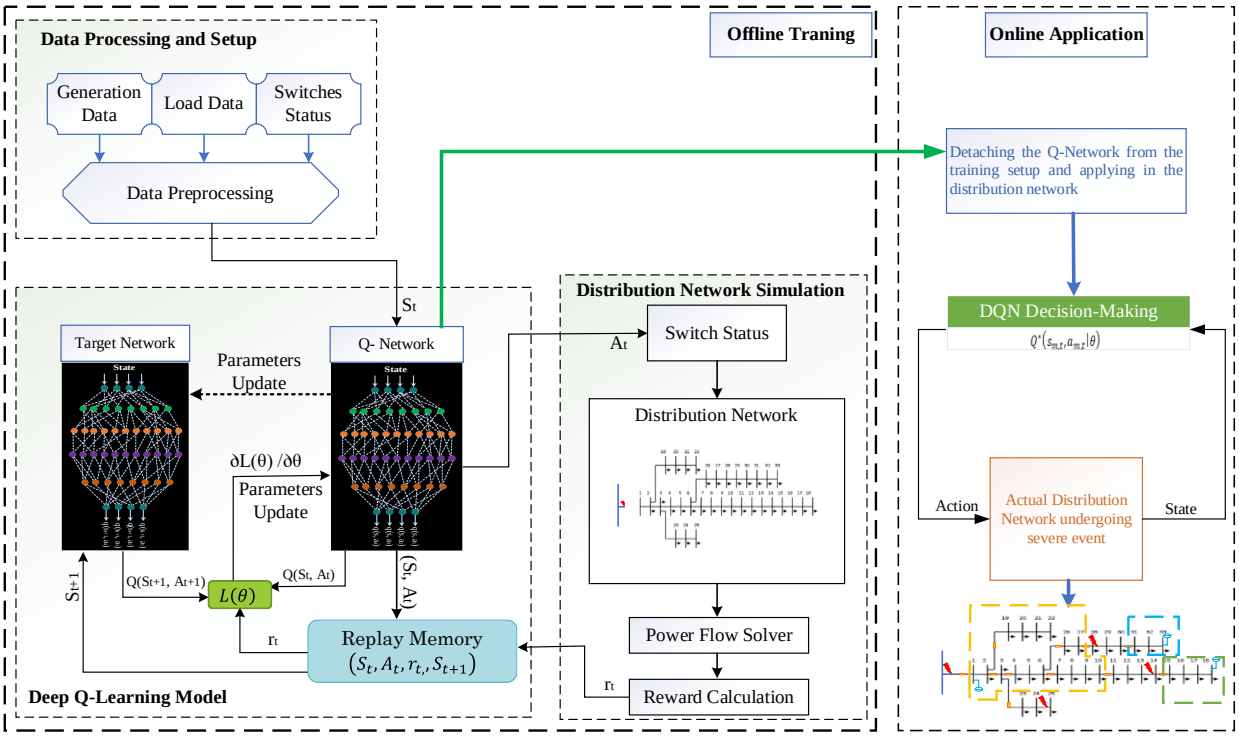

Figure 3.2. The framework of DRL for MG-formation-based service restoration.

3.6 Validation Using IEEE 33-Node Test System

The proposed method is first validated through case studies using the modified IEEE 33-node test system with demand of 3.715 MW and 2.3 MVAr. Pytorch 1.10 and Python 3.9 are used to solve the proposed DRL-based service restoration problem.

3.6.1 The Modified IEEE 33-Node Test System

The modified IEEE 33-node test system, as shown in Figure 3.3, is used in this paper. It contains ten switchable lines and three DGs. Table 3.1 shows parameters of DGs (BSDG means black-start DG, and DDG means dispatchable DG). The node cell concept is used to convert the original 33-node test system into a simplified 14-node-cell system with only switchable lines, as shown in Figure 3.4. The hyper-parameter settings of the DQN for the test system are shown in Table 3.2.

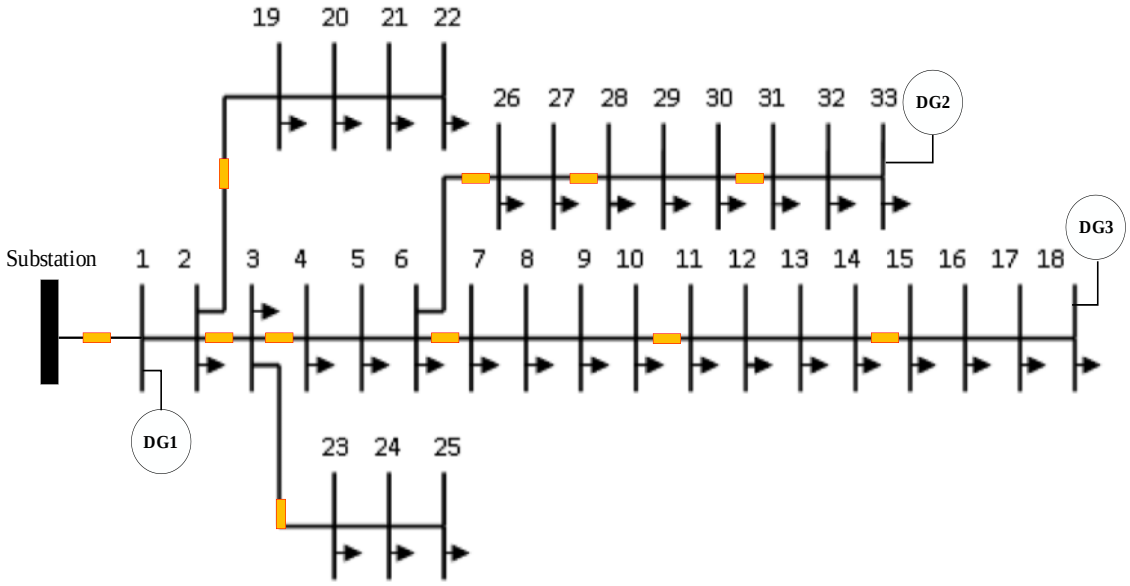

Figure 3.3.The modified IEEE 33-node test system.

Table 3.1. DG parameters for the modified IEEE 33-node test system

Parameters	DG1	DG2	DG3
Node	1	33	18
$P_g^{max}(MW)$	1.5	1.2	1
$P_g^{\min}(MW)$	0.15	0.1	0.1
$Q_g^{max}(MVar)$	1.2	1	0.8
$Q_g^{min}(MVar)$	-0.9	-0.8	-0.8
Status	BSDG/DDG	BSDG/DDG	BSDG/DDG

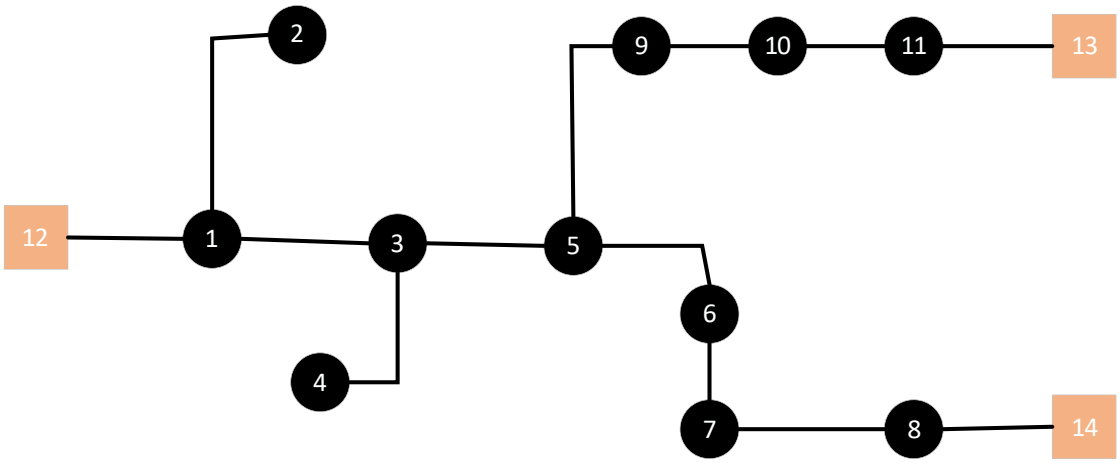

Figure 3.4.The simplified IEEE 33-node test system with 14 node cells.

Table 3.2.Hyper-parameter Settings of the DQN for the Modified IEEE 33-Node Test System

Hyper-parameters	Values
Number of Hidden Layer	3
No. of neurons in hidden layers	50, 50, 50
Learning rate	0.001
Reward discount factor	0.999
Activation function of output layer	Linear
Activation function of hidden layers	ReLU
Optimizer	Adam
Replay memory size	100000
ε_{min}	0.01
ε_{max}	1
ε_{decay}	0.001
Target update	10
Hyper-parameters	Values

3.6.2 Training

The structure of the Q-network is established during training as a neural network with three fully-connected linear layers, all of which have rectified linear units (ReLU). The input layer has the same number of neurons as the state parameters; the hidden layers contain 50 ReLU neurons each; and the output layer has the same number of neurons as the size of the action space.

The training of the proposed method using the test system is performed for 10,000 episodes. The policy Q-network parameters ϑ are initialized with random values. During each episode, an agent selects an action based on the current state of the environment, then this action is applied to the environment, which transitions the agent to a new state, and generates a reward signal. Afterward, the current state, action, reward, and next state are saved in a replay memory. After storing enough experiences, they are used to train the Q-network by minimizing the loss function calculated in (3.28)). The convergence process of the training loss is shown in Figure 3.5. Figure 3.5 shows, as the episode number increases, the average loss of training decreases. After the loss becomes relatively stable with small oscillations, the original DQN can reasonably judge the performance of actions and form dynamic MGs for service restoration during system outages.

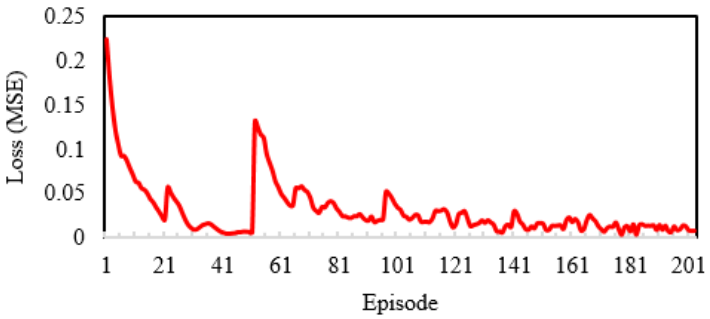

Figure 3.5. The average loss in the training process.

3.6.3 Testing and Implementation

After the DQN is trained properly and learned to make decisions, the following four case studies with different fault scenarios are conducted to test the DQN model and implement it for online applications.

3.6.3.1 Case1

In Case 1, a fault occurs at the substation (Figure 3.6), and the substation must be isolated from the rest of the system. Accordingly, a switch is opened between Node cells 1 and 12 (Figure 3.4) to clear the fault. Note when faulty areas are isolated by opening switches, their connection status in the adjacent matrix will be changed from 1 to 0. In Case 1, before the fault, the connection status between Node cells 1 and 12 was 1 in the adjacent matrix; after the fault, it became 0, i.e., no energization path between the two node cells, so energization agents will not visit node cell 12 during their travels through the system.

As shown in Figure 3.6, three MGs powered by three black-start DGs are formed in Case 1. They can restore 76.31% of active power and 82.61% of reactive power of the entire load, and the computational time for restoration is 0.0004951 seconds. The system is only partially restored as the total capacity of DGs are less than the total load demand. Node numbers and the amount of power restored by each MG are shown in Table 3.3. Table 3.4 shows the output power of DGs when restoring load in Case 1.

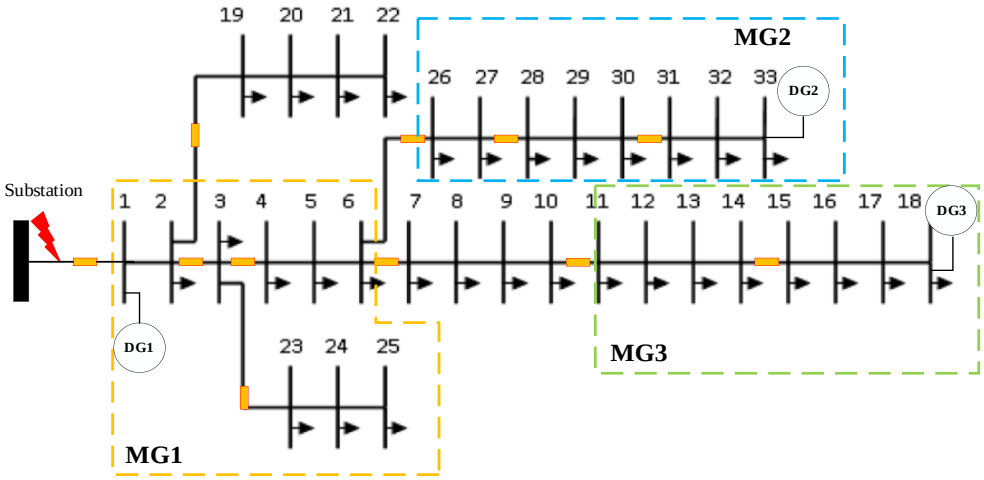

Figure 3.6.Three microgrids formed in the modified IEEE 33-node test system using DQN (Case 1).

Table 3.3. Restored nodes and power of the modified IEEE 33-node test system using DQN (Case 1)

Microgrid	Restored nodes	Restored loads (kW)	Restored loads (kVar)
MG1	1, 2, 3, 4, 5, 6, 23, 24, 25	1360	680
MG2	26, 27, 28, 29, 30, 31, 32, 33	920	950
MG3	11, 12, 13, 14, 15, 16, 17, 18	555	270
$\frac{Total\ resotoredload}{Total\ load}$ *100		76.31%	82.61%
Computational time (Seconds)		0.0004951	

Table 3.4. DG Output Power of the Modified IEEE 33-node Test System (Case 1)

Generation	Active power (kW)	Reactive power (kVar)
DG1	1383.08	694.84
DG2	935.09	967.74
DG3	560.91	276

Figure 3.7 provides a sequential visualization of the restoration path using a learned DQN. The energization agents are coordinated to restore load through the following rules: 1) no loops are formed, 2) the maximum loads are picked up, and 3) DGs energize node cells based on their power capacity. For example, the energization agent connected to Node 18 in Figure 3.6 doesn't have enough capacity to energize Node cell 6 in Step 4. In Step 5, energization agents in yellow

circles can pick up Node cell 2, 4 or 6, and node cell 4 is eventually selected due to the highest load pick-up and the power balance constraints.

The voltage profile of the system after forming three MGs is shown in Figure 3.8. Some nodal voltages are omitted in Figure 3.8 because they are not energized. Phase voltages of all energized buses are within an acceptable range between 0.95 p.u. and 1.05 p.u. Active and reactive power losses for each formed MG are shown in Figure 3.9.

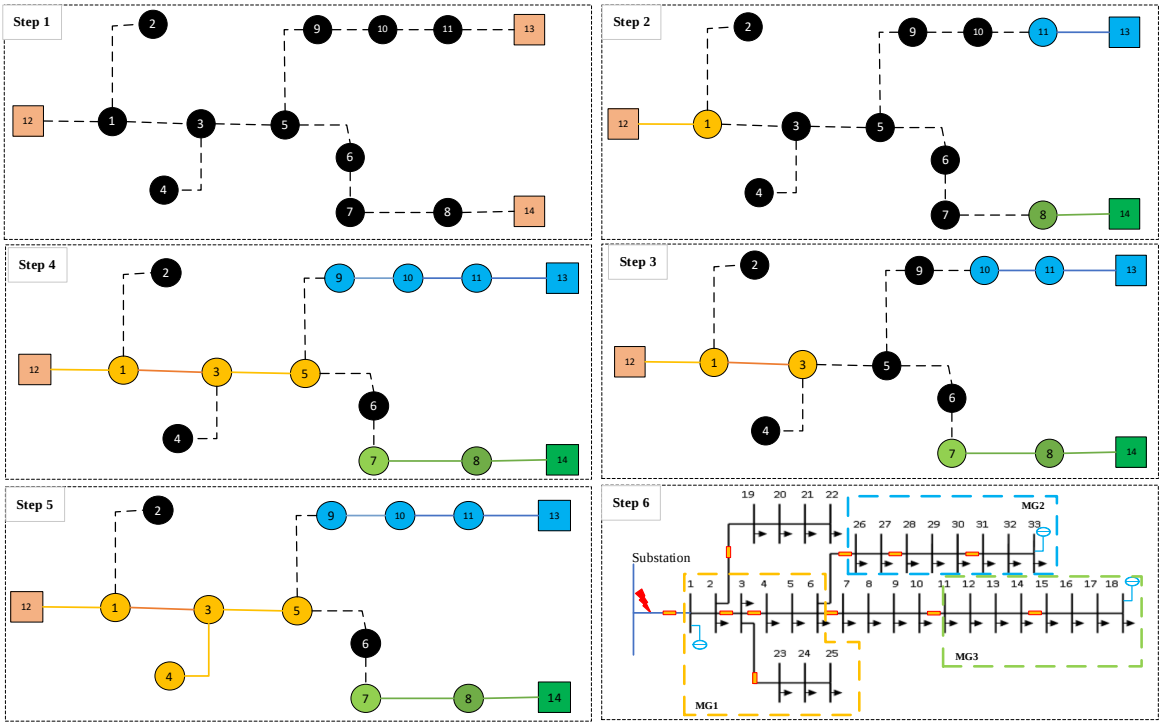

Figure 3.7. The restoration sequences of modified IEEE 33-node system using the DQN in case1.

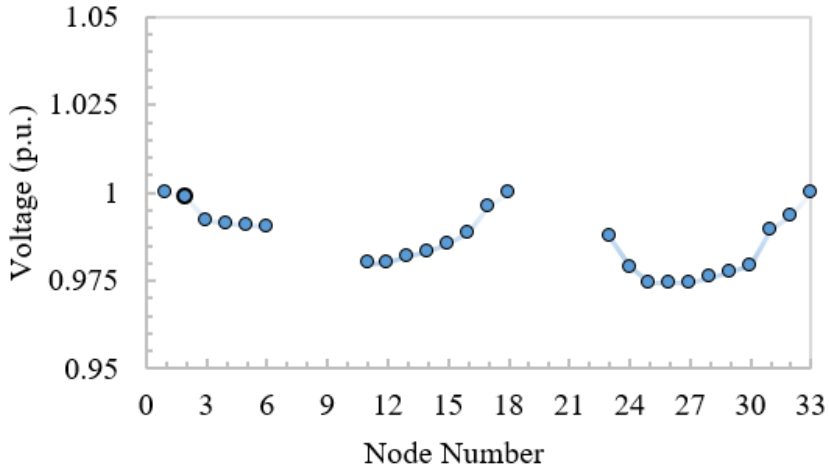

Figure 3.8. Voltage profile of the modified IEEE 33-node test system after forming three MGs (Case 1).

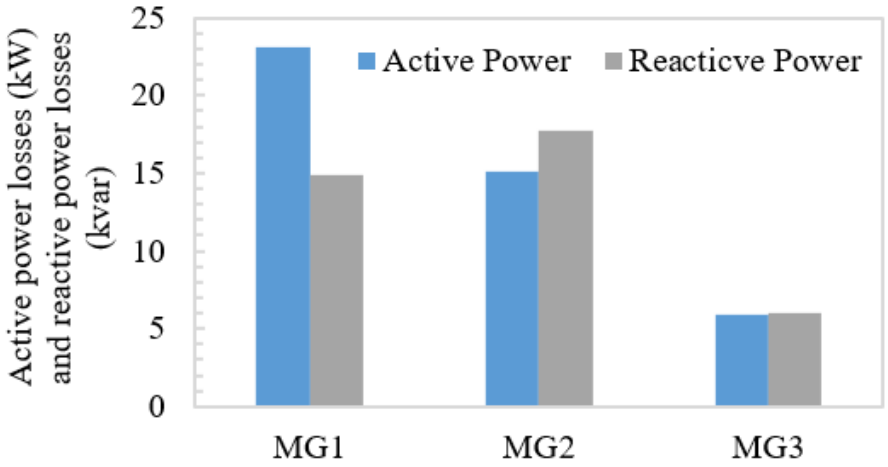

Figure 3.9. Power losses of the modified IEEE 33-node test system in each MG (Case 1).

3.6.3.2 Case2

In Case 2, the substation and the line between nodes 24 and 25 are both faulted in Figure 3.10. Accordingly, Node cells 12 and 4 (Figure 3.4) are isolated from the rest of the system by opening switches, their connection status with the upstream node cells are altered in the adjacent matrix, and they will not be picked up by an energization agent and remain isolated without power during the fault.

The system is partitioned into three MGs as shown in Figure 3.10, each is powered by one black-start DG. Table 3.5 shows the restored node numbers, the amount of active and reactive power restored. Table 3.6 shows the output power of DGs. 74.97% of active power and 80.43% of reactive power for the entire load are restored with an execution time of 0.0004345 seconds. Figure 3.11 and Figure 3.12 indicate the voltage profile of the system after service restoration and power losses in each MG, respectively.

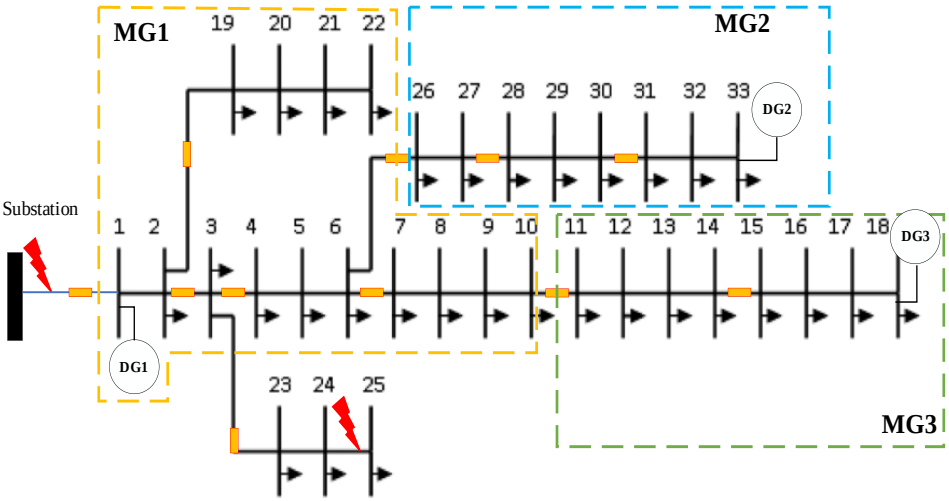

Figure 3.10. Microgrid formation of the modified IEEE 33-node test system using DQN (Case 2).

Table 3.5. Restored Nodes and Power of the Modified IEEE 33-node Test System using DQN (Case 2)

Microgrid	Restored nodes	Restored loads (kW)	Restored loads (kVar)
MG1	1, 2, 3, 4, 5, 6, 7, 8, 9, 10, 19, 20, 21, 22	1310	630
MG2	26, 27, 28, 29, 30, 31, 32, 33	920	950
MG3	11, 12, 13, 14, 15, 16, 17, 18	555	270
$\frac{Total\ resotoredload}{Total\ load}$ *100		74.97%	80.43%
Computational time (Seconds)		0.0004345	

Table 3.6. DG output power of the modified IEEE 33-node test system (Case 2)

Generation	Active power (kW)	Reactive power (kVar)
DG1	1325.07	640.73
DG2	935.09	967.74
DG3	560.91	276

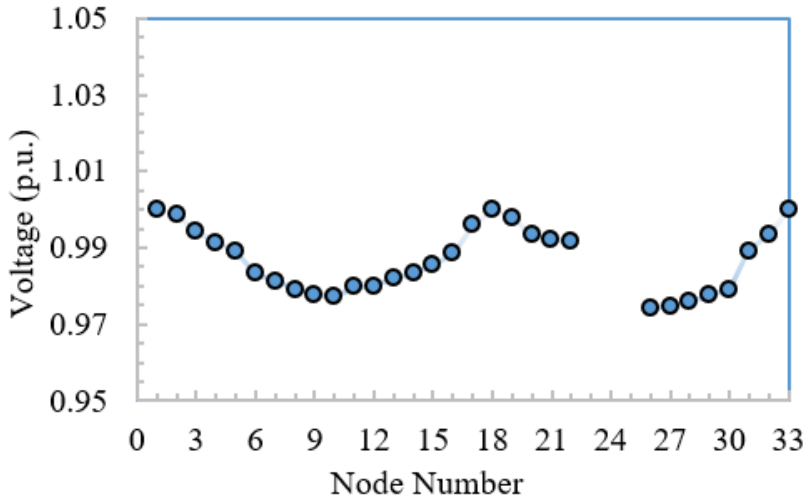

Figure 3.11. Voltage profile of the modified IEEE 33-node test system after forming three MGs (Case 2).

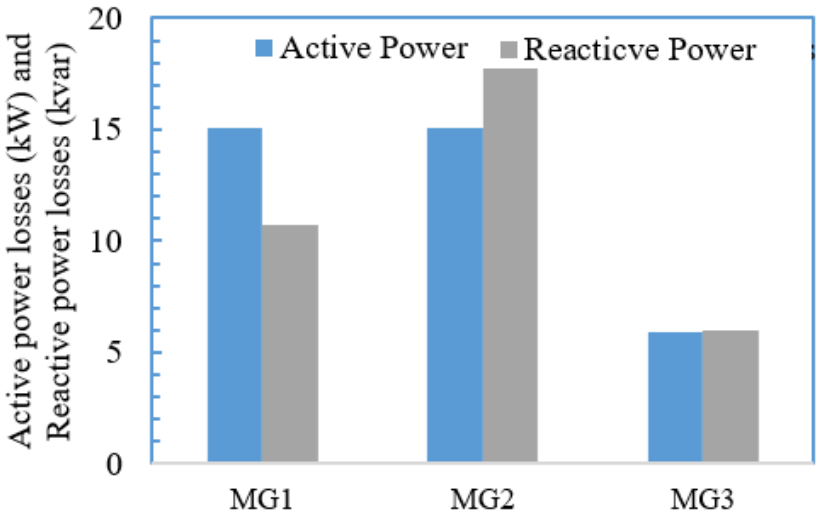

Figure 3.12. Power losses of the modified IEEE 33-node test system in each MG (Case 2).

3.6.3.3 Case3

In Case 3, the substation and DG3 connected to node 18 each have a fault (Figure 3.13), and they are disconnected from the rest of the system by opening switches. Based on available two black-start DGs, DG1 and DG2, 61.37 % of active power and 70.87 % of reactive power for the entire load are restored by forming two MGs in Figure 3.13. The computational time is 0.0004035 seconds in Case 3. Table 3.7 shows the restored node numbers and active and reactive power restored. Table 3.8 shows the output power of DGs in Case 3. Figure 3.14 and Figure 3.15 show

the voltage profile of the system after service restoration and power losses in each MG, respectively.

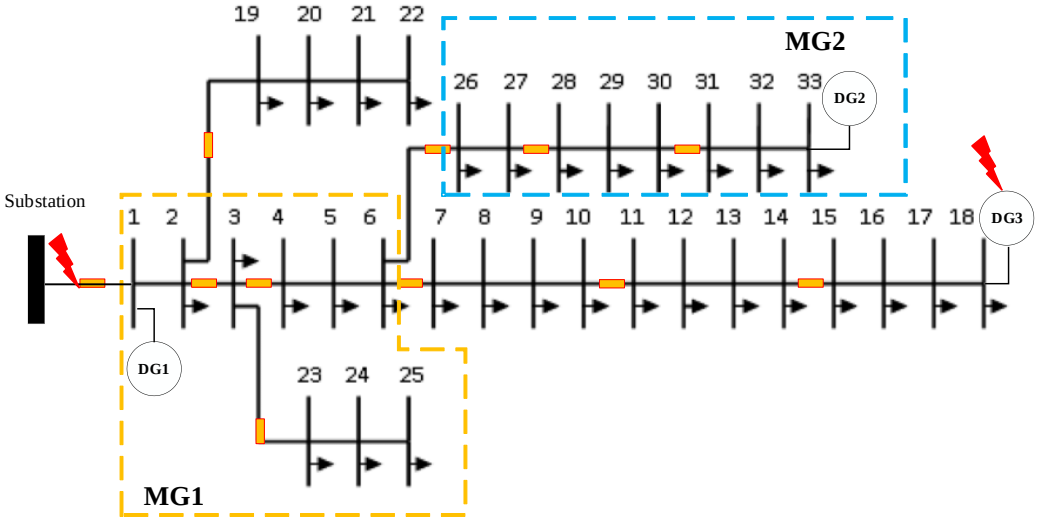

Figure 3.13. Microgrid formation of modified IEEE 33-node system using DQN for Case3.

Table 3.7. Restored nodes and power of the modified IEEE 33-node test system using DQN (Case 3)

Microgrid	Restored Nodes	Restored loads (kW)	Restored loads (kVar)
MG1	1, 2, 3, 4, 5, 6, 23, 24, 25	1360	680
MG2	26, 27, 28, 29, 30, 31, 32, 33	920	950
$\frac{Total\ resotoredload}{Total\ load}$ *100		61.37 %	70.87%
computational time (s)		0.0004035	

Table 3.8. DG output power of the modified IEEE 33-node test system (Case 3)

Generation	Active power (kW)	Reactive power (kVar)
DG1	1383.08	694.83
DG2	935.09	967.74
DG3	-	-

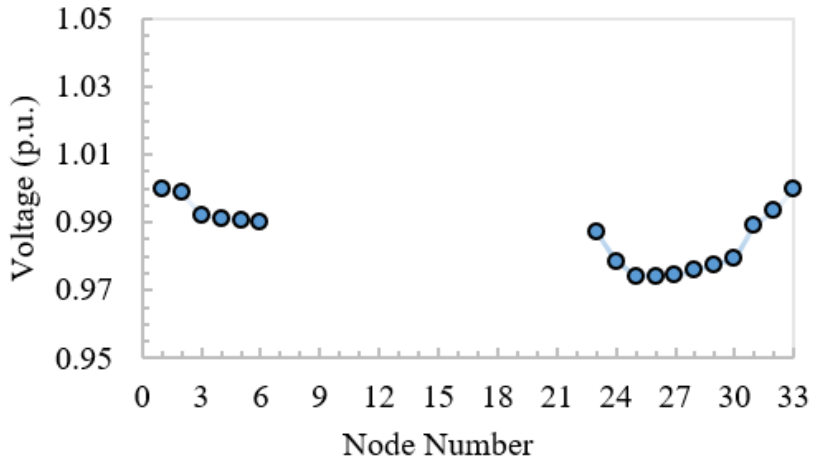

Figure 3.14.Voltage profile of the modified IEEE 33-node test system after forming two MGs (Case 3).

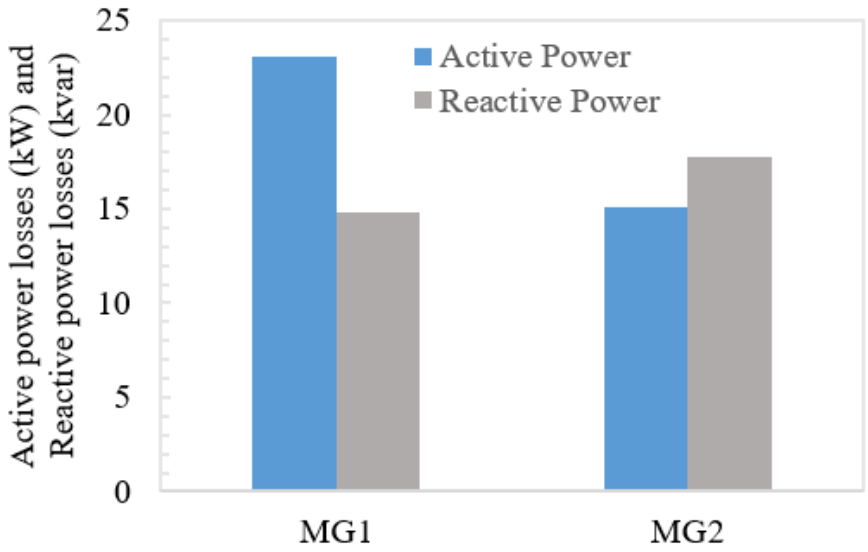

Figure 3.15. Power losses of the modified IEEE 33-node test system in each MG (Case 3).

3.6.3.4 Case4

In Case 4, four faults occur at the substation, the line between nodes 24 and 25, the line between nodes 13 and 14, and the line between nodes 28 and 29 in Figure 3.16. Accordingly, node cells 12, 4, 7, and 10 in Figure 3.4 are isolated from the rest of the system by opening switches, and they will not be selected by energization agents. Using three black-start DGs, three MGs are formed to restore loads in Figure 3.16. The restored node numbers and restored active and reactive power are shown in Table 3.9. Table 3.10 shows the output power of DGs. 57.07% of active power and 42.61% of reactive power of the entire load are restored with the computational time of

0.0004714 seconds. The voltage profile of the system after restoration is shown in Figure 3.17. Power losses in each MG are shown in Figure 3.18.

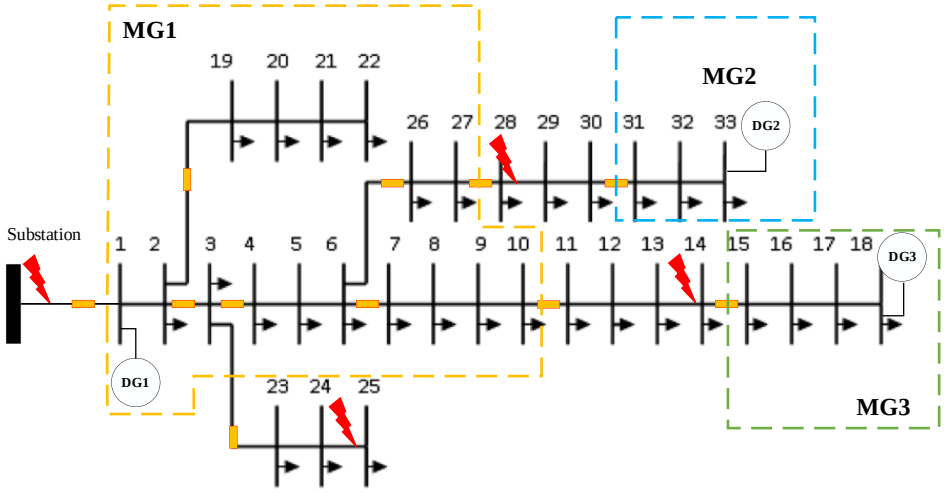

Figure 3.16. Microgrid formation of the modified IEEE 33-node test system using DQN (Case 4).

Table 3.9. Restored nodes and power of the modified IEEE 33-node test system using DQN (Case 4)

Microgrid	Restored Nodes	Restored loads (kW)	Restored loads (kVar)
MG1	1, 2, 3, 4, 5, 6, 7, 8, 9, 10, 19, 20, 26, 27	1430	680
MG2	31, 32, 33	420	210
MG3	15, 16, 17, 18	270	90
$\frac{Total\ resotoredload}{Total\ load}$ *100		57.07%	42.61%
computational time (Seconds)		0.0004714	

Table 3.10. DG output power of the modified IEEE 33-node test system (Case 4)

Generation	Active power (kW)	Reactive power (kVar)
DG1	1449.28	693.34
DG2	420.52	210.78
DG3	270.40	90.40

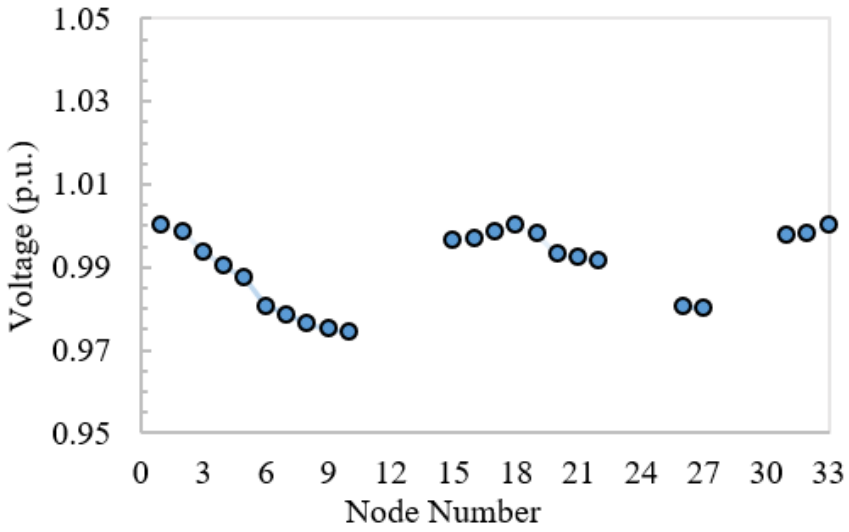

Figure 3.17. Voltage profile of the modified IEEE 33-node test system after forming three MGs (Case 4).

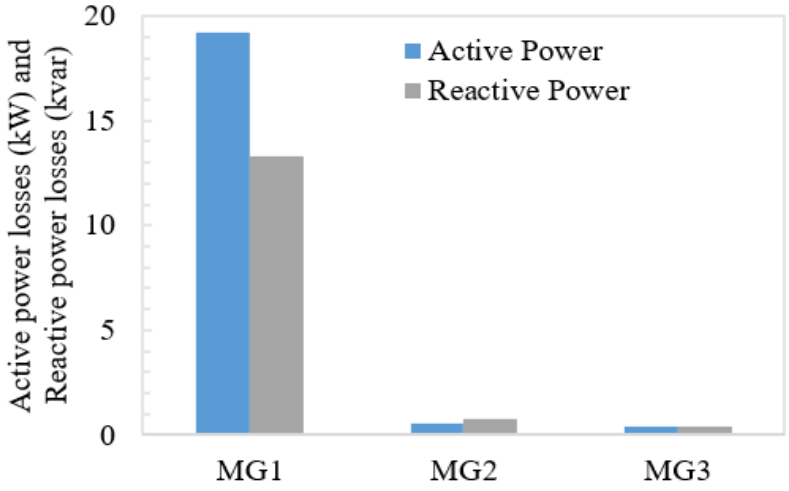

Figure 3.18. Power losses of the modified IEEE 33-node test system in each MG (Case 4).

3.6.4 Performance Comparison with Existing Methods

The proposed restoration method is compared to three existing methods in [10], [11] and [15] for critical loads restoration through MG formation. Ref. [10] uses normal single-commodity flow-based radiality constraints, requires that each subgraph must be a connected graph, and the quantity of closed branches must match the number of subgraphs subtracted from the total number of nodes. Ref. [11] employs the node clustering method to form MGs, allocates each node to a DG, and ensure constraints for connectivity, branch-node, and clustering nodes are met. Ref. [15]

uses the directed multicommodity flow-based model of the spanning tree constraints to form MGs. All three models in [10], [11] and [15] are formulated as a MILP problem and solved using commercial optimization solvers.

To compare the proposed method in this paper with three existing methods in [10], [11] and [15], a case study in [15] with the IEEE 33-node test system is used. The system topology, including information of the fault location, and the placement of DGs and switches, can be found in [15]. Table 3.11 shows the comparison regarding restored loads and computational time. It is found that the proposed method can restore more loads than the methods in [10] and [11], but is on par with the method in [15]. However, from the computational time perspective, the proposed method outperforms all three existing methods. Table 3.12 shows the number of variables and constraints in MG formation models in [11], [10], and [15], in which N, N_r, N_g, N_o, N_c, L, L_o, and L_c represent the total nodes, substation nodes, DG nodes, faulted open nodes, faulted closed nodes, branches, faulted open branches, and faulted close branches, respectively. For a large system, a large number of variables/ constraints are involved, which can greatly increase the computational time and makes their practical use infeasible. However, the proposed method is model-free, can be trained offline and used online to make quick and efficient decisions.

Table 3.11.Comparison among the proposed method and three existing methods in [10], [11], and [15] for service restoration using the modified IEEE 33-node test system

Model	Restored load (kW)	Restoration ratio (%)	Computational time (s)
[11]	1500	40.37%	0.56
[10]	1820	49%	0.75
[15]	2575	69.31%	0.49
The proposed method	2575	69.31%	0.003912

Table 3.12. The number of variables and constraints for three existing methods [15]

	Model [11]	Model [10]	Model [15]
Number of binary Variables	$2N(N_r + N_g) + N + L$	$N + L$	$2N + 3L$
Number of continuous variable	$4N(N_r + N_g)$	$N + 3(N_r + N_g) + 3L$	$2N.L + N + 2(N_r + N_g) + L$
Number of constraints	$(11N - 2N_r - 2N_g + 1)(N_r + N_g) + 2N + N_o + N_c + L + L_o + L_c$	$3N + 3(N_r + N_g) + N_o + N_c + 5L + L_o + L_c + 1$	$N^2 + 2N.L + 3N + 2(N_r + N_g) + N_o + N_c + 3L + L_o + L_c + 1$

3.7 Validation Using a Real Large Distribution Network

The proposed method is further validated using a real 404-node distribution system. This system is one substation within a large distribution network operated by Saskatoon Light and Power in Saskatoon, Canada. The system model was developed using practical data of lines and load of two feeders within the substation provided by Saskatoon Light and Power. The feeders are supplied by the 25/14.4 kV, 33.3 MVA substation. The demand for active and reactive power are 11.605 MW and 7.192 MVar, respectively. The system model in this study was modified with ten black-start DGs, and DG parameters are shown in Table 3.13. The original 404-node system is converted to a simplified system with only switchable lines through the node cell concept, as shown in Figure 3.19. The switch locations are assumed in the system model. To assess online performance of the proposed algorithm after training, three scenarios are conducted for this system using Python and OpenDSS.

Table 3.13.DG parameters in the modified 404-node system model

Name	Node	$P_g^{max}/P_g^{\min}(MW)$	$Q_g^{max}/Q_g^{min}(MVar)$	Status
DG1	1	1.05/0.1	0.8/-0.5	BSDG/DDG
DG2	313	0.9/0.09	0.7/-0.5	BSDG/DDG
DG3	82	0.9/0.09	0.7/-0.5	BSDG/DDG
DG4	147	1.05/0.1	0.8/-0.5	BSDG/DDG
DG5	230	1.2/0.12	0.9/-0.6	BSDG/DDG
DG6	101	1.2/0.12	0.9/-0.6	BSDG/DDG
DG7	183	1.5/0.15	1.2/-0.9	BSDG/DDG
DG8	391	0.5/0.05	0.4/-0.2	BSDG/DDG
DG9	337	0.5/0.05	0.4/-0.2	BSDG/DDG
DG10	279	1.5/0.15	1.2/-0.9	BSDG/DDG

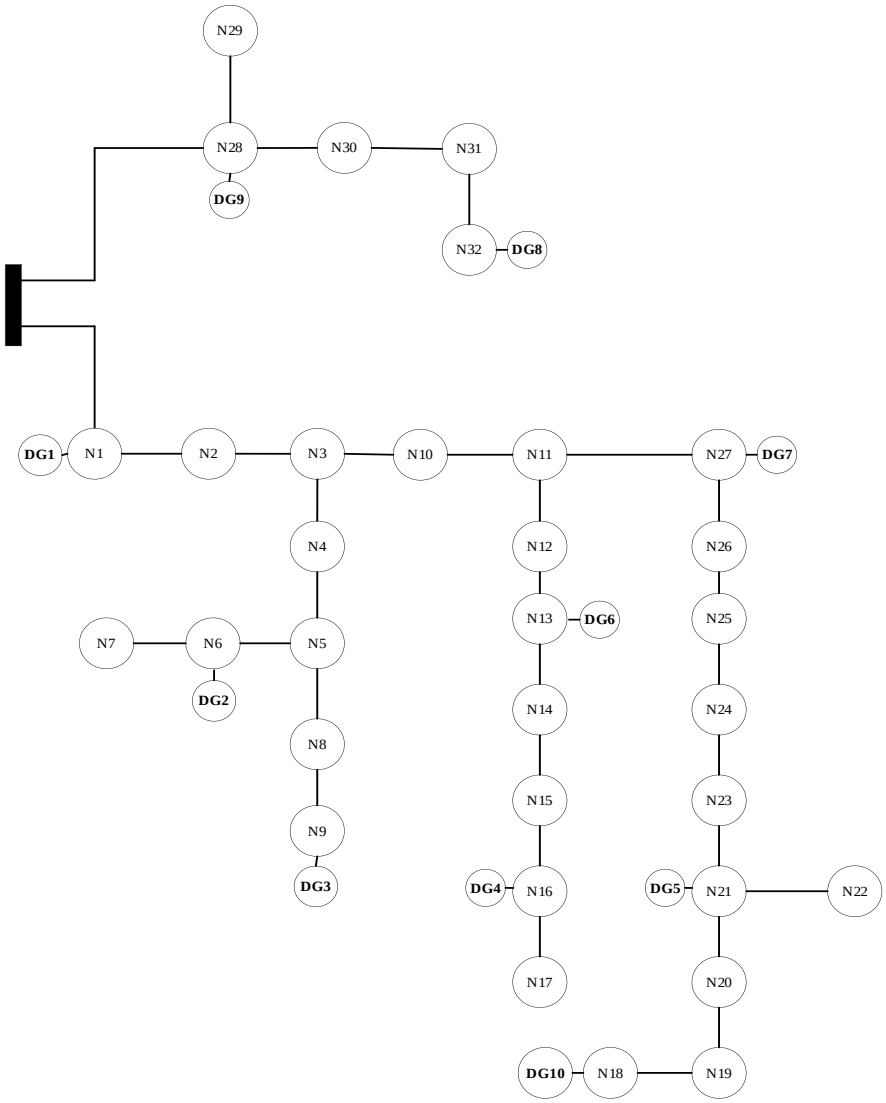

Figure 3.19. The simplified system with 32 node cells through the node cell concept.

3.7.1 Scenario 1

In Scenario 1, a fault occurs at the substation as shown in Figure 3.20. To isolate the affected region, the substation switches are activated and isolate the fault. Ten MGs have been formed (Figure 3.20). Restoration agents energize node cells while ensuring operational and topological constraints are met.

Table 3.14 shows the restored node cell numbers, and 80.66% restored power of the total load with a computational time of 0.013406 seconds. Due to security and power flow constraints, 19.34% of the load has been shed. The DG output power are shown in Table 3.15. The voltage

profile of the restored system is shown inFigure 3.21. Voltage profile of the 404-node system after restoration (Scenario 1).Figure 3.21, and all bus voltages are within acceptable limits. Power losses within each formed MG are shown in Figure 3.22.

Table 3.14. Restored node cells and power of the modified 404-node system using DQN (Scenario 1)

Microgrid	Restored node cells	Restored loads (kW)	Restored loads (kVar)
MG1	N1, N2, N3, N4, N5, N10,	1041.2500	645.3088
MG2	N6, N7	795.8125	493.2003
MG3	N8, N9	825.5625	511.6377
MG4	N16, N17	937.1250	580.7780
MG5	N20, N21, N23	1041.2500	645.3089
MG6	N12, N13	1194.4750	740.2614
MG7	N24, N25, N26, N27	1404.9438	870.7086
MG8	N32	446.2500	276.5635
MG9	N28, N30, N31	476.0000	294.9983
MG10	N18	1197.4375	742.1051
$\frac{Total\ resotoredload}{Total\ load}$ *100		80.66%	80.66%
computational time (s)		0.013406	

Table 3.15. DG output power for the modified 404-node system (Scenario 1)

Generation	Active power (kW)	Reactive power (kVar)
DG1	1043.3627	648.6241
DG2	795.8640	493.6421
DG3	826.1352	512.4591
DG4	937.3487	582.1107
DG5	1041.4337	646.9206
DG6	1194.6908	740.5647
DG7	1405.8361	872.0588
DG8	446.2943	277.8089
DG9	476.2291	250.7190
DG10	1197.6440	742.7900

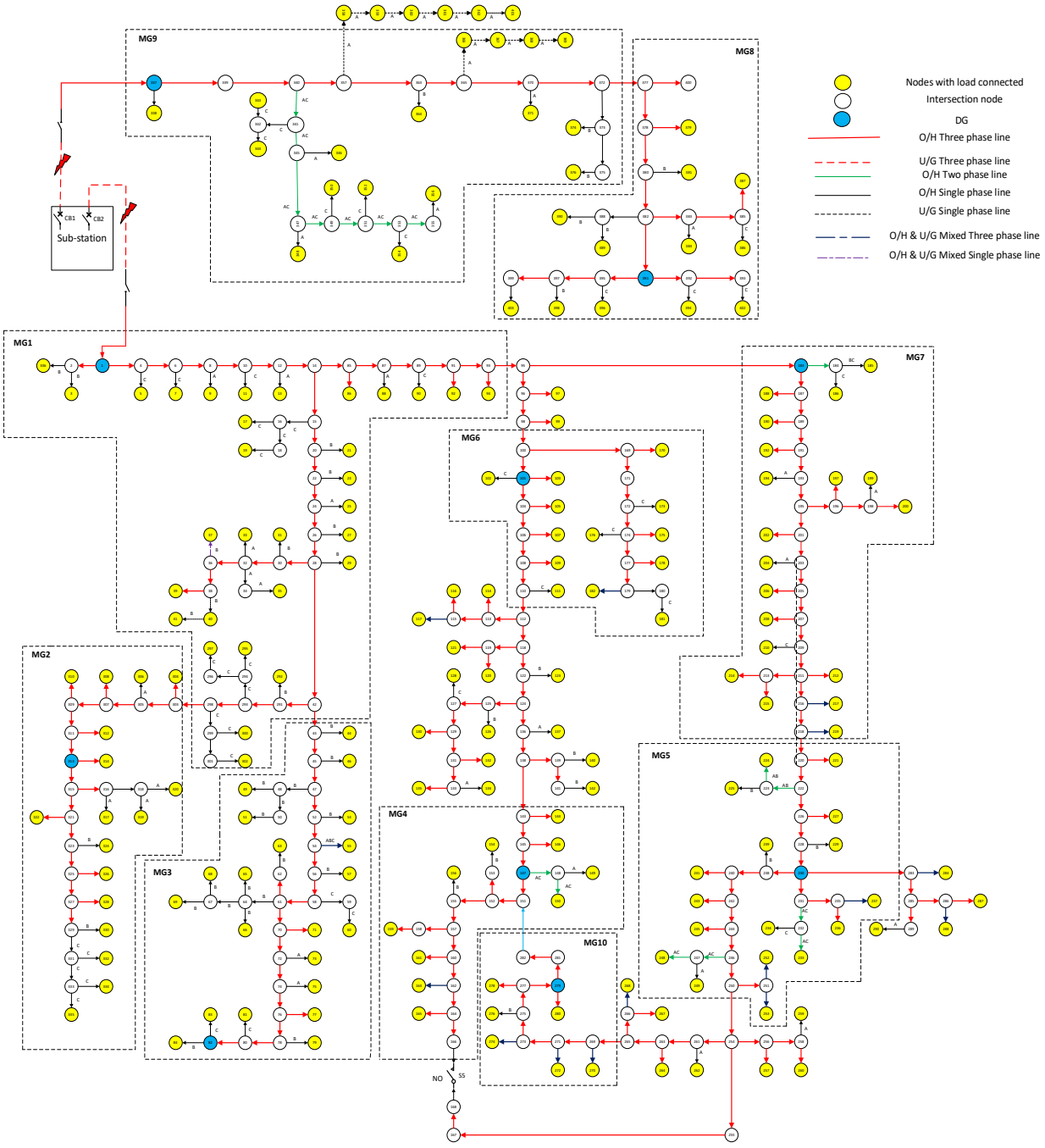

Figure 3.20. Microgrid formation of the 404-node system using DQN (Scenario 1).

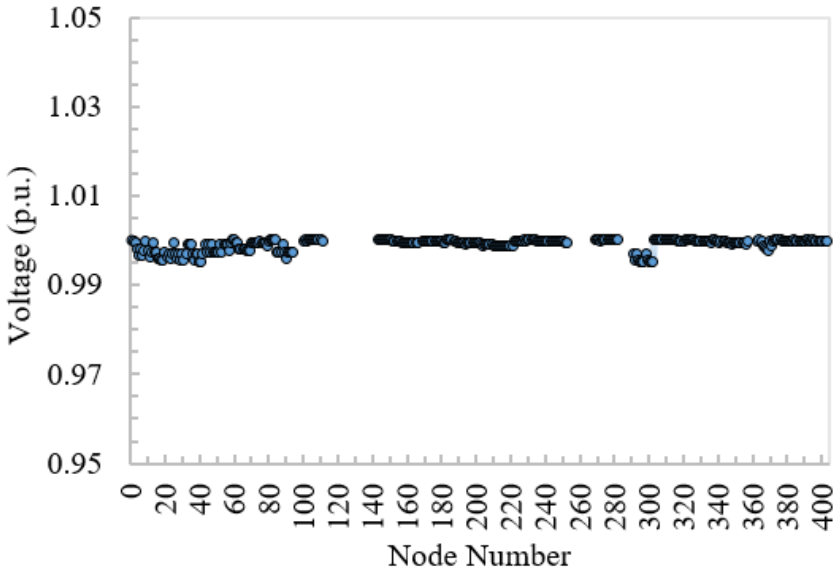

Figure 3.21. Voltage profile of the 404-node system after restoration (Scenario 1).

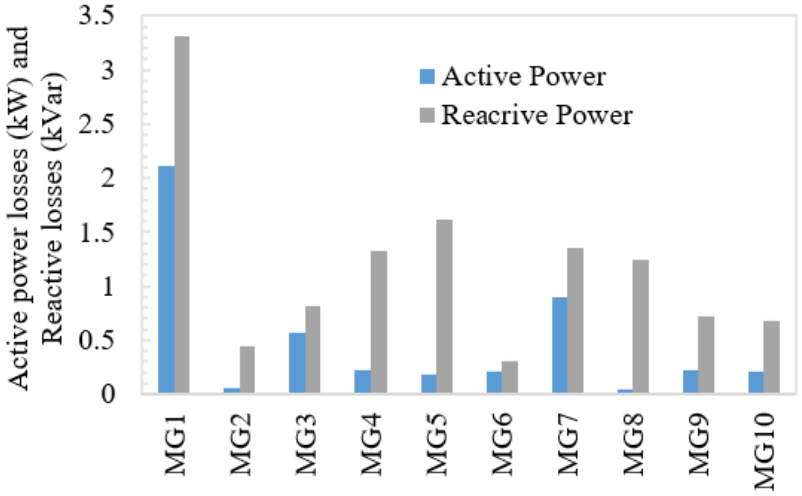

Figure 3.22. Power losses in each MG for the 404-node system (Scenario 1).

3.7.2 Scenario 2

In Scenario 2, 10 faults are applied to the substation and several places in the system as shown in Figure 3.23, and ten MGs are formed. Each MG is energized by a DG. In an effort to restore load, restoration agents work within bounds of the topological and operational constraints to select node cells. Table 3.16 shows the restored node cell numbers, and 63.72% restored power of the total load with a computational time of 0.013716 Seconds. The DG output power are shown

in Table 3.17. The voltage profile following the service restoration is shown in Figure 3.24. Power losses of each formed MG are shown in Figure 3.25.

Table 3.16. The restored node cells and power of the 404-node system using DQN (Scenario 2)

Microgrid	Restored node cells	Restored loads (kW)	Restored loads (kVar)
MG1	N1, N2, N3, N10, N11	699.1250	433.2788
MG2	N4, N5, N6	810.6875	502.4190
MG3	N8, N9	825.5625	511.6377
MG4	N15, N16	699.1250	433.2788
MG5	N21, N22, N23	899.9375	557.7318
MG6	N13, N14	820.8150	508.6877
MG7	N25, N26, N27	594.2563	368.2896
MG8	N32	446.2500	276.5635
MG9	N28, N30	401.6250	248.9048
MG10	N18	1197.4375	742.1051
$\frac{Total\ resotoredload}{Total\ load}$ *100		63.72%	63.72%
computational time (Seconds)		0.013716	

Table 3.17 .DG output power for the 404-node system (Scenario 2)

Generation	Active power (kW)	Reactive power (kVar)
DG1	700.1227	438.2869
DG2	810.8950	503.0603
DG3	826.1352	512.4591
DG4	699.1989	433.8761
DG5	900.0551	560.7991
DG6	820.9023	509.2373
DG7	594.3471	368.8613
DG8	446.2943	277.8089
DG9	401.8250	249.5012
DG10	1197.6440	742.78998

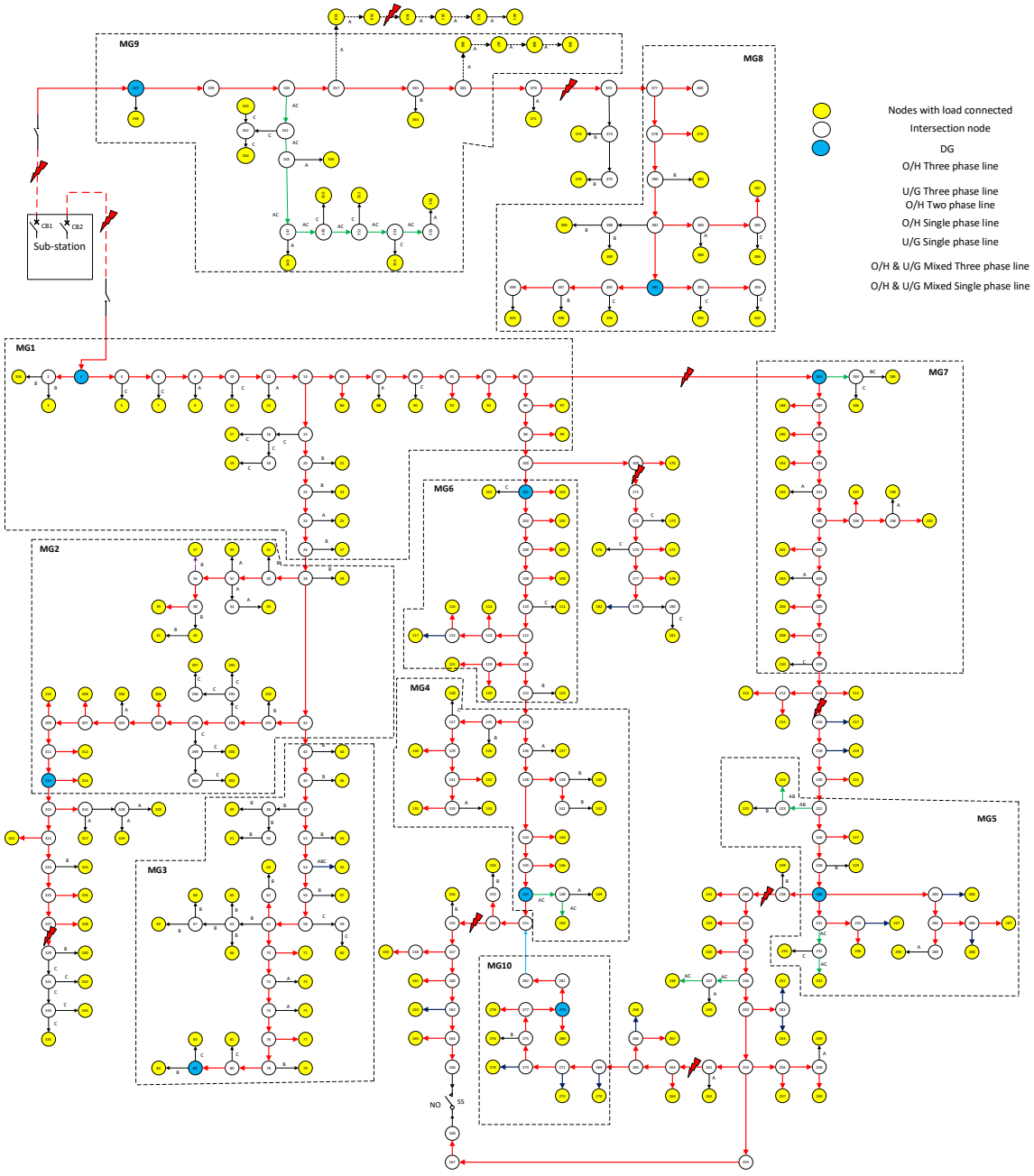

Figure 3.23. Microgrid formation of the 404-node system using DQN (Scenario 2).

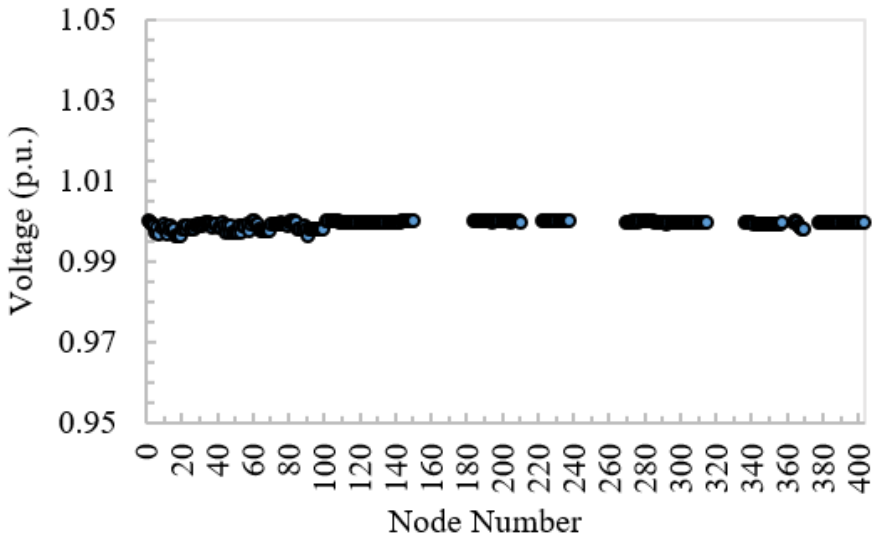

Figure 3.24.Voltage profile of the 404-node system after restoration (Scenario 2).

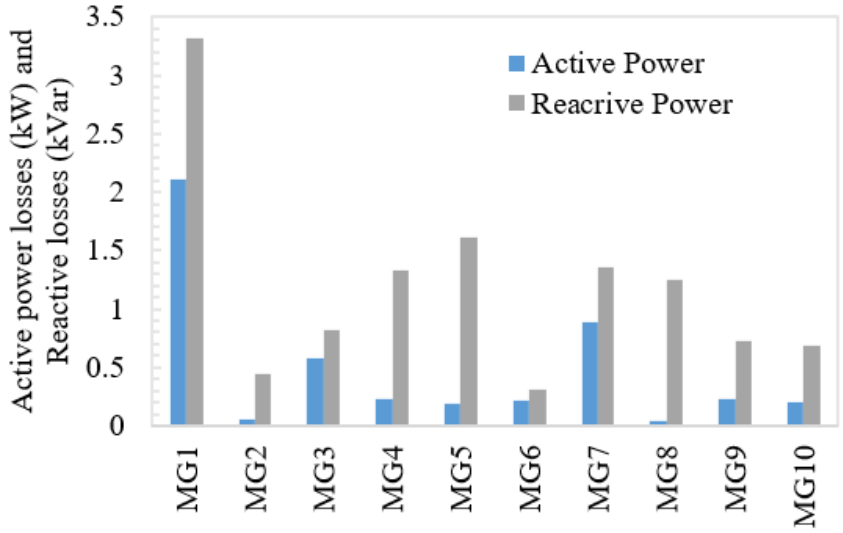

Figure 3.25. Power losses in each MG for the 404-node system (Scenario 2).

3.7.3 Scenario 3

In Scenario 3, a new fault develops at DG3 for Scenario 2, i.e., DG3 has a permanent fault in addition to all faults of Scenario 2. As shown in Figure 3.26, nine MGs are formed using nine black-start DGs in the system. Following DG3's fault, operational boundaries of MG1 and MG2 must be adjusted from Scenario 2 to ensure the maximum load pickup. Table 3.18 shows the restored node cells, and 58.72% restored power of the total load with an execution time of 0.013825 seconds. The DG output power after service restoration is shown in Table 3.19. The

voltage profile after restoration is shown in Figure 3.27. Figure 3.28 shows power losses in each MG.

The proposed MG formation-based service restoration using DRL has shown promising results in a real large 404-node distribution system by efficiently and quickly restoring as many loads as possible. When a new condition arises, MGs can also adjust their boundaries to pick up the maximum amount of load.

Table 3.18. The restored node cells and power of the 404-node system using DQN (Scenario 3)

Microgrid	Restored node cells	Restored loads (kW)	Restored loads (kVar)
MG1	N1, N2, N3, N4, N10, N11	1026.3750	636.0901
MG2	N5, N6, N8	728.8750	451.7161
MG3	N15, N16	699.1250	433.2788
MG4	N21, N22, N23	899.9375	557.7318
MG5	N13, N14	820.8150	508.6877
MG6	N25, N26, N27	594.2563	368.2896
MG7	N32	446.2500	276.5635
MG8	N28, N30	401.6250	248.9048
MG9	N18	1197.4375	742.1051
$\frac{Total\ resotoredload}{Total\ load}$ *100		58.72%	58.72%
computational time (Seconds)		0.013825	

Table 3.19. DG output power for the 404-node system (Scenario 3)

Generation	Active power (kW)	Reactive power (kVar)
DG1	1028.2354	442.0463
DG2	729.0638	452.6724
DG3	-	-
DG4	699.1989	433.8761
DG5	900.0551	560.7991
DG6	820.9023	509.2373
DG7	594.3471	368.8613
DG8	446.2943	277.8089
DG9	401.8250	249.5012
DG10	1197.6440	742.7900

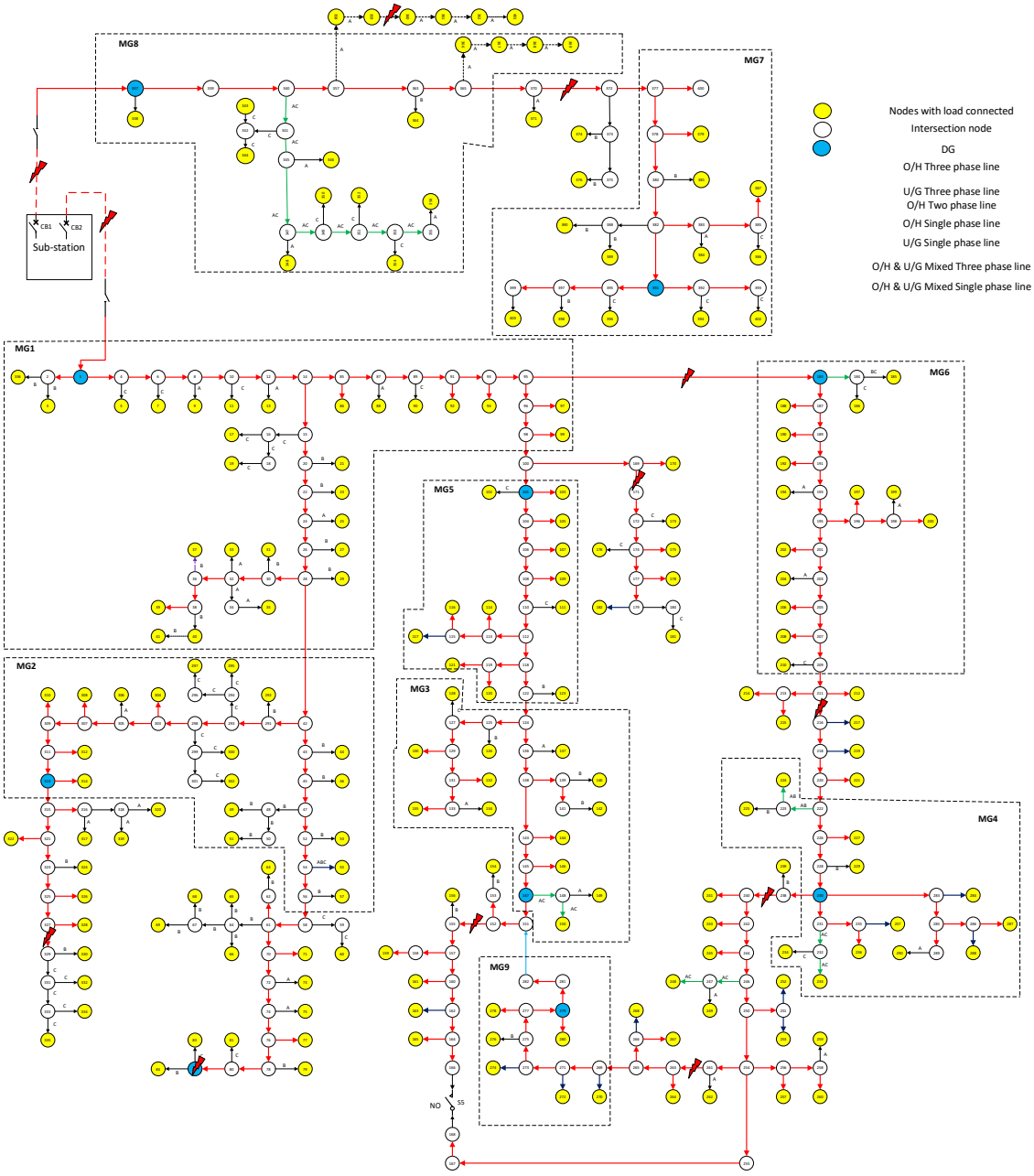

Figure 3.26. Microgrid formation of the 404-node system using DQN (Scenario 3).

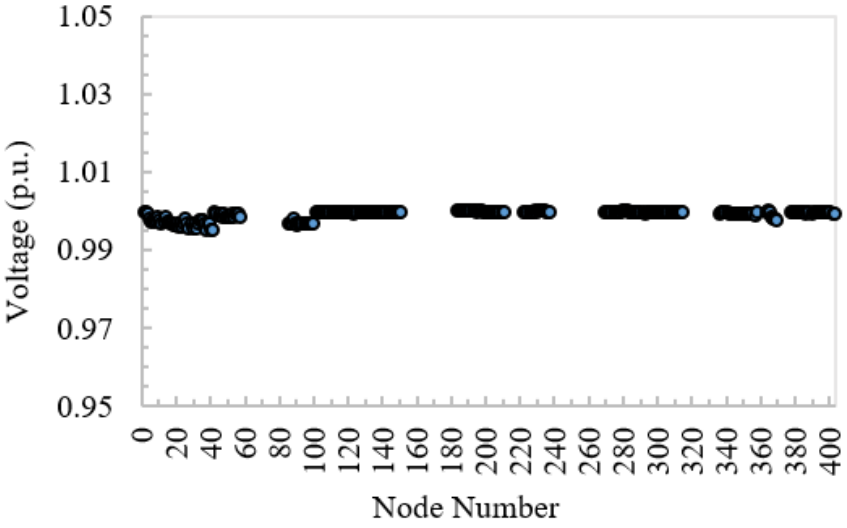

Figure 3.27. Voltage profile of the 404-node system after restoration (Scenario 3).

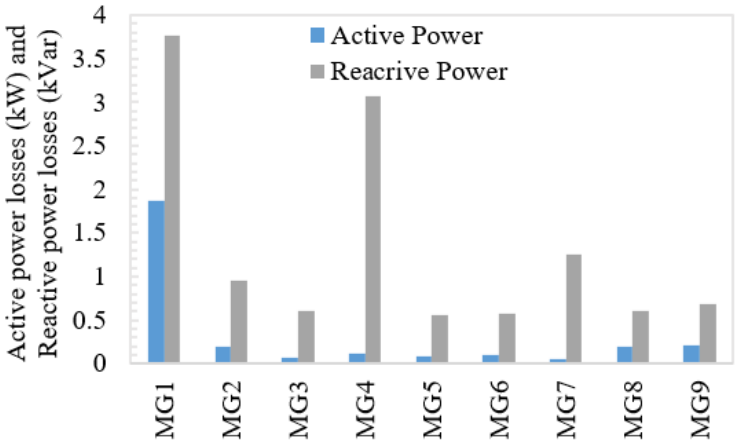

Figure 3.28. Power losses in each MG for the 404-node system (Scenario 3).

3.8 Conclusion

In this paper, a novel dynamic microgrid formation-based service restoration method using deep reinforcement learning for distribution networks is proposed. Through the deep Q-learning technique and a simulator-based environment, the deep reinforcement learning algorithm can effectively learn the optimal control policy and form dynamic microgrids during contingencies for rapid service restoration. It can be trained offline first, and then used in online applications. The proposed method is validated using the modified IEEE 33-node test system and a real large 404-

node distribution system from Saskatoon Light and Power in Saskatoon, Canada. Case studies using a real large distribution system with a very short computational time prove the great potential of the proposed method in large scale distribution grids' online applications. Further development of this method can lead to a powerful tool for electric utilities to realize self-healing and service restoration in distribution grids.

3.9 Appendix

As the first step for a given system, the node cell concept will be used to convert the original system to a simplified system with only node cells and switchable lines. The following two tables show each node cell corresponds to the node numbers of the original system within it for the modified IEEE 33-node test system in Section V, and the large 404-node system in Section VI.

Table 3.20. Node cell mapping for the modified IEEE 33-node test system

Node Cell	Corresponding Nodes
Node cell 1	1, 2
Node cell 2	19, 20, 21, 22
Node cell 3	3
Node cell 4	23, 24, 25
Node cell 5	4, 5, 6
Node cell 6	7, 8, 9, 10
Node cell 7	11, 12, 13, 14
Node cell 8	15, 16, 17, 18
Node cell 9	26, 27
Node cell 10	28, 29, 30
Node cell 11	31, 32, 33

Table 3.21. node cell mapping for the 404-node system

Node Cell	Corresponding Nodes
Node cell 1	1, 2, 3, 336
Node cell 2	4, 5, 6, 7, 8, 9, 10, 11, 12, 13
Node cell 3	14, 15, 16, 17, 18, 19, 20, 21, 22, 23, 24, 25, 26, 27
Node cell 4	28, 29, 30, 31, 32, 33, 34, 35, 36, 37, 38, 39, 40, 41
Node cell 5	291, 292, 293, 294, 295, 296, 297, 298, 299, 300, 301, 302
Node cell 6	303, 304, 305, 306, 307, 308, 309, 310, 311, 312, 313, 314
Node cell 7	315, 316, 317, 318, 319, 320, 321, 322, 323, 324, 325, 326, 327, 328, 329, 330, 331, 332, 333, 334, 335
Node cell 8	42, 43, 44, 45, 46, 47, 48, 49, 50, 51, 52, 53, 54, 55, 56, 57
Node cell 9	58, 59. 60, 61, 62, 63, 64, 65, 66, 67, 68, 69, 70, 71, 72, 73, 74, 75, 76, 77, 78, 79, 80, 81, 82, 83, 84
Node cell 10	85, 86, 87, 88, 89, 90, 91, 92, 93, 94
Node cell 11	95, 96, 97, 98, 99
Node cell 12	169, 170, 171, 172, 173, 174, 175, 176, 177, 178, 179, 180, 181, 182
Node cell 13	101, 102, 103, 104, 105, 106, 107, 108, 109, 110, 111
Node cell 14	112, 113, 114, 115, 116, 117, 118, 119, 120, 121, 122, 123
Node cell 15	124, 125, 126, 127, 128, 129, 130, 131, 132, 133, 134, 135, 136, 137, 138, 139, 140, 141, 142
Node cell 16	143, 144, 145, 146, 147, 148, 149, 150
Node cell 17	151, 152, 153, 154, 155, 156, 157, 158, 159, 160, 161, 162, 163, 164, 165, 166
Node cell 18	269, 270, 271, 272, 273, 274, 275, 276, 277, 278, 279, 280, 281, 282
Node cell 19	254, 255, 256, 257, 258, 259, 260, 261, 262, 263, 264, 265, 266, 267, 268
Node cell 20	238, 239, 240, 241, 242, 243, 244, 245, 246, 247, 248, 249, 250, 251, 252, 253
Node cell 21	230, 231, 232, 233, 234, 235, 236, 237
Node cell 22	283, 284, 285, 286, 287, 288, 289, 290
Node cell 23	222, 223, 224, 225, 226, 227, 228, 229
Node cell 24	211, 212, 213, 214, 215, 216, 217, 218, 219, 220, 221
Node cell 25	201, 202, 203, 204, 205, 206, 207, 208, 209, 210
Node cell 26	183, 187, 188, 189, 190, 191, 192, 193, 194, 195, 196, 197, 198, 199, 200
Node cell 27	184, 185, 186
Node cell 28	337, 338, 339, 340, 341, 342, 343, 344, 345, 346, 347, 348, 349, 350, 351, 352, 353, 354, 355, 356
Node cell 29	358, 359, 360, 361, 362, 401
Node cell 30	357, 363, 364, 365, 366, 367, 368, 369
Node cell 31	370, 371, 372, 373, 374, 375, 376
Node cell 32	377, 400, 378, 379, 380, 381, 382, 383, 384, 385, 386, 387, 388, 389, 390, 391, 392, 393, 394, 395, 396, 397, 398, 399, 402, 403

3.10 Reference

[1] B. Chen, Z. Ye, C. Chen, and J. Wang, "Toward a MILP modeling framework for distribution system restoration," IEEE Trans. Power Syst., vol. 34, no. 3, pp. 1749–1760, 2018.

[2] Y.-L. Ke, "Distribution feeder reconfiguration for load balancing and service restoration by using G-nets inference mechanism," IEEE Trans. Power Deliv., vol. 19, no. 3, pp. 1426–1433, 2004.

[3] X. Liang, M. A. Saaklayen, M. A. Igder, S. M. R. H. Shawon, S. O. Faried, and M. Janbakhsh, "Planning and Service Restoration through Microgrid Formation and Soft Open Points for Distribution Network Modernization: a Review," IEEE Trans. Ind. Appl., 2022.

[4] M. A. Igder, X. Liang, and M. Mitolo, "Service Restoration through Microgrid Formation in Distribution Networks: A Review," IEEE Access, 2022.

[5] J. Zhao, F. Li, S. Mukherjee, and C. Sticht, "Deep Reinforcement Learning based Model-free On-line Dynamic Multi-Microgrid Formation to Enhance Resilience," IEEE Trans. Smart Grid, 2022.

[6] Y. Huang, G. Li, C. Chen, Y. Bian, T. Qian, and Z. Bie, "Resilient distribution networks by microgrid formation using deep reinforcement learning," IEEE Trans. Smart Grid, vol. 13, no. 6, pp. 4918–4930, 2022.

[7] F. S. Gazijahani, J. Salehi, M. Shafie-Khah, and J. P. Catalão, "Spatiotemporal splitting of distribution networks into self-healing resilient microgrids using an adjustable interval optimization," IEEE Trans. Ind. Inform., vol. 17, no. 8, pp. 5218–5229, 2020.

[8] X. Liu, M. Shahidehpour, Z. Li, X. Liu, Y. Cao, and Z. Bie, "Microgrids for enhancing the power grid resilience in extreme conditions," IEEE Trans. Smart Grid, vol. 8, no. 2, pp. 589–597, 2016.

[9] C. Abbey et al., "Powering through the storm: Microgrids operation for more efficient disaster recovery," IEEE Power Energy Mag., vol. 12, no. 3, pp. 67–76, 2014.

[10] T. Ding, Y. Lin, G. Li, and Z. Bie, "A new model for resilient distribution systems by microgrids formation," IEEE Trans. Power Syst., vol. 32, no. 5, pp. 4145–4147, 2017.

[11] C. Chen, J. Wang, F. Qiu, and D. Zhao, "Resilient distribution system by microgrids formation after natural disasters," IEEE Trans. Smart Grid, vol. 7, no. 2, pp. 958–966, 2015.

[12] Y. Vilaisarn, Y. R. Rodrigues, M. M. A. Abdelaziz, and J. Cros, “A Deep Learning Based Multiobjective Optimization for the Planning of Resilience Oriented Microgrids in Active Distribution System,” IEEE Access, vol. 10, pp. 84330–84364, 2022.

[13] S. Cai, Y. Xie, Q. Wu, M. Zhang, X. Jin, and Z. Xiang, “Distributionally robust microgrid formation approach for service restoration under random contingency,” IEEE Trans. Smart Grid, vol. 12, no. 6, pp. 4926–4937, 2021.

[14] M. N. Ambia, K. Meng, W. Xiao, and Z. Y. Dong, “Nested formation approach for networked microgrid self-healing in islanded mode,” IEEE Trans. Power Deliv., vol. 36, no. 1, pp. 452 464, 2020.

[15] S. Lei, C. Chen, Y. Song, and Y. Hou, “Radiality constraints for resilient reconfiguration of distribution systems: Formulation and application to microgrid formation,” IEEE Trans. Smart Grid, vol. 11, no. 5, pp. 3944–3956, 2020.

[16] M. Salimi, M.-A. Nasr, S. H. Hosseinian, G. B. Gharehpetian, and M. Shahidehpour, “Information gap decision theory-based active distribution system planning for resilience enhancement,” IEEE Trans. Smart Grid, vol. 11, no. 5, pp. 4390–4402, 2020.

[17] Z. Wang and J. Wang, “Self-healing resilient distribution systems based on sectionalization into microgrids,” IEEE Trans. Power Syst., vol. 30, no. 6, pp. 3139–3149, 2015.

[18] K. S. A. Sedzro, X. Shi, A. J. Lamadrid, and L. F. Zuluaga, “A heuristic approach to the post disturbance and stochastic pre-disturbance microgrid formation problem,” IEEE Trans. Smart Grid, vol. 10, no. 5, pp. 5574–5586, 2018.

[19] S. A. Arefifar, Y. A.-R. I. Mohamed, and T. H. El-Fouly, “Supply-adequacy-based optimal construction of microgrids in smart distribution systems,” IEEE Trans. Smart Grid, vol. 3, no. 3, pp. 1491–1502, 2012.

[20] Y. Du, H. Tu, X. Lu, J. Wang, and S. Lukic, “Black-start and service restoration in resilient distribution systems with dynamic microgrids,” IEEE J. Emerg. Sel. Top. Power Electron., 2021.

[21] T. Zhao and J. Wang, “Learning sequential distribution system restoration via graph-reinforcement learning,” IEEE Trans. Power Syst., vol. 37, no. 2, pp. 1601–1611, 2021.

[22] Q. Huang, R. Huang, W. Hao, J. Tan, R. Fan, and Z. Huang, “Adaptive power system emergency control using deep reinforcement learning,” IEEE Trans. Smart Grid, vol. 11, no. 2, pp. 1171–1182, 2019.

[23] T. Qian, C. Shao, X. Wang, and M. Shahidehpour, “Deep reinforcement learning for EV charging navigation by coordinating smart grid and intelligent transportation system,” IEEE Trans. Smart Grid, vol. 11, no. 2, pp. 1714–1723, 2019.

[24] B. Wang, Y. Li, W. Ming, and S. Wang, “Deep reinforcement learning method for demand response management of interruptible load,” IEEE Trans. Smart Grid, vol. 11, no. 4, pp. 3146–3155, 2020.

[25] Q. Zhang, K. Dehghanpour, Z. Wang, and Q. Huang, “A learning-based power management method for networked microgrids under incomplete information,” IEEE Trans. Smart Grid, vol. 11, no. 2, pp. 1193–1204, 2019.

[26] M. M. Hosseini and M. Parvania, “Resilient Operation of Distribution Grids Using Deep Reinforcement Learning,” IEEE Trans. Ind. Inform., vol. 18, no. 3, pp. 2100–2109, 2021.

[27] R. S. Sutton and A. G. Barto, Reinforcement learning: An introduction. MIT press, 2018.

[28] Z. Zhang, D. Zhang, and R. C. Qiu, “Deep reinforcement learning for power system applications: An overview,” CSEE J. Power Energy Syst., vol. 6, no. 1, pp. 213–225, 2019.

[29] S. H. Oh, Y. T. Yoon, and S. W. Kim, “Online reconfiguration scheme of self-sufficient distribution network based on a reinforcement learning approach,” Appl. Energy, vol. 280, p. 115900, 2020.

[30] X. Wang et al., “Deep reinforcement learning: a survey,” IEEE Trans. Neural Netw. Learn. Syst., 2022.

4 Optimal Switch Placement to Enhance Microgrid Formation-based Service Restoration Using Reinforcement Learning in Distribution Networks

4.1 Abstract

In this paper, an effective optimal switch placement method is proposed using the binary particle swarm optimization to minimize unsupplied loads and the total number of switches as the objective function through the multiobjective optimization technique. The optimally placed switches offer a significant improvement on service restoration when compared to randomly placed switches, which has been proven using our previously proposed dynamic microgrid formation and deep reinforcement learning-based service restoration method. Case studies are performed to validate these methods using the IEEE 33-node test system and a real 404-node distribution network system operated by Saskatoon Light and Power in Canada.

4.2 Introduction

Uninterrupted reliable power supply in distribution networks is a primary concern for distribution system operators [1]. To improve reliability, electric utilities are making significant investments in their systems [2], [3]. Faults are inevitable in distribution grids, and proactive measures must be taken to mitigate negative impact of such events. Protection and isolation devices, including circuit breakers, reclosers, and remote-controlled switches, can significantly improve the reliability of the system. Modern automated distribution networks rely heavily on sectionalizing and automatic switches, which are instrumental in isolating faulted areas when potential faults arise. This proactive measure has a direct positive impact on reducing customer outages. However, sectionalizing switches have a relatively high cost, so system planners must ensure optimal placement of these switching devices considering a trade-off between potential investment costs and reliability improvement.

Identifying optimal locations of switches in a distribution system requires optimization techniques [4]. Conducting optimization can be computationally expensive, and often exhibits

multiple local optima, necessitating global search methods, such as population-based algorithms, to generate reliable outcomes [5], [6]. Heuristic evaluation techniques, including the genetic algorithm (GA) [7], ant colony algorithm (ACO) [8], particle swarm optimization (PSO) [9] and immune algorithm (IA) [10], have been extensively use to address a diverse range of combinatorial problems, including the power system analysis and control system design. In [8], a combination of the mixed fuzzy logic and ACO methods are used for optimal switch placement in a distribution system featuring distributed generation (DG) sources, and the weighted sum of objective functions is used to analyze impacts on both economic costs and the network reliability. In [10], IA is employed to determine optimal placement of switching devices with the objective to minimize both investment costs of line switches and the total cost of customer service outages. In [7], a hybrid algorithm incorporating both fuzzy logic and genetic algorithms (GAs) is utilized to improve the system average interruption duration index, but this algorithm requires a considerable number of network parameters. In [9], a three-state variation of the PSO method is introduced to determine optimal number and position of sectionalizer switches in distribution networks with the cost of outage as the objective function.

Integer programming is another class of methods to solve optimization problems for optimal switch placement. In [11], an effective method for optimizing the system average interruption duration index is introduced using a mixed integer linear programming (MILP) approach. MILP is used in [12] to minimize customer outage costs in networks with and without alternative supply paths. To simultaneously optimize allocation of sectionalizing switches and protective devices, mixed integer nonlinear programming (MINLP) techniques are employed in [13], and the optimization problem can be solved by commercial solvers using the branch-and-bound algorithm. As the complexity of optimization problems increases, the number of test solutions in the branch and bound algorithm grows exponentially, which limits the size of the network that can be effectively solved.

In this paper, an effective algorithm based on the binary particle swarm optimization (BPSO) is used to optimize the switch placement in distribution networks. Input information required for the proposed algorithm includes the power system topology and load point data. To evaluate the fitness of the solution, the objective function minimizes unsupplied loads and the number of switches.

We have proposed a dynamic microgrid (MG) formation-based service restoration method

using deep reinforcement learning (DRL) for distribution systems previously, but the number of switches and their locations in the system are assumed. To further improve the restoration performance using this method, optimal switch placement appears to be a necessary step. In this paper, optimal placement of switches is firstly conducted, then the results are used in the proposed service restoration to evaluate if a better restoration can be achieved.

The main contributions of the paper include

1) An effective optimal switch placement is proposed using the binary particle swarm optimization with minimizing unsupplied loads and the total number of switches as the objective function.
2) The optimally placed switches are then used in the proposed dynamic microgrid formation-based service restoration method using DRL. The IEEE 33-node test system and a real 404-node distribution system operated by Saskatoon Light and Power, a Canadian electric utility in Saskatoon, Canada, are used for validations.

The paper is arranged as follows: In Section 4.3, the problem formulation is presented; in Section 4.4, the proposed algorithm for switch placement is explained; the effectiveness of the proposed approach is then evaluated in Sections 4.5 and 4.6, utilizing both the IEEE 33-node system and a practical distribution network from Saskatoon Light and Power, respectively; finally, Section 4.7 presents the concluding remarks of this study.

4.3 Problem Formulation

The proposed BPSO algorithm for switch placement in this study is inspired by the binary variant of the PSO, which is an adaptation of the original continuous version introduced in [14] initially. The algorithm can determine a switch configuration in the system that effectively minimizes unsupplied loads with the network topology and the demand associated with each load point as parameters. The network topology is represented by using the graph theory, and an incidence matrix is established with details, such as nodes, edges, weights, and their respective interconnections in the network under investigation.

4.3.1 Particle Swarm Optimization Algorithm

Swarm intelligence-inspired optimization techniques, such as PSO, have gained popularity due to their inherent flexibility and robustness traits. PSO leverages the principle of swarming

theory in conjunction with the evolutionary computation to achieve optimal outcomes. The swarm population, which comprises of *M* agents, each containing *N* particles, is effectively represented by a $M \times N$ matrix. Each swarm serves as an agent to address a *N*-dimensional optimization problem at hand. A larger value of *M* indicates a higher degree of exploration within the solution space. The revised version of the original PSO approach presented in [15] offers an alternative interpretation of the concept of position and velocity in discrete values. In this approach, each particle's position is restricted to a binary value, 0 or 1. Meanwhile, the particle's velocity is measured by the number of bits that change in each iteration as defined by (4.1), and it is updated throughout the process accordingly.

$$V_{i+1} = V_i + C_1.Rand_1.\Delta X_{1,i} + C_2.Rand_2.\Delta X_{2,i} \quad (4.1)$$

$$\Delta X_{1,i} = pbest_i - X_i \quad (4.2)$$

$$\Delta X_{2,i} = gbest_i - X_i \quad (4.3)$$

where C_1 and C_2 are learning factors. $Rand_1$ and $Rand_2$ are randomly generated values within the range of [0, 1]. The particle best value ($pbest$), the global best value ($gbest$), and the particle position (X) are integers in {0, 1}. V_i is a probability value in the range of [0, 1]. A logical transformation, known as $S(V_i)$, is used in this paper, which can be precisely defined by the following rule:

$$X_i = \begin{cases} 1 & rand(0,1) < S(V_i) \\ 0 & otherwise \end{cases} \quad (4.4)$$

$$S(V_i) = \frac{1}{1 + \exp(-V_i)} \quad (4.5)$$

where $S(V_i)$ is the sigmoid transformation. The term $rand(0,1)$ refers to a randomly generated number that follows a uniform distribution in the range of [0, 1].

Within each iteration (*i*), the particles associated with each agent are randomly initialized as either 1 or 0 to obtain the initial solution. The fitness of the current solution is then evaluated

by calculating the objective function. Once the results for all agents are calculated, the $pbest$ value is also determined. The most appropriate $pbest$ value from the set of $pbest$ for all agents at iteration *i* is then assigned to $gbest$. After incrementing the proposed solution by 1, a new iteration starts, and the fitness of the subsequent solution is once again evaluated using the objective function. If a better-fitted outcome is discovered, $gbest$ is updated accordingly. The procedure terminates once a specified number of iterations is reached or a particular objective function value is achieved, at this point, $gbest$ is the final solution of the problem.

The output of the discrete PSO for the switch placement problem are Boolean values (1 or 0), 1 means a switch in the respective branch, and 0 means no switch. Each swarm's dimension (*dim*) is related to the maximum number of potential switches within a distribution network, which can be represented as follows:

$$dim = NC + NO - CB \tag{4.6}$$

where *NC*, *NO*, and *CB* denote the total number of branches in the distribution network, the number of normally open switches, and the number of circuit breakers, respectively.

4.3.2 Objective Function

The objective function evaluates solutions of each particle swarm, which only relies on the network topology and the demand of customer per load point, and does not involve any reliability data, i.e. it is independent of the failure rates of network components. Each solution (*x*) has a collection of switches that minimize the number of affected customers (unsupplied) in the event of outages. This procedure effectively simplifies the objective function. In this switch placement algorithm, the objective function (*OF*) includes two member functions, F_{UL} and F_{NSW}. The function F_{UL} calculates the number of unsupplied loads due to outages, and the function F_{NSW} determines the number of switches included in the solution *x*. When there is a fault in the network, some switches are opened to isolate the fault while ensuring that the maximum possible load is supplied. The objective function is expressed as follows:

$$OF(x) = w_u F_{UL}(x) + w_r F_{NSW}(x) \tag{4.7}$$

where w_u and w_r are weight coefficients used to determine the relative importance of different objective terms, and can be selected based on priorities of stakeholders. These weight coefficients must follow constrains in (8) and (9).

$$w_u + w_r = 1 \quad (4.8)$$

$$w_u, w_r \geq 0 \quad (4.9)$$

In the initial stage, the weight coefficients are set as w_u = 1 and w_r = 0, indicating that the priority is to supply more loads than minimizing the cost to determine a benchmark value for the number of switches. In the second stage, the weight of the cost objective function is assigned a nonzero value. In case studies, the values of w_u and w_r are both set to 0.5, reflecting an equal importance and priority of both objectives. Other weight coefficients are also used in this study to show their influences. When $w_u > w_r$, the optimization algorithm prioritizes presenting more reliable but expensive solutions; when $w_u > w_r$, the algorithm presents a cheaper but less reliable solutions.

The F_{UL} function can be expressed as follows:

$$F_{UL} = \frac{\sum_{j=1}^{B} d_j}{TD} \quad (4.10)$$

where *B* is the total number of branches in the distribution network. d_j is the amount of load demand that is switched off due to a fault on the *jth* branch. *TD* is the total amount of load demand that are normally supplied by the distribution network. Therefore, the function F_{UL} evaluates the amount of demand that remains unsupplied by a specific set of switches, considering all possible contingencies.

The F_{NSW} function can be expressed as follows:

$$F_{NSW} = \frac{N_x}{TS} \quad (4.11)$$

F_{NSW} is calculated by taking into account the number of switches in the current iteration solution,

denoted by N_x, and the number of switches obtained from the first stage algorithm solution, denoted by TS of the x_{gbest}.

4.4 The Switch Placement Algorithm

The proposed BPSO-based switch placement approach can be implemented by following the steps:

1) Step 1: Topology information. A distribution network is represented by the graph theory to define nodes, edges, weight, and their relationships.
2) Step 2: Initialization. A swarm of particles are randomly initialized with positions and velocities in the search space.
3) Step 3: Evaluation. The fitness of each particle in the swarm is evaluated using (4.7). (4.10) for each proposed solution (x_i) of iteration i is determined by analyzing all contingencies by
    3.1 Assuming a contingency on branch j.
    3.2 Finding the shortest path between the source node and the source-side node of a short circuit.
    3.3 Locating a normally closed switch along this path and deactivating it to isolate the fault. If there is no such switch available, the circuit breaker or recloser of the feeder must be opened to isolate the fault.
    3.4 Identifying a normally closed switch between the other node of the short circuit and the last node of the feeder and opening it to achieve complete isolation of the fault.
    3.5 Identifying all load points that become isolated as a result of opening a normally closed switch.
4) Step 4: Update $pbest$. For each particle, update its $pbest$ if the current position has a better fitness than the previous $pbest$.
5) Step 5: Update $gbest$. Update $gbest$ for the swarm based on the particle with the best fitness among all $pbest$.
6) Step 6: Update velocity. Update the velocity of each particle using (4.1)-(4.3).
7) Step 7: Update position. Update the position of each particle using (4.4) and (4.5).
8) Step 8: First stage termination. Repeat Steps 3 to 7 until a termination criterion is met for

the first stage, reaching a maximum number of iterations.

9) Step 9: Update information for the second stage. Update weight coefficients, w_u and w_r, and the number of the maximum iteration (IterMax).
10) Step 10: The second stage termination. Randomly initialize a swarm of particles with position and velocities, then repeat Steps 3 to 7 until a termination criterion is met for the second stage.
11) Step 11: State solution: State $gbest$ as a final solution for determining the optimal switch configuration in the distribution network.

The flowchart of the proposed switch placement algorithm is shown in Figure 4.1, where s is the stage number, *i* is the iteration number, *a* is the swarm number, and *A* is the swarm size.

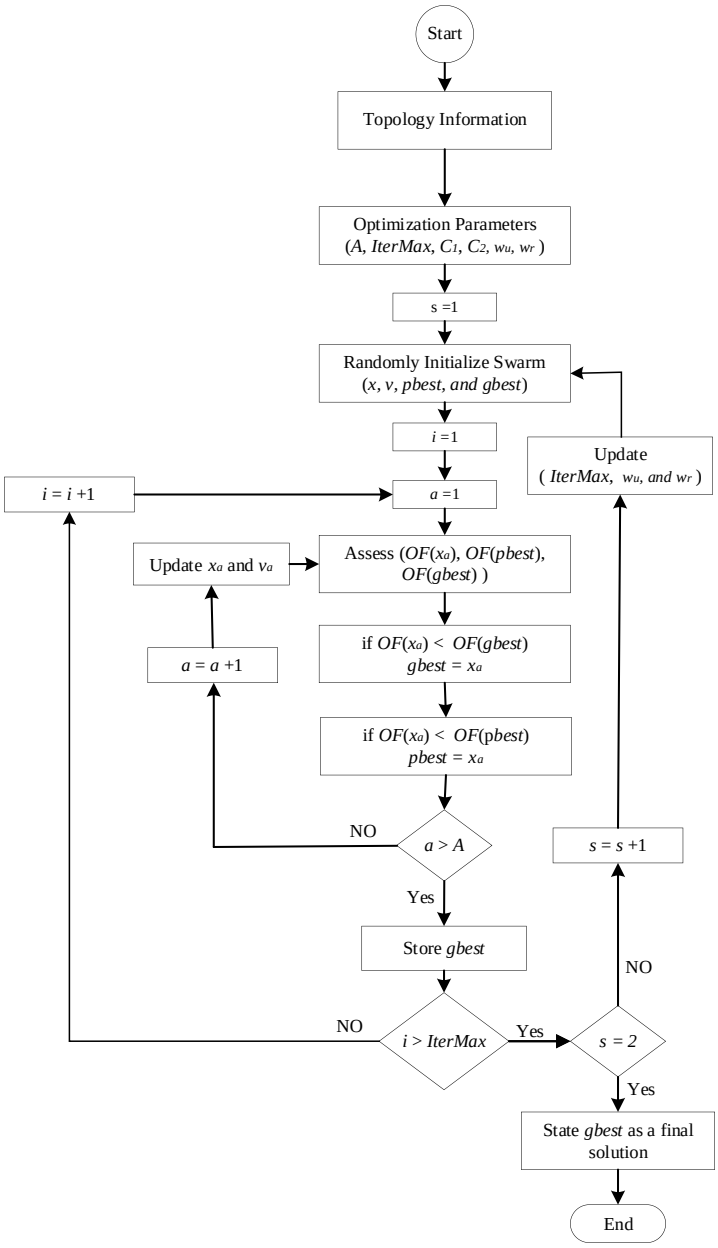

Figure 4.1. Flowchart of the proposed switch placement algorithm.

4.5 Validation of the Proposed Switch Placement Method Using the IEEE 33-node Test System

To validate the proposed switch placement method, the IEEE 33-node test system in Figure 4.2 is used in this paper. It has 32 lines with a demand of 3.715 MW and 2.3 MVAr. We first analyze the switch placement problem, and then evaluate their impact on the microgrid formation-

based service restoration using deep reinforcement learning. Python 3.9 is used to solve the optimization problem.

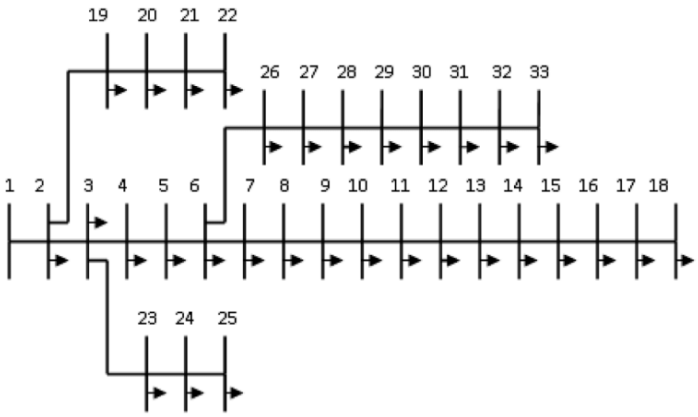

Figure 4.2. The IEEE 33-node test system [16].

4.5.1 The Switch Placement Optimization

The BPSO is applied to find an optimal configuration of switches shown in Table 4.1. Three solutions are compared based on the priority weights of objectives, the number of switches, the best solution OF value, the worst solution OF value, the mean OF value, standard deviation (STD), and the switch locations. For solution 1, the weight coefficients w_u and w_r are both set to 0.5, leading to a total of 15 switches placed, and the switch locations are provided in Table 4.1. By installing switches at these specified locations, the network can be reconfigured to isolate faults and reroute power in case of outages, thereby minimizing the number of customers affected. Distribution grid operators consider various factors, such as load demand, line capacity, reliability, and cost-effectiveness, when determining the number of switches to be installed on lines [17], [18].

To demonstrate the effect of different factors, two different weight priorities to minimize unsupplied loads and the number of switches are considered in addition to equal weight. The choice of weight values for the two objectives in the objective function has a significant impact on the number of switches and the overall objective function value. Compared to Solution 1, Solution 2 places more weight on reducing unsupplied loads, resulting in a lower objective function value of 0.62431 and a total of 19 switches installed. Solution 3 places more weight on minimizing the number of switches installed, resulting in a higher objective function value of 0.7901 and a total of 7 switches installed. Therefore, different weight values can be selected to achieve the desired

balance between unsupplied loads and the number of switches installed.

To evaluate the performance of the proposed optimization method, objective function (OF) values are analyzed for the best and worst solutions, and the mean and standard deviation (STD) of OF values for all solutions. For Solution 1 the best solution is the one with the lowest OF value of 0.7182, and the worst solution is the one with the highest OF value of 0.7869. The mean of the OF values is 0.7467, which is the average OF value of all solutions found by the algorithm; and the STD of the OF values is 0.0169, which represents the spread of the OF values around the mean. A low STD value indicates that the solutions found by the algorithm are consistently good.

Table 4.1. Comparative analysis of switching solutions with different objective weights in IEEE 33-node system

Solution (#)	Priority Weights of Objectives	Number of Switches	Best Solution OF	Worst Solution OF	Mean	STD	Switch Location
1	W_u = 0.5 and W_r = 0.5	15	0.7182	0.7869	0.7467	0.0169	(Substation, 1), (3, 4), (6, 7), (8, 9), (10, 11), (14, 15), (2, 19), (20, 21), (3, 23), (23, 24), (24, 25), (6, 26), (27, 28), (29, 30), (31, 32)
2	W_u = 0.6 and W_r = 0.4	19	0.6243	0.6754	0.6507	0.0193	(Substation, 1), (2, 3), (3, 4), (5, 6), (6, 7), (7, 8), (8, 9), (11, 12), (14, 15), (16, 17), (19, 20), (3, 23), (23, 24), (24, 25), (6, 26), (27, 28), (29, 30), (30, 31), (31, 32)
3	W_u = 0.4 and W_r = 0.6	7	0.7901	0.8484	0.8199	0.0209	(Substation, 1) (12, 13), (13, 14), (14, 15), (3, 23), (23, 24), (24, 25)

4.5.2 Service Restoration through Microgrid Formation using Deep Reinforcement Learning

Using our previously proposed dynamic microgrid formation and deep reinforcement learning-based service restoration method, the optimal switch placement can significantly improve restoration in distribution networks compared to randomly placed switches with arbitrary numbers and locations, as shown in Table 4.2. The improvement of 10.84% of active power demand and 65.29% of reactive power demand have been made compared to randomly placed switches. The graphical representation of the microgrid formation-based service restoration method using optimal switch placement for the IEEE 33-node test system is depicted in Figure 4.3, forming three

microgrids.

Table 4.2. Comparison of MG-based service restoration using DRL: optimal vs random switch placement

Microgrid	Restored Nodes		Restored loads (kW)		Restored loads (kVar)	
MG1	Optimal switch placement	Randomly switch Placement	Optimal switch placement	Randomly switch Placement	Optimal switch placement	Randomly switch Placement
	1, 2, 3, 4, 5, 6, 7, 8, 9, 10, 23, 24	1, 2, 3, 4, 5, 6, 7, 8, 9, 10, 19, 20, 26, 27	1460	1430	720	680
MG2	30, 31, 32, 33	31, 32, 33	620	420	810	210
MG3	15, 16, 17, 18	15, 16, 17, 18	270	270	90	90
$\frac{Total\ resotoredload}{Total\ load}$ *100			63.26%	57.07%	70.43%	42.61%
Service Restoration Improvement			10.84%		65.29%	

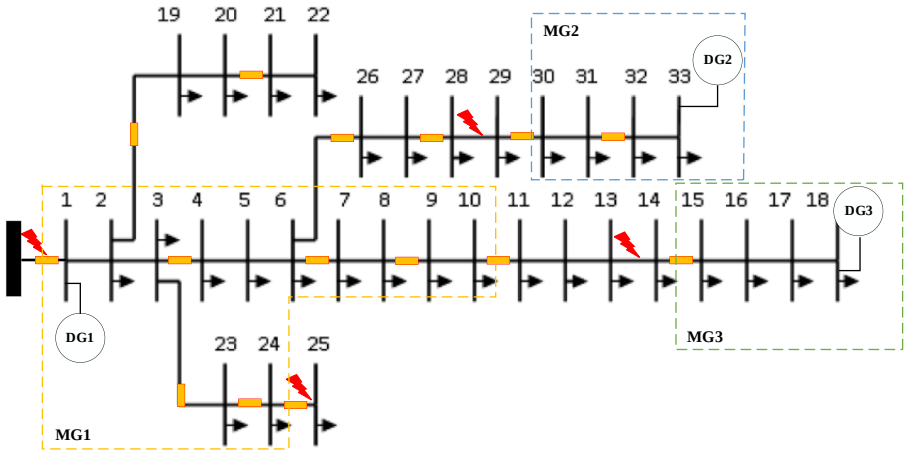

Figure 4.3. Microgrid formation-based service restoration in IEEE 33-node test system.

4.6 Validation Through a Real Large 404-node Distribution System

The proposed method is further verified through a real 404-node distribution system consisting of two distribution feeders. This system is one 25/14.4 kV, 33.3 MVA substation in the distribution network operated by Saskatoon Light and Power in Saskatoon, Canada, with a real power demand of 11.605 MW and a reactive power demand of 7.192 MVar. The system model was developed using the data provided by Saskatoon Light and Power.

4.6.1 Switch Placement Optimization

Through the utilization of the novel BPSO-based switch placement approach, the optimal

configurations of switches for varying priority coefficients of objectives have been obtained, as depicted in Table 4.3. For Solution 1, a total of 40 switches are required, located at specific lines in the network with the same weights of 0.5 for both objective functions. The second solution prioritizes minimizing the unsupplied loads, achieved a lower OF value of 0.5957 and 56 switches. The third solution emphasizes reducing the number of switches, obtained a higher OF value of 0.84098 and 27 switches. Their objective function (OF) values for the best and worst solutions, along with the mean and STD of the OF values for all the solutions are shown in this table.

4.6.2 Service Restoration through Microgrid Formation using Deep Reinforcement Learning

To demonstrate the influence of optimal switch placement on service restoration using the proposed restoration method, the real 404-node system is used. First, the system is converted into node cells, which only contain switchable lines. Figure 4.4 provides a graphical representation of this conversion. The appendix contains tables that present the correspondence between node cells and their respective node numbers in the original system for both optimal and random switch placement strategies.

The results of this study is shown in Table 4.4. An improvement of 6.5% of active power and 7% of reactive power can be achieved when compared to randomly placed switches.

Figure 4.5 illustrates the graphical representation of the microgrid formation-based service restoration approach employed in the 404-node system with ten microgrids formed.

Table 4.3.Comparative Analysis of Switching Solutions with Different Objective Weights in the real world system

Solution (#)	Priority Weights of Objectives	Number of Switches	Best Solution OF	Worst Solution OF	Mean	STD	Switch Location
1	W_u = 0.5 and W_r = 0.5	40	0.60771	0.61545	0.6128	0.0027	(Substation, 1), (4, 6), (14, 15), (28, 30), (293, 298), (298, 299), (307, 309), (311, 313), (316, 318), (325, 327), (327, 329), (42, 43), (56, 58), (61, 64), (74, 76), (95, 96), (100, 169), (172, 174), (101, 104), (108, 110), (112, 113), (125, 127), (122, 124), (147, 151), (152, 155), (95, 183), (207, 209), (218, 220), (226, 228), (230, 238), (240, 242), (246, 250), (263, 265), (265, 269), (279, 151), (Substation, 337), (357, 358), (365, 366), (365, 370), (377, 378)
2	W_u = 0.6 and W_r = 0.4	56	0.5957	0.61005	0.60468	0.005	(Substation, 1), (6, 8), (12, 14), (15, 20), (22, 24), (28, 30), (36, 38), (293, 294), (299, 301), (305, 307), (311, 313), (316, 318), (323, 325), (325, 327), (42, 43), (47, 48), (52, 54), (58, 61), (61, 64), (74, 76), (14, 85), (85, 87), (87, 89), (95, 96), (100, 169), (101, 104), (112, 113), (118, 122), (122, 124), (124, 136), (139, 141), (145, 147), (155, 157), (160, 162), (162, 164), ('95', '183'), ('189', '191'), ('195', '196'), (205, 207), (220, 222), (222, 226), (228, 230), (230, 231), (244, 246), (261, 263), (265, 269), (269, 271), (271, 273), (279, 151), (Substation, 337), (345, 347), (351, 353), (353, 355), (365, 370), (377, 378), (382, 391)
3	W_u = 0.4 and W_r = 0.6	27	0.84098	0.85605	0.84830	0.0057	(Substation, 1), (28, 30), (298, 303), (313, 315), (321, 323), (329, 331), (47, 48), (72, 74), (78, 80), (89, 91), (98, 100), (110, 112), (118, 122), (129, 131), (124, 136), (138, 139), (191, 193), (193, 195), ('196', 198), (218, 220), (230, 283), (250, 254), (279, 151), (0, 337), (347, 349), (372, 373), (395, 397)

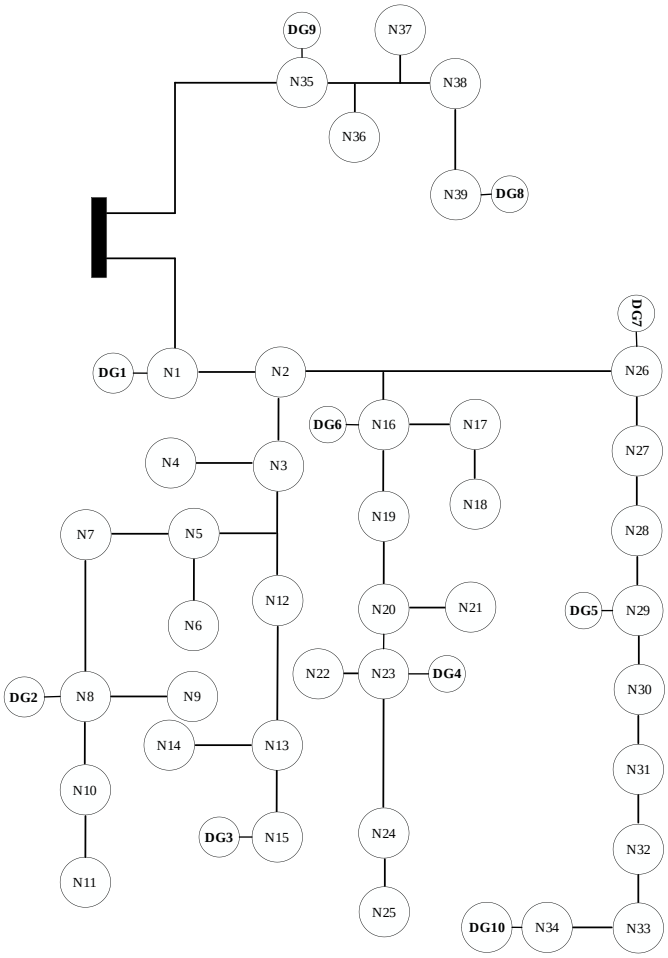

Figure 4.4. Node cells formation of Saskatoon Light and Power system.

Table 4.4. Comparison of MG-based service restoration using DRL: optimal vs random switch placement

Microgrid	Restored Node Cells		Restored loads (kW)		Restored loads (kVar)	
MG1	Optimal switch placement	Randomly switch Placement	Optimal switch placement	Randomly switch Placement	Optimal switch placement	Randomly switch Placement
	N1, N2, N3, N4	N1, N2, N3, N10, N11	989.1875	699.1250	626.8714	433.2788
MG2	N5, N6, N7, N8, N9	N4, N5, N6	632.1875	810.6875	391.79461	502.4190
MG3	N12, N13, N14, N15	N8, N9	825.5625	825.5625	511.6377	511.6377
MG4	N22, N23	N15, N16	699.125	699.1250	433.27879	433.2788
MG5	N28, N29	N21, N22, N23	944.5625	899.9375	585.3872	557.7318
MG6	N16, N19, N20, N21	N13, N14	917.49	820.8150	577.82791	508.6877
MG7	N26	N25, N26, N27	575.6625	594.2563	356.7650	368.2896
MG8	N39	N32	446.25	446.2500	276.5609	276.5635
MG9	N35, N37	N28, N30	401.625	401.6250	248.9048	248.9048
MG10	N33, N34	N18	1442.875	1197.4375	894.2136	742.1051
$\frac{Total\ resotoredload}{Total\ load}$ *100			67.85%	63.72%	68.18 %	63.72%
Service Restoration Improvement			6.5 %		7 %	

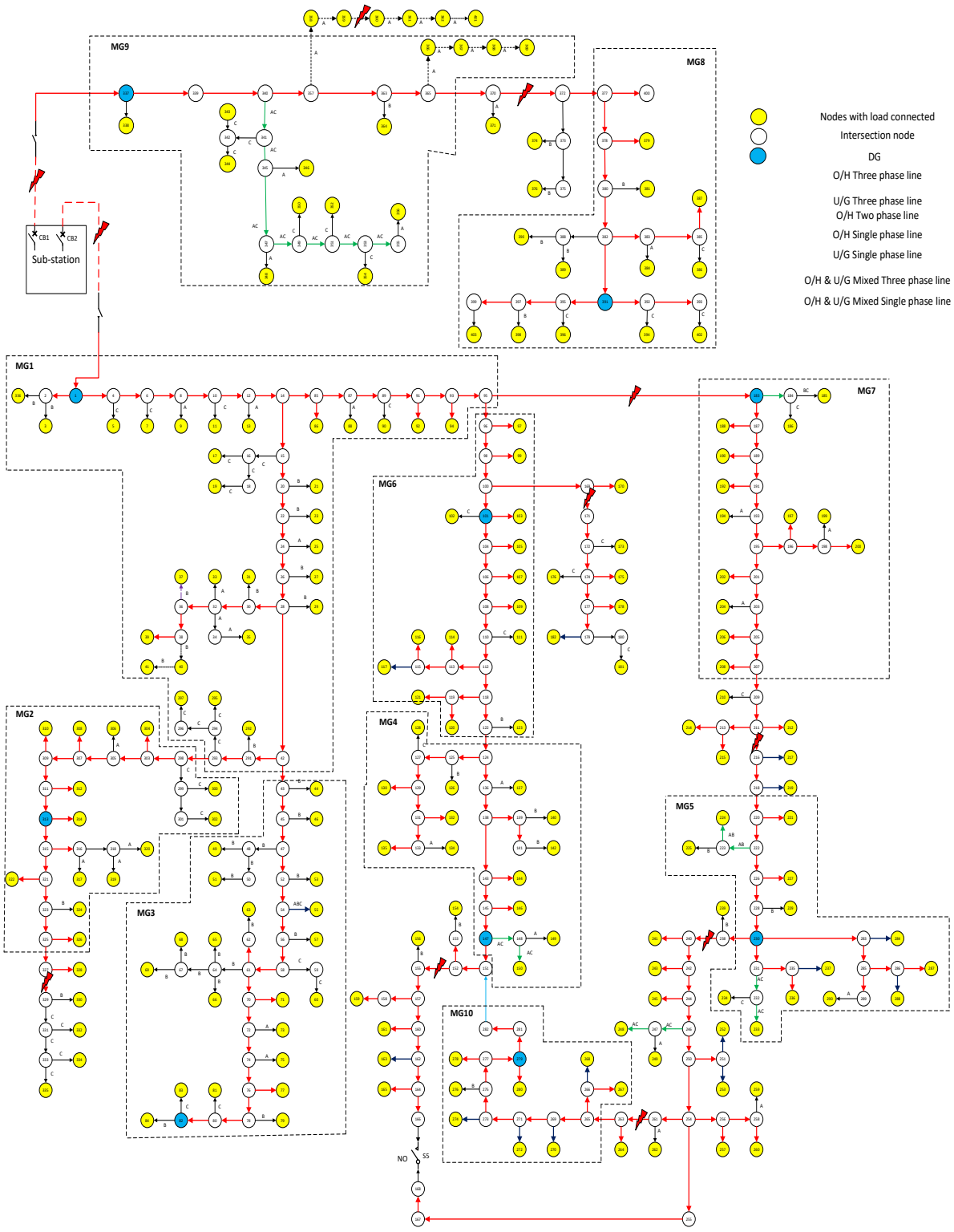

Figure 4.5. Microgrid formation-based service restoration in the Saskatoon Light and Power distribution network.

4.7 Conclusion

In this paper, a multi-objective BPSO-based optimization algorithm is proposed for the optimal placement of switches by considering two objective functions: minimizing the number of unsupplied loads and installed switches. The optimization with different weight values for the objective functions is considered. The optimally placed switches are used in our previously proposed dynamic microgrid formation and deep reinforcement learning-based service restoration method, significant improvement of restored load can be made compared to randomly placed switches. This is validated by IEEE 33-node test system, and the 404-node Saskatoon light and Power system.

4.8 Reference

[1] F. Shen, Q. Wu, and Y. Xue, “Review of service restoration for distribution networks,” J. Mod. Power Syst. Clean Energy, vol. 8, no. 1, pp. 1–14, 2019.

[2] Z. Galias, “Tree-structure based deterministic algorithms for optimal switch placement in radial distribution networks,” IEEE Trans. Power Syst., vol. 34, no. 6, pp. 4269–4278, 2019.

[3] Y. Du and D. Wu, “Deep reinforcement learning from demonstrations to assist service restoration in islanded microgrids,” IEEE Trans. Sustain. Energy, vol. 13, no. 2, pp. 1062–1072, 2022.

[4] Z. Li, W. Wu, X. Tai, and B. Zhang, “Optimization model-based reliability assessment for distribution networks considering detailed placement of circuit breakers and switches,” IEEE Trans. Power Syst., vol. 35, no. 5, pp. 3991–4004, 2020.

[5] V. Calderaro, V. Lattarulo, A. Piccolo, and P. Siano, “Optimal switch placement by alliance algorithm for improving microgrids reliability,” IEEE Trans. Ind. Inform., vol. 8, no. 4, pp. 925–934, 2012.

[6] J. R. Bezerra, G. C. Barroso, R. P. S. Leão, and R. F. Sampaio, “Multiobjective optimization algorithm for switch placement in radial power distribution networks,” IEEE Trans. Power Deliv., vol. 30, no. 2, pp. 545–552, 2014.

[7] H. N. Alves, “A hybrid algorithm for optimal placement of switches devices in electric distribution systems,” IEEE Lat. Am. Trans., vol. 10, no. 6, pp. 2218–2223, 2012.

[8] H. Falaghi, M.-R. Haghifam, and C. Singh, “Ant colony optimization-based method for placement of sectionalizing switches in distribution networks using a fuzzy multiobjective approach,” IEEE Trans. Power Deliv., vol. 24, no. 1, pp. 268–276, 2008.

[9] A. Moradi and M. Fotuhi-Firuzabad, “Optimal switch placement in distribution systems using trinary particle swarm optimization algorithm,” IEEE Trans. Power Deliv., vol. 23, no. 1, pp. 271–279, 2007.

[10] C.-S. Chen, C.-H. Lin, H.-J. Chuang, C.-S. Li, M.-Y. Huang, and C.-W. Huang, “Optimal placement of line switches for distribution automation systems using immune algorithm,” IEEE Trans. Power Syst., vol. 21, no. 3, pp. 1209–1217, 2006.

[11] A. Shahbazian, A. Fereidunian, and S. D. Manshadi, “Optimal switch placement in distribution systems: A high-accuracy MILP formulation,” IEEE Trans. Smart Grid, vol. 11, no. 6, pp. 5009–5018, 2020.

[12] A. Abiri-Jahromi, M. Fotuhi-Firuzabad, M. Parvania, and M. Mosleh, “Optimized Sectionalizing Switch Placement Strategy in Distribution Systems,” IEEE Trans. Power Deliv., vol. 27, no. 1, pp. 362–370, Jan. 2012, doi: 10.1109/TPWRD.2011.2171060.

[13] A. Heidari, Z. Y. Dong, D. Zhang, P. Siano, and J. Aghaei, “Mixed-integer nonlinear programming formulation for distribution networks reliability optimization,” IEEE Trans. Ind. Inform., vol. 14, no. 5, pp. 1952–1961, 2017.

[14] J. Kennedy and R. Eberhart, “Particle swarm optimization,” in Proceedings of ICNN’95-international conference on neural networks, IEEE, 1995, pp. 1942–1948.

[15] J. Kennedy and R. C. Eberhart, “A discrete binary version of the particle swarm algorithm,” in 1997 IEEE International conference on systems, man, and cybernetics. Computational cybernetics and simulation, IEEE, 1997, pp. 4104–4108.

[16] P. S. Meera and S. Hemamalini, “Optimal siting of distributed generators in a distribution network using artificial immune system,” Int. J. Electr. Comput. Eng., vol. 7, no. 2, p. 641, 2017.

[17] R. Billinton and S. Jonnavithula, “Optimal switching device placement in radial distribution systems,” IEEE Trans. Power Deliv., vol. 11, no. 3, pp. 1646–1651, 1996.

[18] J. N. Ahour, M. Rostami, V. T. Majd, M. Rashidbeygi, and H. Moazen, “Optimal switch placement with revised genetic algorithm in distribution system,” in 2016 21st Conference on Electrical Power Distribution Networks Conference (EPDC), IEEE, 2016, pp. 54–59.

5 Conclusions and Future Work

5.1 Summary and Conclusions

In this thesis, a service restoration method in distribution networks through dynamic microgrid formation and deep reinforcement learning is proposed. By using the deep Q-learning technique within a simulated environment, the proposed deep reinforcement learning algorithm is capable of acquiring an optimal control policy, enabling dynamic formation of microgrids during contingencies, thus facilitating a swift service restoration. An initial offline training phase can be conducted to establish the model's learning, which can subsequently be employed for online applications. The proposed method is verified using the IEEE 33-node test system, and a real 404-node distribution system from Saskatoon Light and Power.

To illustrate the critical role of optimal switch placement to improve service restoration in distribution networks, an optimal switch placement method is introduced through a multi-objective optimization algorithm based on BPSO. The algorithm considers two objective functions: minimizing unsupplied loads and the number of switches. The optimization process incorporates different weight values assigned to the objective functions, allowing a flexible trade-off analysis between the two objectives. The switches are then used with the proposed service restoration method to evaluate the improvement on restored loads. The proposed approach is validated using the IEEE 33-node test system and the real 404-node distribution system from Saskatoon Light and Power.

5.2 Future Work

The following recommendations are suggested for the future research:

1) A safe deep reinforcement learning approach can be developed to effectively address the Markov Decision Process (MDP) under various constraints for service restoration. This method incorporates safety layer in training section to ensure safe behaviors of the reinforcement learning agent during the decision-making process.
2) To accurately model the service restoration problem in distribution networks, it is necessary to incorporate dynamic behaviors of induction motor loads and

distributed generators (DGs), taking into account transient operational constraints, such as voltage dips and over-current limits during the starting of induction motor loads. This modification in the problem formulation allows for a more realistic and comprehensive consideration of transient behaviors of the system, leading to improved decision-making and effective service restoration strategies.

Appendix

Publications (Jan. 2021 – Apr. 2023):

1. **Mosayeb Afshari Igder,** Xiaodong Liang, and Massimo Mitolo, "Service restoration through microgrid formation in distribution networks: A review," *IEEE Access*, vol. 10, pp. 46618 – 46632, Apr 2022.
2. Xiaodong Liang, Md Abu Saaklayen, **Mosayeb Afshari Igder**, Shah Mohammad Rezwanul Haque Shawon, Sherif O. Faried, and Mehrnoosh Janbakhsh, "Planning and Service Restoration through Microgrid Formation and Soft Open Points for Distribution Network Modernization: a Review," *IEEE Transactions on Industry Applications*, vol. 58, no. 2, pp. 1843-1857, Mar-Apr 2022.
3. Mehdi Abbasipour, **Mosayeb Afshari Igder,** and Xiaodong Liang, " A novel hybrid neural network-based day-ahead wind speed forecasting technique," *IEEE Access*, vol. 9, pp 151142 - 151154, Nov 2021.
4. Xiaodong Liang, Md Abu Saaklayen, **Mosayeb Afshari Igder**, Shah Mohammad Rezwanul Haque Shawon, and Sherif O. Faried, "Microgrid Formation and Service Restoration in Distribution Systems: a Review," *Proceedings of 2021 56th IEEE Industry Applications Society (IAS) Annual Meeting, Virtual Conference*, October 10 - 14, 2021.
5. Mehdi Abbasipour, **Mosayeb Afshari Igder,** and Xiaodong Liang, "Data-driven wind speed forecasting techniques using hybrid neural network methods," *Proceedings of 2021 IEEE Canadian Conference of Electrical and Computer Engineering (CCECE)*, pp. 1-6, Virtual Conference, Sept. 12-17, 2021.